UNIVERSIDAD DE CÁDIZ

FACULTAD DE CIENCIAS DEL MAR Y AMBIENTALES

DEPARTAMENTO DE FÍSICA APLICADA

ONDAS INTERNAS EN EL GOLFO DE CÁDIZ: IMPLICACIONES OCEANOGRÁFICAS Y MORFOSEDIMENTARIAS

TESIS DOCTORAL

David Roque Atienza

Cádiz, 2022

ONDAS INTERNAS EN EL GOLFO DE CÁDIZ: IMPLICACIONES OCEANOGRÁFICAS Y MORFOSEDIMENTARIAS

Memoria presentada por D. David Roque Atienza para optar al grado de Doctor por la Universidad de Cádiz

Fdo.: David Roque Atienza

Los directores:

Dr. D. Miguel Bruno Mejías
Catedrático de Universidad
Dpto. Física Aplicada
Universidad de Cádiz

Dr. D. Francisco Javier Hernández-Molina
Professor in Sedimentary Geology
Dpt. of Earth Sciences
Royal Holloway University of London

D. MIGUEL BRUNO MEJÍAS, Catedrático del Departamento de Física Aplicada de la Universidad de Cádiz, y D. FRANCISCO JAVIER HERNÁNDEZ-MOLINA, Professor del Departamento de Earth Science de la Universidad Royal Holloway of London,

HACEN CONSTAR:

Que el trabajo recogido en la Memoria de Tesis Doctoral, titulada "ONDAS INTERNAS EN EL GOLFO DE CÁDIZ: IMPLICACIONES OCEANOGRÁFICAS Y MORFOSEDIMENTARIAS", presentada por el Licenciado en Ciencias del Mar D. David Roque Atienza, ha sido realizada bajo su dirección y autorizan su presentación y defensa para optar al grado de Doctor por la Universidad de Cádiz.

Puerto Real, 22 de Octubre de 2022

Tabla de contenidos

Capítulo 1

INTRODUCCIÓN

1.1 Objetivos y justificación de la Tesis

El objetivo principal de la presente Tesis doctoral, desarrollada en el departamento de Física Aplicada de la Universidad de Cádiz, es el análisis de la variabilidad temporal que gobierna el régimen de corrientes y otras propiedades físicas en el Golfo de Cádiz, poniendo especial énfasis en el papel que tienen los procesos de corta escala espacio-temporal, como los fenómenos de ondas internas generadas en el talud, en la definición de estas estructuras, así como su influencia en la morfología del talud continental. Concretamente los objetivos específicos de esta tesis son conocer el papel de las distintas masas de agua existentes en el Golfo de Cádiz en la generación de ondas internas en la plataforma y el talud continental, su relación entre la variabilidad de los flujos del agua central NorAtlántica hacia el Estrecho de Gibraltar y la intensificación y localización de la masa de agua Mediterránea. Además, se quiere valorar, de manera general, las implicaciones que estos procesos físicos pueden tener sobre la morfología del fondo marino del talud continental.

Los estudios asociados a la Tesis se han llevado a cabo en el marco de diferentes Proyectos de Investigación nacionales [CTM2012-39599-C03-01; CTM2013-49048-C2-2; CTM2016-75129-C3-3, CGL2016-80445-R (AEI/FEDER, UE))] e internacionales (OCASO).

Como parte de los requisitos existentes por la Universidad de Cádiz, uno de los capítulos de la Tesis Doctoral ha sido publicado en una revista científica internacional de SCI, Ocean Science en el año 2019, (https://doi.org/10.5194/os-15-1381-2019) y que es presentado en el capítulo 3.

Existen numerosos estudios donde se observan que los procesos de corto periodo pueden contribuir de manera notable a la dinámica de los procesos de mezcla en el talud y en la plataforma y de esta manera influir en la definición de estructuras mesoescalares que dominan la dinámica del Golfo de Cádiz.

El conocimiento del papel de las corrientes de fondo y los procesos oceanográficos asociados, incluyendo procesos intermitentes (mareas, ondas internas, ...), está evolucionando rápidamente. Muchos de estos procesos son poco conocidos, en parte debido a que las observaciones directas son limitadas, si bien pueden generar importantes rasgos deposicionales y/o erosivos a escalas temporales de corto o largo periodo (Hernández-Molina et al., 2016; Rebesco et al., 2014). Para un mejor conocimiento de la sedimentación marina profunda se requiere la interpretación de estos procesos oceanográficos, cuál es su evolución espacial y temporal, cómo afectan a las corrientes de fondo y cómo se ven afectados por la topografía submarina. Sin embargo, dada su complejidad y su variable naturaleza tridimensional y temporal, es necesario que estos procesos se integren en un marco oceanográfico y climatológico con un enfoque multidisplinar que incluyan la Geología y la

oceanografía Física. Esta integración requiere de una mayor compilación de datos oceanográficos y un mejor conocimiento de la morfología del fondo marino (Rebesco et al., 2014).

Con esta tesis se pretende avanzar en el conocimiento de la importancia que tienen los procesos de corto periodo, abordando su estudio desde dos puntos de vista: i) El análisis de las observaciones obtenidas en campañas oceanográficas y en fondeos; ii) Su correlación con los rasgos morfosedimentarios del talud del Golfo de Cádiz.

Los objetivos específicos de esta tesis son los siguientes:

1. Determinar cuál es el papel de las distintas masas de agua existente en el Golfo de Cádiz.
2. Definir cuál es la implicación existente entre estas masas de agua en la generación de ondas internas en el talud continental.
3. Conocer la relación entre la variabilidad de flujos del Agua Central NorAtlántica hacia el Estrecho de Gibraltar y la intensificación de la masa de agua Mediterránea.
4. Evaluar la implicación de la masa de agua Antártica intermedia modificada en la dinámica regional y su posible interacción con la masa de agua Mediterránea.
5. Establecer las implicaciones de estos procesos físicos sobre la morfología del fondo marino del talud continental.

1.2 Localización del área de estudio

El Golfo de Cádiz es una región del océano Atlántico Norte al sur de la península ibérica, y adyacente al Estrecho de Gibraltar (Figura 1.1). Geográficamente vamos a definir las fronteras del mismo, siendo el límite superior de esta región la costa suroccidental de la península ibérica, concretamente la región del Algarve y la costa de Huelva. Por otro lado, las costas de Cádiz, la costa atlántica marroquí y el Estrecho de Gibraltar forman la frontera oriental.

En el caso de la parte occidental y meridional no existe ningún accidente geográfico reseñable con el que se tenga ningún límite en la región, por lo que este límite se pone en aguas abiertas y teniendo la longitud de 9º Oeste como límite al oeste y la latitud de 35º Norte como límite inferior de esta subcuenca.

Geológicamente, se encuentra sobre el límite de las placas Euroasiática y africana, a través de la zona de fractura de Azores-Gibraltar, caracterizado por un régimen de convergencia oblicua. Esta limitado por el macizo Ibérico y la cuenca del Algarve por el norte y, en la parte oriental por el arco orogénico de la cordillera bético-rifeña. En sus fondos oceánicos destacan multitud de relieves submarinos correspondientes en su gran mayoría a volcanes extintos. La mayor parte del golfo de Cádiz se sitúa sobre la corteza continental ibérica o africana que se

adelgaza hacia el oeste. El cabo de Santa María, situado en Faro (Portugal) divide en dos regiones las plataformas continentales, siendo más amplia y con menor pendiente en la parte oriental de este cabo (parte española) con anchuras comprendidas entre los 30 -50 kilómetros. Al oeste del cabo la plataforma se estrecha teniendo la plataforma una anchura de entre 15-20 kilómetros y apareciendo cañones submarinos como el de Portimao.

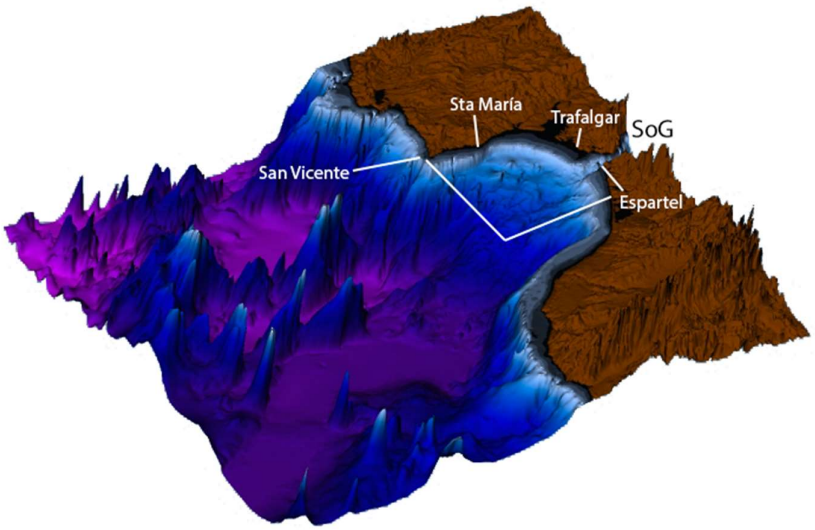

Figura 1.1. Entorno geográfico del Golfo de Cádiz. En la imagen aparecen los principales cabos del Golfo de Cádiz. Las líneas blancas marcan el límite del Golfo de Cádiz

1.3 Marco oceanográfico

El Golfo de Cádiz es una región muy interesante desde el punto de vista oceanográfico ya que es una zona donde confluyen muchas masas de agua de distintas regiones.

Los estudios de circulación de masas de agua en el Golfo de Cádiz se han iniciado en fechas relativamente recientes. Uno de los primeros trabajos es el de (Stevenson, 1977) y en él se determinan algunos rasgos de la circulación superficial en el Golfo de Cádiz, como el frente de Huelva. Sin embargo, la gran mayoría de los trabajos posteriores se han centrado en la circulación intermedia del agua mediterránea vertida a través del Estrecho de Gibraltar y en los meddies (Mediterranean Eddies) formados en el golfo de Cádiz (Ambar and Howe, 1979; Bower et al., 1995; Hernández-Molina et al., 2006, Sanchez-Leal et al 2017). La razón del

estudio de la salida del agua Mediterránea es la importancia que tiene a nivel global la interacción de esta masa de agua salina y caliente en la circulación termohalina a gran escala del océano Atlántico. El estrecho de Gibraltar es un punto muy importante en el golfo de Cádiz, ya que es la zona que conecta el Mediterráneo con el océano Atlántico. El sistema de circulación en el estrecho de Gibraltar es un sistema bicapa (Farmer et al., 1988; Price et al., 1993) donde en el parte superficial se encuentra el agua menos densa atlántica que entra hacia el Mediterráneo y en la parte inferior, se encuentra el agua Mediterránea, más densa, que sale hacia el Atlántico, realizando un viaje por el Golfo de Cádiz para mezclarse con las aguas Atlánticas(Sánchez-Leal et al., 2017).

La formación del agua Mediterránea que sale por el estrecho de Gibraltar, son aguas intermedias y profundas cuyo origen se ubica en el Mediterráneo occidental, con salinidades superiores a 38 y relativamente cálidas (12ºC).

La salida de agua Mediterránea produce sobre 1 Sv (10^6 m^3s^{-1}) según (Naranjo et al., 2015).Esta agua Mediterránea, una vez que pasa el umbral de Espartel, en la parte occidental del estrecho de Gibraltar, circula a lo largo del Golfo de Cádiz como una corriente gravitacional por debajo del agua más ligera Atlántica(Figura 1.2). Una vez pasada la longitud de 6.5 Oeste, el agua Mediterránea se dirige hacia el Norte debido a la topografía del fondo y a la fuerza de Coriolis y a la formación de Meddies (Iorga and Lozier, 1999).

Existen varias ramificaciones del agua Mediterránea en todo el golfo de Cádiz, delimitadas por la profundidad. Según diversos autores(Ambar, 1983; Ambar and Howe, 1979; Hinrichsen and Tomczak, 1993; Madelain, 1970, Zenk 1975a) existen 3 ramificaciones entre los 500 y 1200 metros, aunque recientemente (Sánchez-Leal et al., 2017) ha definido mejor estas arterias descomponiéndolas en 5.

En relación a la circulación en las capas superiores los primeros trabajos existentes se han centrado en la dinámica de afloramientos al sur de la costa portuguesa (Fiuza et al., 1982), fenómenos que han vuelto a ser abordados más recientemente en los trabajos de (Folkard et al., 1997; Relvas and Barton, 2002; Sánchez et al., 2006). La circulación tradicional de estas aguas en el Golfo de Cádiz lleva un sentido horario a lo largo de toda la plataforma desde la costa portuguesa hasta el estrecho de Gibraltar.

Posteriormente, (Criado-Aldeanueva et al., 2006; García-Lafuente et al., 2006), han estudiado el patrón de circulación superficial del Golfo de Cádiz. Sus esfuerzos se han centrado en la parte norte del Golfo de Cádiz y en la identificación de las masas de agua existentes en la región. En esta circulación aparece un nuevo factor que afecta al patrón de circulación, el viento (Fiuza et al., 1982). La corriente superficial responde a los cambios de viento, observándose como los vientos del Oeste (ponientes) generan afloramientos en la costa portuguesa. Por el contrario, vientos del Este (levantes), bloquean estos afloramientos y generan una conexión entre las dos contracorrientes costeras.

El agua Atlántica presente en el Golfo de Cádiz tiene 2 tipos de masas de agua. La primera es el Agua Central Noratlántica Oriental (*Eastern North Atlantic Central Water*, ENACW), con unas características bien definidas tanto en la de salinidad (35,7-36,25) como de temperatura (12ºC-16ºC) (Gascard and Richez, 1985). Esta masa de agua tiene una mayor salinidad que el Agua Central Noratlántica Occidental debido a la interacción con el agua Mediterránea (Mauritzen et al., 2001).

La ENACW se forma primero por una fuerte evaporación y luego por un enfriamiento invernal posterior a lo largo del Frente de las Azores (Pollard and Pu, 1985; Ríos et al., 1992). Desde aquí circula hacia el sur penetrando en el Golfo de Cádiz (Figura 1.2).

En la parte más superficial, y debido al intercambio de flujos con la atmosfera, aparece una modificación de la ENACW con temperaturas superiores a los 16ºC, menor salinidad, debido a las entradas de agua dulce en la región, denominada Agua Superficial Atlántica (*Surface Atlantic Water*, SAW). La SAW tiene un rango de profundidad entre la superficie y los 100 metros, mientras que la ENACW tiene un rango de profundidad entre los 250 hasta los 700 metros.

Las interacciones entre las masas de agua son zonas muy interesantes, siendo la más activa, la interacción entre el agua Mediterránea y la Atlántica (*Atlantic Mediterranean Interface*, AMI). Esta interacción muestra unos gradientes muy altos de salinidad y temperatura, así como variación en la profundidad. La AMI puede encontrarse tanto en la columna del agua como cerca del fondo. Si la interfaz se encuentra cerca del fondo, ésta puede generar rasgos deposicionales y erosivos sobre el fondo. El agua Mediterránea fuera de los principales canales ha sido observada entre los 250-300 metros en la parte oriental de la plataforma del Golfo de Cádiz (M.J. Bellanco and R.F. Sánchez-Leal, 2016; Sánchez-Leal et al., 2017), siendo el límite superior de esta masa de agua la salinidad de 36.3 correspondiente con el límite de la plataforma continental. Cerca del cabo de Trafalgar, el agua Mediterránea ha sido observada a 200 metros de profundidad (Criado-Aldeanueva et al., 2006; Vargas-Yañez et al., 2002).

En la parte inferior de la masa de agua Mediterránea, se encuentra en el Golfo de Cádiz el agua Nortlántica profunda (*North Atlantic Deep Water*, NADW) (Figura 1.2). Esta masa de agua tiene como formación la mezcla de aguas Árticas en la corriente noruega con las aguas Mediterráneas en estas latitudes. Suele ser una masa de agua fría (3-8 ºC) y una salinidad de 34.95-35.2, y a unas profundidades cercanas a los 1500 metros(Meincke et al., 1975; Price et al., 1993; Serra et al., 2005; Thorpe, 1976).

Tradicionalmente, estas son las masas de agua que han sido estudiadas en el Golfo de Cádiz, aunque también han sido descritas por diversos autores la presencia de otras aguas intermedias que interaccionan con estas masas de agua conocidas.

Por un lado, tenemos el agua intermedia Subártica (*SubArctic Intermediate Water*, SAIW). Esta agua está formada por el enfriamiento invernal de las aguas superficiales en tres regiones

principales: noroeste del Atlántico Norte, al norte del frente subártico, la zona profunda de Porcupine y el norte del Golfo de Vizcaya (Van Aken, 2001). Una parte significativa de la variedad de agua formada en las dos últimas regiones progresa por debajo de la corriente del Atlántico Norte y fluye hacia el margen del Atlántico Este, penetrando en el Golfo de Cádiz, moviéndose en un rango de profundidad de 400-800 metros (Cabeçadas et al., 2002; Carracedo et al., 2016).

Finalmente aparece otra agua intermedia en el Golfo de Cádiz, que proviene de la otra región polar, y se llama Agua Antártica intermedia (*Antarctic Intermediate Water*, AAIW). A escala global, el AAIW es una de las aguas intermedias más relevantes, ya que es un componente importante de la superior de la circulación meridional *(Meridional Overtuning Circulation*, MOC) en el giro subtropical del Hemisferio Sur (Pahnke et al., 2008b; Talley, 2003). Se caracteriza por una salinidad mínima y una alta concentración de nutrientes entre los 500 a 1500 metros de profundidad con un núcleo central a 900 metros.(Cabeçadas et al., 2002; Hernández-molina et al., 2014; Louarn and Morin, 2011) han definido el AAIW en el Golfo de Cádiz, existiendo una interacción entre la AAIW y el agua Mediterránea.

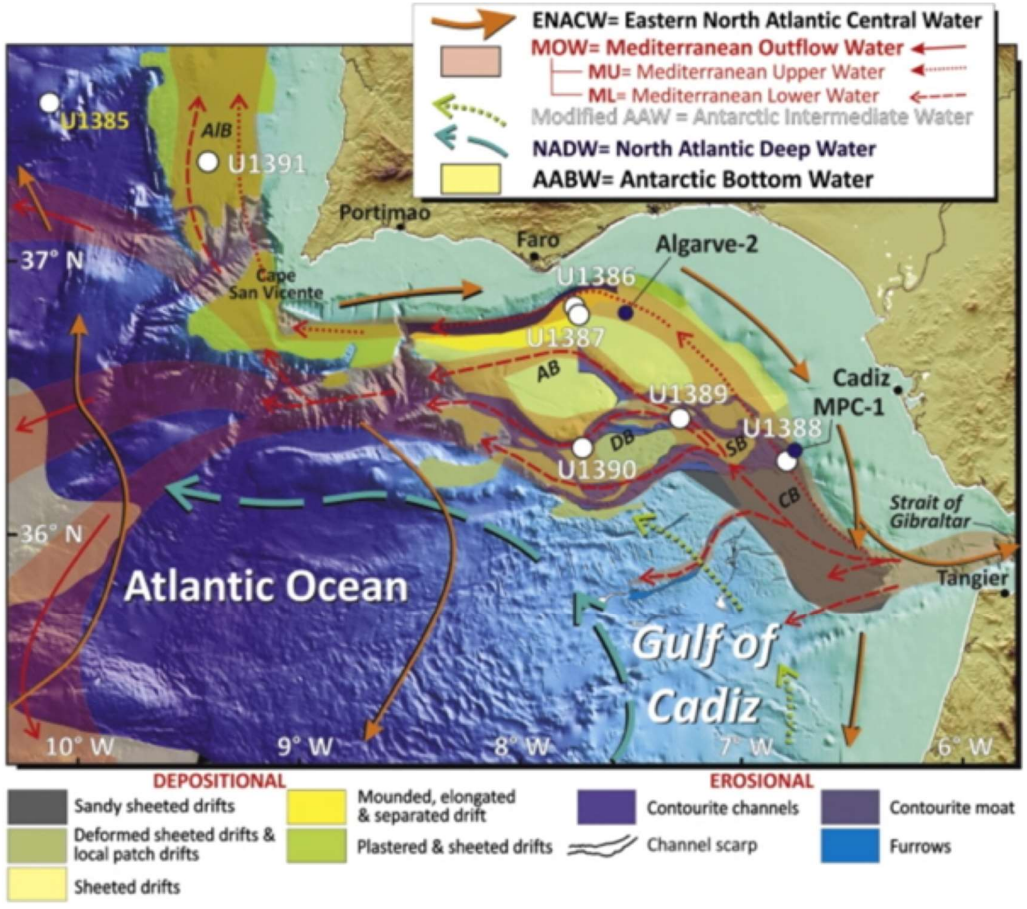

Figura 1.2. Esquema de las masas de agua existentes en el Golfo de Cádiz, así como las características geomorfológicas del talud medio del Golfo de Cádiz. Imagen obtenida de Hernández-Molina et al 2016.

1.4 Importancia de los procesos oceanográficos en el fondo marino

Las corrientes geostróficas asociadas a las masas de agua que circulan paralelas a los márgenes continentales, así como procesos oceanográficos asociados tales, como, eddies, procesos de desbordamiento desde la plataforma, mareas (barotrópicas y baroclinas) y, ondas internas son procesos que controlan la morfología de los fondos marinos, así como los tipos de sedimentos y su biota asociada (Hernández-Molina et al., 2016; Lozano et al., 2020; Rebesco et al., 2014) (Figura 1.3).

El conocimiento sobre dichos procesos oceanográficos y las escalas temporales y espaciales en las que afectan en los medios marinos profundos es escaso, principalmente por la escasez de las observaciones directas y los estudios de modelización de los mismos (Hernández-Molina et al., 2016; Hunter et al., 2007).

Las corrientes pueden ser barotrópicas o baroclinas. Los flujos barotrópicos son corrientes con superficies de presión constante paralelas a superficies de densidad constante. En general, estos flujos son impulsados por gradientes de presión causados por la pendiente de la superficie del mar. Estos flujos barotrópicos incluyen mareas, corrientes potenciados por el viento y olas superficiales. Por el contrario, los flujos baroclínicos son corrientes con superficies de presión constante que no son paralelas a superficies de densidad constante. Estos flujos suelen estar impulsados por gradientes de presión causados por la densidad horizontal. Ejemplos de flujos baroclinos incluyen las ondas y mareas internas que se propagan sobre las picnoclinas en aguas estratificadas. Su velocidad típica se correlaciona con la fuerza de su gradiente de densidad. Las corrientes baroclinas se encuentran interactuando a lo largo del fondo oceánico, de los taludes y en los cañones submarinos (Shanmugam, 2013).

Las ondas internas pueden determinar el ángulo de la pendiente promedio de los márgenes continentales (entre 2º y 4º), que es un orden de magnitud menor que el ángulo de fricción interna del sedimento marino (Cacchione et al., 2002b). A su vez, pueden generar campos de dunas sedimentarias (Droghei et al., 2016).

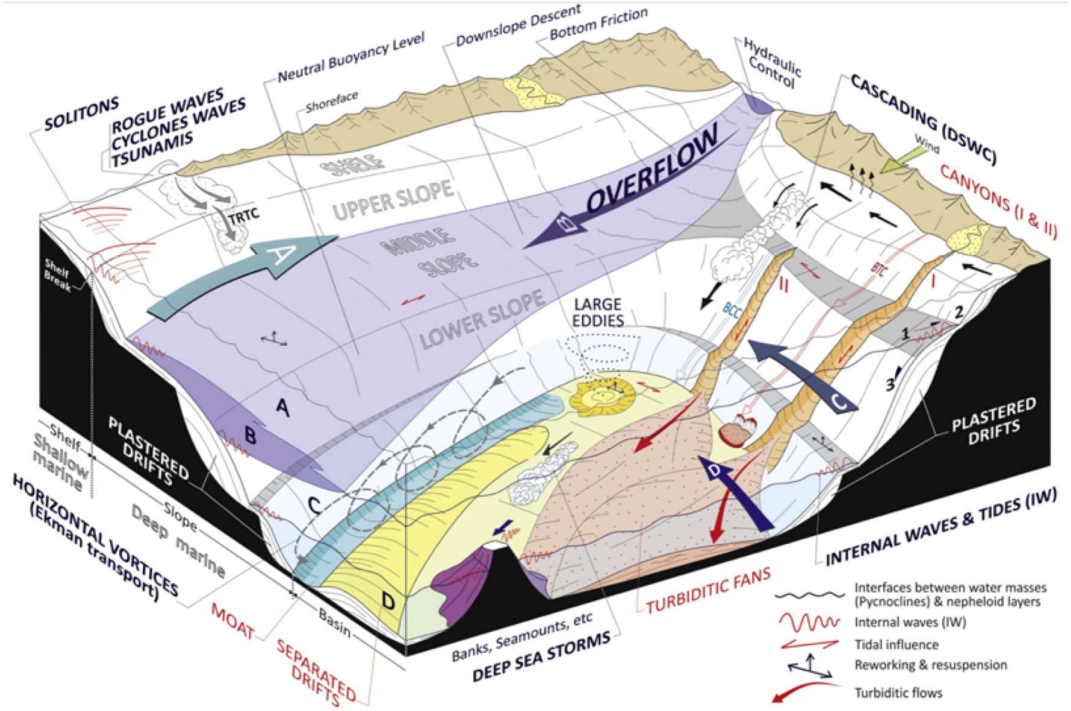

Figura 1.3. Figura que representa los posibles procesos oceanográficos en ambiente de aguas profundos. Además de las corrientes de densidad y desbordes, la velocidad en el fondo marino también puede verse afectada por corrientes barotrópicas o procesos intermitentes como cascadas, remolinos gigantes, tormentas de aguas profundas, vórtices, ondas internas, mareas internas, tsunamis y olas ciclónicas. Imagen obtenida de Rebesco et al 2014.

1.5 Estructura de la Tesis

A partir de los objetivos y planteamientos propuestos, la presente Tesis Doctoral está organizada con la siguiente estructura:

En el **Capítulo 2**, se describen detalladamente todos los valores experimentales, tanto los obtenidos mediante campañas oceanográficas como los obtenidos mediante el uso de varias bases de datos, utilizados a lo largo de este estudio. Además, se detallan los distintos modelos numéricos que han sido utilizados para la realización de este trabajo.

En el **Capítulo 3**, se explica la variabilidad estacional de las distintas masas de agua intermedias existentes en el Golfo de Cádiz, y el papel que realizan las interacciones entre ellas. El contenido de este capítulo está publicado en la revista Ocean Science (https://doi.org/10.5194/os-15-1381-2019).

El **Capítulo 4** se demuestra como los efectos dinámicos producidos por la marea en el talud continental oriental del Golfo de Cádiz juega un rol fundamental en la relación entre las

distintas masas de agua existentes en esta zona y qué efectos conllevan en la morfología del fondo.

En el **Capítulo 5**, se presentan los resultados del papel del forzamiento atmosférico en la modulación de las masas de agua que caracterizan la columna en el talud continental de la parte oriental del Golfo de Cádiz.

En el **Capítulo 6**, se detallan las conclusiones más importantes que se derivan de este trabajo.

En el **Capítulo 7**, se plantean posibles líneas de investigación que pueden salir a partir de este trabajo.

Finalmente, en el **Capítulo 8** se incluyen las referencias bibliográficas citados a lo largo de esta Tesis Doctoral.

Capítulo 2

DATOS Y METODOLOGÍA

2.1 Introducción

En este capítulo se va a proceder a comentar los distintos conjuntos de datos que han sido necesarios para conseguir los objetivos planteados. A su vez, se comentarán las técnicas de análisis realizadas a los datos para obtener la información necesaria en el estudio de cada fenómeno.

2.2 Bases de datos oceanográficas

Actualmente, existen diversas bases de datos oceanográficas (tabla 2.1) con las que se puede obtener múltiple información. El uso de estas bases de datos es fundamental para poder observar tendencias estacionales a lo largo del tiempo. La estacionalidad de las masas de agua en el Golfo de Cádiz ha sido estudiada con estas bases de datos obteniendo muchos perfiles que han sido recogido por distintas plataformas oceanográficas (CTDs, Boyas Argo, XCTD, ...). La distribución temporal de los perfiles obtenidos va desde 1900 hasta 2013, aunque el grueso de los datos ha sido adquirido después de 1950.

Data base	Temporal range	Link
WOD	1900-2013	https://www.nodc.noaa.gov/OC5/WOD13/data13geo.html
WOCE	1990-1999	http://www.ewoce.org/data/index.html
Medatlas	1900-2010	https://odv.awi.de/data/ocean/medatlasii/
Coriolis	1990-2012	https://odv.awi.de/data/ocean/coriolis-cora-3-dataset/
Seadatanet	1930-2010	https://www.seadatanet.org/
WOA	1955-2009	https://www.nodc.noaa.gov/OC5/SELECT/woaselect/woaselect.html

Tabla 2.1.- Detalles de las diferentes bases de datos utilizadas en el análisis

Se han utilizado todas las bases de datos para obtener el máximo de perfiles oceanográficos y poder cubrir de manera más completa el Golfo de Cádiz, para poder discernir como fluctúan las masas de aguas intermedias.

Los parámetros seleccionados para este estudio obtenidos de estas bases de datos, han sido la profundidad, temperatura, salinidad, densidad y concentración de oxígeno.

Además de estos datos históricos obtenidos en las bases de datos, también han sido utilizados datos de World Ocean Atlas 2013 (WOA, https://www.nodc.noaa.gov/OC5/woa13/), que son un conjunto de datos climatológicos que han sido analizados objetivamente en cuadrículas de 0.125x0.125º obteniéndose las misma variables existentes en las bases de datos.

2.3 Datos oceanográficos *in situ*

Para poder responder a las hipótesis planteadas en esta Tesis, ha sido necesario obtener datos *in situ* en el Golfo de Cádiz.

En primer lugar, se va a hablar de las campañas oceanográficas de las cuales se han obtenidos datos para obtener la información necesaria.

Diversas campañas oceanográficas de la Universidad de Cádiz (Golfo 2001, Medout 2011, Estrecho 2008) han sido utilizadas para completar las bases de datos que se han comentado en el apartado anterior. Concretamente los datos utilizados han sido los que se han obtenido con un Seabird Scientific SBE 911plus CTD, siendo un total de 200 perfiles los que han sido añadido a la base de datos.

Por otro lado, han sido utilizados datos de campañas oceanográficas del Instituto Español de Oceanografía (IEO), en la zona de la plataforma oriental de Cádiz con el fin de poder observar las masas de agua existentes. Los datos obtenidos han sido los parámetros físico-químicos de la columna de agua, por medio de un Seabird Scientific SBE 911plus CTD, así como los datos de velocidad de corrientes obtenidos con un Lowered Acoustic Doppler Current Profiler (LADCP)fijado en la roseta oceanográfica. Las campañas donde se han realizado estos perfiles han sido ARSA, Ecoreclutas y STOCAS-Ingres, todas realizadas en octubre del 2014. Estos datos han sido cedidos por parte del investigador responsable del Instituto Español de Oceanografía Ricardo Sánchez Leal.

Los datos batimétricos y sísmicos utilizados provienen de los proyectos IEO Indemares y Contouriber (Proyecto de Ciencia y Tecnologías Marinas CTM 2008-06399-C04/MAR, CTM 2012-39599-C03, INPULSE (CTM2016 75129 C3 1 R MINECO) y LIFE+ INDEMARES/CHICA (LIFE 07/NAT/E/000732)), de los cuales se obtienen los detalles de la morfología del fondo fundamentales para entender la sinergia existente entre la morfología del fondo y los efectos oceanográficos.

En segundo lugar, han sido colocados dos fondeos oceanográficos en el talud continental oriental del Golfo de Cádiz con el fin de entender los procesos físicos en la zona. Ambos

fondeos se realizaron con el buque oceanográfico Malaspina perteneciente al Instituto Hidrográfico de la Armada Española. Este fondeo fue financiado en parte por el proyecto MOWER.

El fondeo más profundo ha sido colocado a una profundidad de 235 metros, en la parte distal de una terraza ubicada en el talud superior. Este fondeo estaba compuesto por un correntímetro doppler (Acoustic Doppler Current Profiler, ADCP) Workhorse 75 Khz de la compañía RDI fondeado a 10 metros del fondo y con una configuración de tamaño de celda de 4 metros y una distancia de blanqueo de 2.8 metros. El intervalo de muestreo ha sido cada 2 minutos. En la parte inferior de este ADCP, se instaló un correntímetro monopunto Aanderaa Current Meter (RCM7), a 5 metros del fondo para poder observar los valores de corrientes en la parte más profunda, con el mismo intervalo de muestreo que el realizado por el otro correntímetro. Este fondeo fue liberado por razones desconocidas antes de tiempo, pudiéndose obtener un total de 18 días de datos.

En la parte más somera de la terraza del talud superior se instaló otro fondeo, en este caso una cadena de termistores de la marca NKE modelo S2T600. La profundidad de este fondeo ha sido de 185 metros. Un total de 50 termistores han sido utilizados cada 2 metros cubriendo la columna de agua entre los 170 metros y los 70 metros. Los termistores han sido colocados cada 2 metros y el intervalo de muestreo ha sido cada minuto, para poder obtener la máxima resolución temporal. En la parte superior del fondeo se instaló un sensor de presión Aquatec Aqualogger 520 PT para poder observar si existió alguna fluctuación en la cadena de termistores en la vertical obteniéndose resultados negativos (la cadena siempre quedó en la vertical y nunca fluctuó en la vertical).

Respecto a los datos del nivel del mar *in situ*, han sido obtenidos de Puertos del Estado, dentro del sistema de Mareógrafos de Puertos del Estado (REDMAR), los cuales son accesibles vía OpenDAP (http://opendap.puertos.es/thredds/catalog.html). Tienen una resolución temporal horaria.

2.4 Datos atmosféricos

Los valores atmosféricos que han sido utilizados para este trabajo provienen de varias series de datos. Concretamente los datos de viento provienen de los datos reanalizados ERA-Interim (Dee et al 2011), que pueden ser descargados en la siguiente dirección (https://www.ecmwf.int/en/forecasts/datasets/browse-reanalysis-datasets), cuya resolución espacial es de 0.125x0.125º. Para el caso del análisis de las masas de agua intermedias el periodo temporal de estudio ha sido desde 1979-2018.

De este mismo modelo, se han obtenido datos de presión atmosférica respecto al nivel medio del mar (Mean Sea Level Pressure, MSLP) en la zona del mar de Liguria. En este caso los datos obtenidos tienen una resolución espacial de 0.25x0.25º y una resolución temporal horaria.

Para los regímenes de viento en la plataforma continental, se ha tomado el modelo como mayor resolución disponible en la zona. En este caso es el modelo MM5 (Modelo de mesoescala de quinta generación, Penn State/NCAR) (Georg a et al., 1994)). Este modelo se ha implementado para la región de Andalucía y centrado en el estrecho de Gibraltar con una resolución máxima de 3.3 km (Reyes 2015). En este caso se han trabajado con los datos de viento a 10 metros de altura del nivel del mar para ambas componentes, con resolución temporal horaria.

2.5 Medidas de corrientes superficiales a partir del sistema de radares costeros de alta frecuencia

El sistema de Radar de alta frecuencia está operado por Puertos del Estado. Para el año de estudio, tenía colocadas 3 antenas CODAR Seasonde en el estrecho de Gibraltar (Tarifa, Punta Carnero y Ceuta), que posteriormente fueron ampliadas con una cuarta antena colocada en la punta de Camarinal (Figura 1.1). Gracias a este sistema se obtienen mapas horarios de corrientes superficiales de la zona oriental del estrecho de Gibraltar, los cuales son accesibles vía OpenDAP (http://opendap.puertos.es/thredds/catalog.html). Los datos obtenidos con este sistema de observación ya han sido contrastados por diversos autores como (Chioua et al., 2017), entre otros.

La corriente superficial en el estrecho de Gibraltar, se ha analizado a partir de un transecto transversal extraído de los datos del sistema de radares de alta frecuencia (5.4492º W, 35.9503-36.0315ºN). Dicha serie temporal cuenta con el mismo periodo que la duración del fondeo de los termistores con el fin de poder ver la interacción entre la zona de estudio y el estrecho de Gibraltar. Además, con el fin de determinar si estas relaciones ocurren de manera recurrente, se ha extraído para el mismo transecto transversal, la serie temporal para todo el 2019.

2.6 Modelos numéricos

Para poder complementar el análisis de los mecanismos hidrodinámicos más relevantes se ha utilizado el modelo hidrodinámico barotrópico UCA2D (Alvarez et al., 1999). Este modelo hidrodinámico es un modelo bidimensional, en diferencias finitas de muy alta resolución que resuelve numéricamente las ecuaciones de conservación de masa y momento integradas

verticalmente, mediante un esquema semiimplícito de Crank-Nicolson en una cuadrícula escalonada Arakawa-C. Los arrastres del fondo y del viento están parametrizados por la llamada "ley del muro". En los límites abiertos, el sistema se fuerza con los parámetros armónicos de elevación y corrientes para las constituyentes de marea deseadas. En este caso, el dominio de la cuadricula es de 1 x 1 Km cubre el Golfo de Cádiz y el Estrecho de Gibraltar. La batimetría utilizada ha sido obtenida de ETOPO-1 (www.ngdc.noaa.gov) y de cartas náuticas editadas por el Instituto Hidrográfico de la Armada Española (IHM). El modelo fue forzado en los límites abiertos este y oeste por el flujo barotrópico medio (Z0) y el principal componente de marea semidiurna M2, inferido de los datos de reanálisis IBI_REANALYSIS_PHYS_005_002 (www.copernicus.eu) y los resultados del modelo de González et al 2013, ejecutándose durante 10 ciclos de mareas con un intervalo de tiempo de 5 segundos. Los datos de los últimos 5 ciclos se utilizaron para el análisis armónico, una vez asegurada la estabilidad numérica y la conservación de energía. La validación de los resultados del modelo en este dominio proporciona errores rms de 4.6 cm y 3.6º para la amplitudes y constantes de fase, respectivamente de la elevación de marea y 7.3 cm/s y 4.9º para corrientes (Gomiz, 2017). El uso de este modelo está destinado para simular la corriente barotrópica de marea y calcular el forzamiento barotrópico de las mareas internas.

Finalmente, se han utilizado datos de nivel medio del mar del modelo SAMPA. Es un modelo de circulación regional cerca del estrecho de Gibraltar que proviene del modelo de circulación global del Instituto de tecnología de Massachusetts (Marshall et al., 1997) . El dominio espacial cubre el golfo de Cádiz- estrecho de Gibraltar y mar de Alborán. Su resolución horizontal en las fronteras abiertas es de 8-10 km con mayor resolución en el Estrecho (300-500 m). Los forzamientos en las fronteras mareales y meteorológicos vienen del modelo descrito en (Carrère and Lyard, 2003) y del modelo HAMSOM (Álvarez Fanjul et al., 2001). En la superficie, el modelo es forzado cada 3 horas con valores de viento obtenidos por la agencia española de meteorología (AEMET) a través del modelo HiRLAM (Cats, 1996).

Capítulo 3

SEASONAL VARIABILITY OF THE INTERMEDIATE WATER MASSES IN THE GULF OF CÁDIZ: IMPLICATIONS OF THE ANTARCTIC AND SUBARCTIC SEESAW

Roque D., Parras-Berrocal I., Bruno M., Sánchez-Leal R. F., Hernández-Molina F.J. Seasonal variability of intermediate water masses in the Gulf of Cadiz: implications of the Antarctic and Subarctic seesaw. Ocean Science, 15,1381-1397,2019. https://doi.org/10.5194/os-15-1381-2019

Abstract. Global circulation of intermediate water masses has been extensively studied; however, its regional and local circulation along continental margins and variability and implications on sea floor morphologies are still not well known. In this study the intermediate water mass variability in the Gulf of Cádiz (GoC) and adjacent areas has been analysed and its implications discussed. Remarkable seasonal variations of the Antarctic Intermediate Water (AAIW) and the Subarctic Intermediate Water (SAIW) are determined. During autumn a greater presence of the AAIW seems to be related to a reduction in the presence of SAIW and Eastern North Atlantic Central Water (ENACW). This interaction also affects the Mediterranean Water (MW), which is pushed by the AAIW toward the upper continental slope. In the rest of the seasons, the SAIW is the predominant water mass reducing the presence of the AAIW. This seasonal variability for the predominance of these intermediate water masses is explained in terms of the concatenation of several wind-driven processes acting during the different seasons. Our finding is important for a better understanding of regional intermediate water mass variability with implications in the Atlantic Meridional Overturning Circulation (AMOC) but further research is needed in order to decode their changes during the geological past and their role, especially related to the AAIW, in controlling both the morphology and the sedimentation along the continental slopes.

Key words: Intermediate Water Mass circulation; Seasonal variability; Antarctic Intermediate Water; Subarctic Intermediate Water; Mediterranean Water; Gulf of Cádiz; Atlantic meridional overturning circulation.

3.1 Introduction

The intermediate water masses, their circulation and associated oceanographic processes are essential to understanding global Thermohaline Circulation (THC). Concretely, these water masses take part of the Meridional Overturning Circulation (MOC) carrying a significant part of the meridional heat, freshwater and nutrient transports in the global ocean. Also, it is an important oceanic sink for anthropogenic CO_2 (Sabine et al., 2004). In figure 3.1 shown is a general sketch of the main circulation patterns that these intermediate water masses describe in the Atlantic Ocean.

Although their circulation at global scale has been extensively studied (Rahmstorf, 2006), the spreading, interactions and the regional implications of these intermediate waters along continental margins are still not well known. At a global scale, the Antarctic Intermediate Water (AAIW) is one of the most relevant intermediate waters, since it is an important component of the upper branch of the MOC in the Southern Hemisphere subtropical gyre (Pahnke et al., 2008a; Talley, 2003). It is characterised by a salinity minimum and high nutrient concentration between 500-800 m to ca. 1500 m depth (Tsuchiya et al. 1992), with its main core located at 900 m (Fig. 3.2). The AAIW spreads along the eastern boundaries of all major oceans, although its original characteristics are best observed in the Southern Hemisphere (Stramma and England 1999).

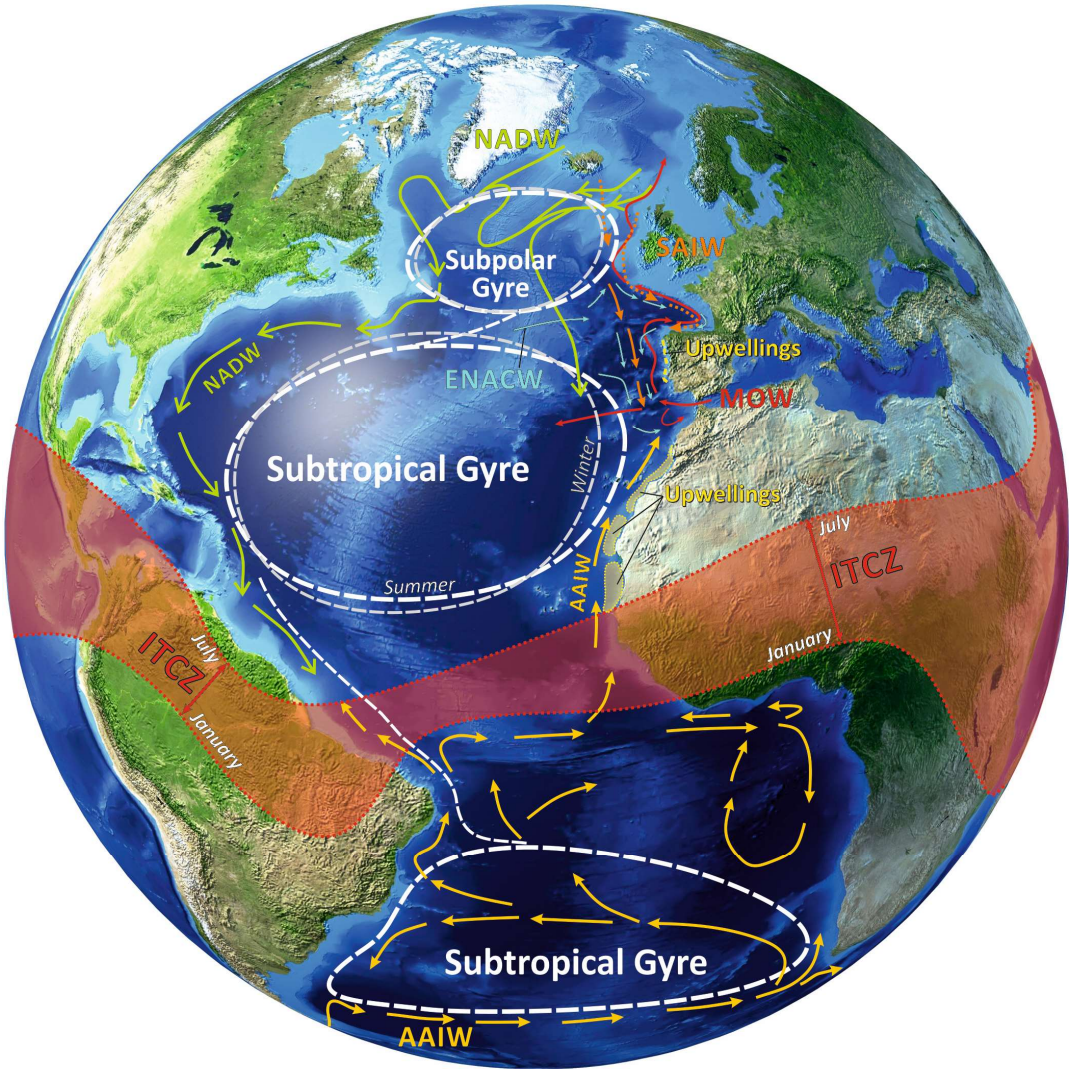

Figure 3.1. Sketch of the intermediate waters circulation in the Atlantic Ocean. The position of the main gyres, the Intertropical Confluence Zone (ITCZ) and circulation of the AAIW, SAIW, ENACW and MW w<are indicated. (Compilation based on; Krauss et al., 1987; Stramma and Siedler, 1988; Faugères et al., 1993; Iorga and Lozier 1999; Pickart et al., 1999; Stramma and England, 1999; Coulbourne and Foote, 2000; Lavander et al., 2000; Rhein, 2000; Fratantoni, 2001; Raymo et al., 2004; Mackie, 2005; Peliz et al., 2005, 2009; Rahmstorf, 2006; Stein, 2007; Gil et al., 2008; Yashayaev, and Clarke, 2008; Hernández-Molina et al., 2011 and references therein; Cheng et al., 2012; Pérez et al., 2013*).*

Several authors have reported a significant time variability of the AAIW presence in the North Atlantic between glacial and inter-glacial periods (Oppo 2000; Curry and Oppo 2005; Jung et al. 2010; Makou, Oppo, and Curry 2010; Muratli et al. 2010; Wainer et al. 2012). The AAIW is well identified year-round in the eastern boundary of the North Atlantic. It spreads along the African coastline up to approximately 28.5 °N but during autumn it can extend up to 32 °N (Tsuchiya et al. 1992; Machín and Pelegrí 2009) and even into the Gulf of Cádiz (GoC) (Cabeçadas, Brogueira, and Gonçalves 2002; Louarn and Morin 2011; Hernández-Molina et al. 2014), where it interacts with the MW, perhaps restricting the spreading of the

latter, especially between summer and winter (Cabeçadas et al., 2002; Knoll et al., 2002; Louarn & Morin, 2011).

Traditionally, only two intermediate water masses are considered in the GoC (van Aken, 2000; Ambar and Howe, 1979a; Baringer and Price, 1997): The Eastern North Atlantic Central Water (ENACW) and the Mediterranean Outflow Water (MW) (Fig. 3.2). The ENACW is formed by strong evaporation first and further winter cooling later along the Azores Front (Pollard and Pu, 1985; Ríos et al., 1992). From here, it circulates southward penetrating into the GoC in the 250 - 700 m depth range. Here, the ENACW interacts actively with the MW close to the western side of the Strait of Gibraltar (Louarn and Morin, 2011) and with the upper MW core (Ambar and Howe, 1979a) further west, throughout the GoC continental slope (Louarn and Morin 2011; Bellanco and Sánchez-Leal 2016).

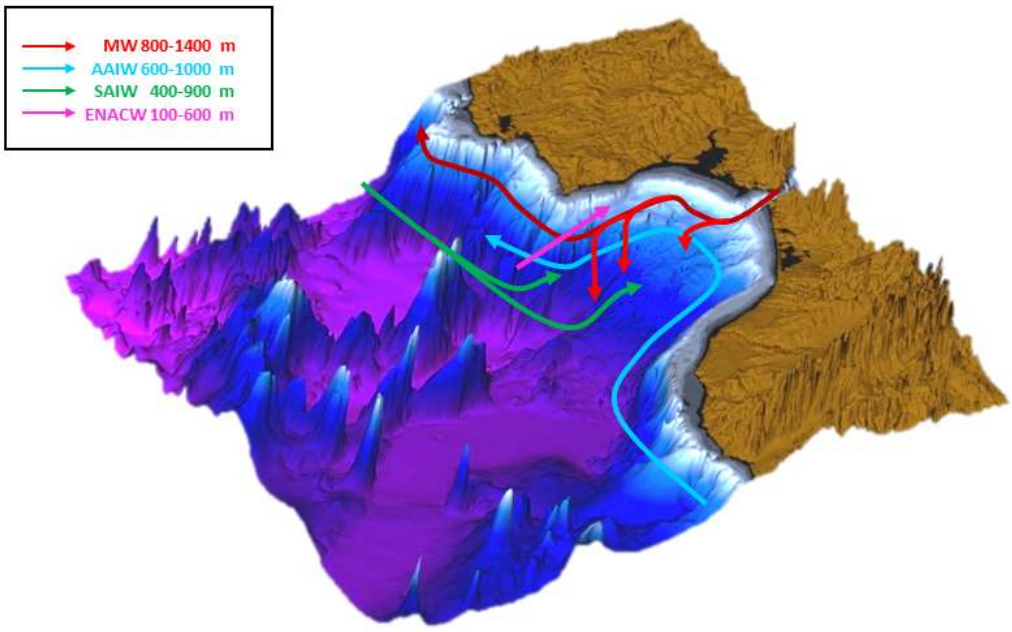

Figure 3.2. Illustration of intermediate water mass circulation in the GoC. The red line indicates the MW along the Spanish and Portuguese coast. The blue line is for the AAIW coming from the African coast from the south. The green line is for the modified SAIW coming from the northwest of the Iberian Peninsula. The purple line is for the ENACW coming from the western part of the GoC.

Another important intermediate water mass in the GoC is the Subarctic Intermediate Water (SAIW). It is formed by winter cooling of surface water in three main regions: a) North Western North Atlantic, north of the subarctic front, b) the Porcupine Seabight, and c) northern Bay of Biscay (Van Aken, 2001). A significant part of the variety of water formed in the latter two regions progresses below the North Atlantic Current and flows towards the Eastern Atlantic margin, penetrating into the GoC from a south-southwestern direction and moving in the depth range of 400-800 m (Cabeçadas et al., 2002).

In several works, the SAIW and the ENACW have been referred to as the lower and upper ENACW (Louarn and Morin 2011; Carracedo et al. 2014) or as subpolar and subtropical origin ENACW (Voelker et al., 2015). Following (van Aken, 2000; Van Aken, 2001) , we use the former denominations. Currently, there is a lack of information about the seasonal variability of these intermediate water masses in the region.(M.J. Bellanco and R.F. Sánchez-Leal, 2016) analysed the interaction between the upper MW core and the ENACW on the upper GoC continental slope. The authors suggested an enhanced upper MW core and a less stratified ENACW in winter, resulting in an upslope expansion of the MW core and a more effective mixing with the overlaying ENACW. In contrast, they noted a weakened and deeper MW core and a thicker ENACW during late summer and early autumn.

The study by (Machín and Pelegrí, 2009) is relevant for consideration of the seasonal variations of the AAIW water within the GoC. Although focussed on the Canary Islands region, the authors reported a clear AAIW increase during autumn when compared with other seasons. The question whether this AAIW increase has implications on the other water masses circulating in the region is addressed in the present paper. Therefore, our main aims are: a) to determine the AAIW extension and variability vicinity the GoC; b) to identify its interplays with other intermediate water masses; c) to hypothesise about its implication on the continental margin morphology. We analyse a large conductivity, temperature, and depth (CTD) and oxygen concentration profile database extracted from various providers, complemented with the World Ocean Atlas (WOA13).

3.2 Data set and methodology

3.2.1 Data set

In order to identify water masses coming from remote locations we considered a study area spanning from 30°- 40° North and 15°-5.5° West (Fig. 3.3). The domain includes the GoC and the surrounding areas into the GoC (African coast, Portugal Coast and Strait of Gibraltar). We have gathered all available observations from WODB, WOCE, MEDATLAS, CORIOLIS, SEADATANET databases (Table 3.1), complemented with data from other individual cruises, carried out by the University of Cádiz (Golfo 2001, Medout 2011, Estrecho 2008). The temporal distribution of profiles span from 1900-2013, although the bulk of the data was acquired after 1950. The resulting product consists of a database including vertical profiles of temperature, salinity, density and dissolved oxygen concentration. The latter will be used to discern the AAIW from the SAIW and the ENACW (Carracedo et al., 2014; Hernández-Molina et al., 2014; Louarn and Morin, 2011; Machín and Pelegrí, 2009). We also included

the World Oceanographic Atlas monthly objectively analysed (1° grid) climatological fields (https://www.nodc.noaa.gov/OC5/woa13/).

To study the seasonal variability, we grouped observations into 3-month seasonal bins, starting in December (i.e., winter spans December through February, spring spans March through April, and so on). Since the analysis will be focused on intermediate water masses, we only used the observations taken within the 400-1000 m depth range. Figures 3.3 and 3.4 show the seasonal distribution of vertical profiles as well as the WOA data nodes. The figures reveal the homogeneous spatial distribution of profiles.

Data base	Temporal range	Link
WOD	1900-2013	https://www.nodc.noaa.gov/OC5/WOD13/data13geo.html
WOCE	1990-1999	http://www.ewoce.org/data/index.html
Medatlas	1900-2010	https://odv.awi.de/data/ocean/medatlasii/
Coriolis	1990-2012	https://odv.awi.de/data/ocean/coriolis-cora-3-dataset/
Seadatanet	1930-2010	https://www.seadatanet.org/
WOA	1955-2009	https://www.nodc.noaa.gov/OC5/SELECT/woaselect/woaselect.html

Table 3.1. Details of the different databases used in the analysis.

In addition, to examine the possible mechanisms behind the time variability of water masses we used monthly wind data taken from the ERA-Interim reanalysis (Dee et al., 2011) spanning 1979-2018, downloaded from https://www.ecmwf.int/en/forecasts/datasets/archive-datasets/browse-reanalysis-datasets. The spatial data resolution is 0.125 x 0.125 degrees. These monthly wind data will be analysed in combination with the monthly WOA data.

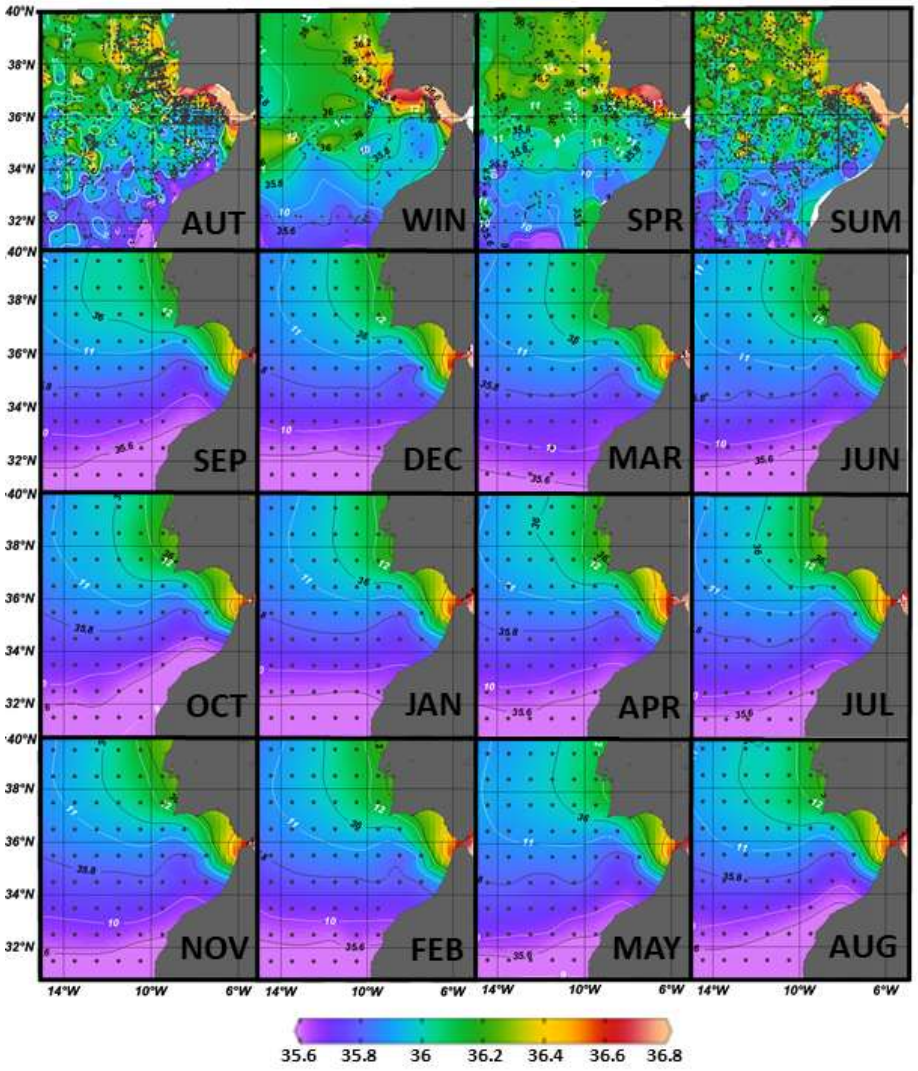

Figure 3.3. Observed salinity on the isopycnic surface σ= 27.5 for the different seasons (top row). The rows below show the same distributions for each climatological month as shown by WOA data. The white lines represent the temperature values at density σ= 27.5.

3.2.2 Optimum Multiparameter Analysis

In order to quantify the percentage in which each water mass was presented in the studied area we applied the Optimum Multiparameter Analysis (OMP) to each seasonal dataset. This technique assumes that the value of any sea water property, measured at each depth in the ocean, is the result of the mixing of a certain number of water masses present in the region (Tomczak and Large, 1989). It has become a standard tool in oceanography to resolve water mass mixing in regional scales studies (Álvarez et al., 2004; Johnson, 2008; Louarn and Morin, 2011; Pardo et al., 2012; Poole and Tomczak, 1999).

Mathematically, it implies solving an overdetermined system of linear equations which is composed of (n+1) equations, 'n' being the number of unknown variables, the fraction (percentage) of each water mass present in the mixing. As an example, for a problem with four water masses the following system of equations would apply:

$$x_1T_1+x_2T_2+x_3T_3+x_4T_4 = T_o \quad (1)$$

$$x_1S_1+x_2S_2+x_3S_3+x_4S_4 = S_o \quad (2)$$

$$x_1C_1+x_2C_2+x_3C_3+x_4C_4 = C_o \quad (3)$$

$$x_1+x_2+x_3+x_4 = 1 \quad (4)$$

where the x_{is} are the fraction (percentage) of each water mass present (subscript i take the values 1,2,3,4); T_o, S_o and C_o, the observed temperature, salinity and concentration of some conservative property (i.e. oxygen) at each point; T_{is}, S_{is} and C_{is} are the characteristic values of properties for each water mass type.

The analysis is restricted to the depth range of 400-1000 m and considers the following four water mass types: AAIW, SAIW, ENACW and MW and the resulting percentages are binned into 9 boxes 1º x 1º (see figure 3.6). The characteristic values of properties for these water masses in the GoC region have been taken from (Louarn and Morin, 2011) (Table 3.2). Note that the difference in S and T between the AAIW and SAIW is very small and can only be distinguished by their oxygen concentration. For this reason, we have chosen oxygen as the other conservative property in the OMP analysis.

WATER MASS TYPE	Temperature (º C)	Salinity	Oxygen (µmol/Kg)
AAIW	10.25	35.62	167
ENACW	16.374	36.289	225.93
SAIW	10.659	35.434	185.2
MW	13.9	36.64	180

Table 3.2. Values of physical-chemical variables taken for the different water masses.

3.2.3 Principal component analysis

The principal component analysis (PCA) is a statistical procedure that allows the transformation of a set of observations, which contain variables possibly correlated among them, into a set of values of uncorrelated variables called principal components (Pearson, 1901). When the problem under study contains a large number of observations the maximum number of principal components to be sought for is equal to the number of variables. This transformation is defined in such a way that the first principal component has the largest possible variance, and the successive components progressively reduce their variance.

This technique has been applied, using the MATLAB function PCA on the fractions of the four water mass types determined in the OMP analysis previously described, in order to identify common patterns of behaviour among them while they change with the seasons. Therefore, the variables of our PCA problem are these fractions of each water mass type (AAIW, ENACW, SAIW, MW) at each of the 9 boxes 1ºx1º shown in figure 3.6. Note that there are 36 variables (4 in each box) in the performed PCA. Subsequently, the values of these variables, through the different seasons, are arranged into four rows and the resulting file is subjected to the PCA. The resulting principal components (*PCs*) may be expressed as:

$$PC_k(t) = \sum_{i=1}^{nv} C_k^i \, [x_i(t) - \bar{x}_i] \qquad (5)$$

Where t stands for the time (season); indexes k and i do it for the given PC and variables respectively, being nv the number of analysed variables (36 in our case); $\bar{x}_i$ is the average value of the given variables through the different seasons . In this way, each PC is built as a linear combination of the observed variables xi weighted by a set of coefficients Ckj. At the same time, matrix algebra allows us to write the inverse problem:

$$x_i(t) = \bar{x}_i + \sum_{k=1}^{nc} C_k^i \, PC_k(t) \qquad (6)$$

Where *nc* is the number of considered *PCs*. Therefore, each of the observed values of the variables x_i may be expressed as a linear combination of the resolved *PCs* weighted by the coefficients C_k^i already introduced.

Now the absolute values that take these coefficients for a given *PC* along the different variables enable us to identify which of them are related to that *PC*. In order to visualise the temporal patterns contained in the resolved *PCs*, it is worthwhile to separate the products ($C_k^i.PC_k$) corresponding to each climatic season for each *PC*. Note that the values of these products represent deviations of the variables with respect to their time averaged values, as equation (6) indicates. Later, using these quantities, we will be able to map the seasonal variability contained in each *PC* and assess how intense is its manifestation in the different spatial locations of the studied area.

3.3 Results

3.3.1 Spatial distribution of physical- chemical properties

As a first step of the data analysis, several spatial representations of the different variables have been elaborated:

a. Representation of the spatial distribution of the variables on the isopycnic surface of 27.5 which best characterizes the position of the AAIW core in the region (Van Aken, 2001; Cabeçadas et al., 2002; Hernández-Molina et al., 2014; Louarn and Morin, 2011).

b. Representation of vertical sections of the variables along the meridional section at a latitude of 36º N which meets two important conditions: (i) To allow an adequate identification of the AAIW pathway by the GoC and (ii) To contain a high number of profiles covering as homogeneously as possible, during the different seasons, the given vertical sections.

3.3.1.1 Spatial distribution on the 27.5 isopycnic surface

Figures 3.3 and 3.4 show, respectively, the distributions of salinity and oxygen concentration on the 27.5 isopycnic surface, for the seasonal values contained in the observed data (upper row) and for the monthly values provided by the WOA database (following three rows).

Concerning the observed data, we found low oxygen concentration values (Fig. 3.4) coincident with low salinity values (Fig. 3.3), attributable to the AAIW presence (see Table 3.2), penetrating from lower latitudes into the GoC in all seasons, although it is remarkable that this penetration is more accentuated and closer to the African coast in autumn but also in summer. Note also that the lowest presence of AAIW is found in spring (Fig. 3.3 and 3.4).

The monthly distributions shown by the WOA data on the 27.5 isopycnic, roughly agree with the previous commented behaviour. It must be noted that in this case these data do not offer such a detailed spatial resolution of the region closer to the continental margin as the observed data do. However, those maps allow us to gain insight into the intra-annual variability of the AAIW distribution close to the GoC. In this sense, attending to the oxygen concentration distribution, which offers the most marked differences with the other water masses (see table 3.2), we can see that the major entrance of the AAIW close to the African coast occurs in November. At the same time, we can see that the spreading of the AAIW toward the GoC is more restricted during the spring months, only slightly suggested in March by the salinity distribution and in April by the oxygen distribution. In addition, in May, June and July this spreading is re-stablished, albeit to a lesser extent than in autumn.

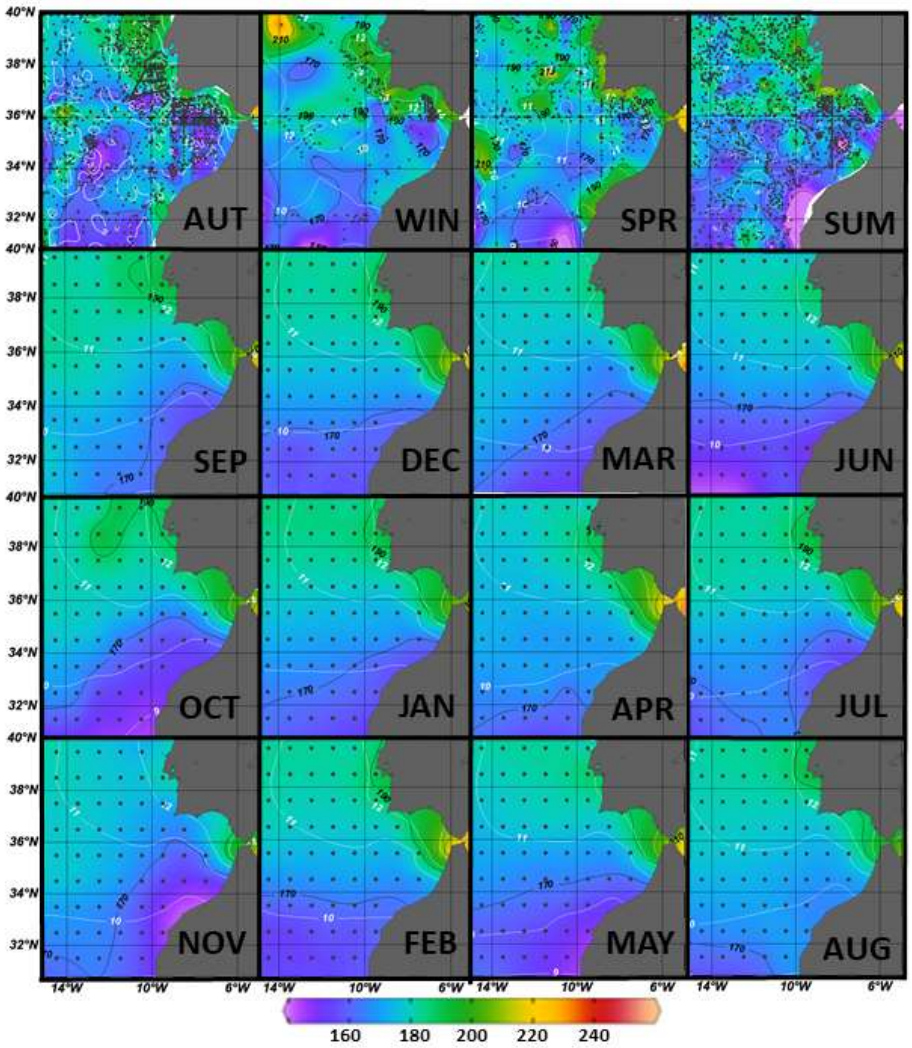

Figure 3.4. Observed oxygen concentration on the isopycnic surface σ= 27.5 for the different seasons (top row). The rows below show the same distributions for each climatological month as shown by WOA data. The white lines represent the temperature values at density σ= 27.5.

3.3.1.2 Vertical section distribution in zonal direction at latitude 36 º N

Figure 3.5 shows the zonal distribution of dissolved oxygen, salinity and temperature along 36º N. Low oxygen values characteristic of the AAIW occur year-long in the 700-1200 m depth range. As suggested before, the lowest oxygen concentrations occur in autumn close to the African continental slope. This increased AAIW presence close to the African Coast in autumn was already reported (Knoll et al., 2002; Machín and Pelegrí, 2016, 2009; Tsuchiya et al., 1992), although at lower latitudes.

In summer, the low oxygen zone spreads zonally, extending to Cape San Vicente (Fig. 3.5). In winter, the low oxygen signal is less evident, relative oxygen values are higher, perhaps suggesting weaker AAIW presence in winter. Note that salinity and temperature distributions are not helpful to discern between AAIW and SAIW (see table 3.2).

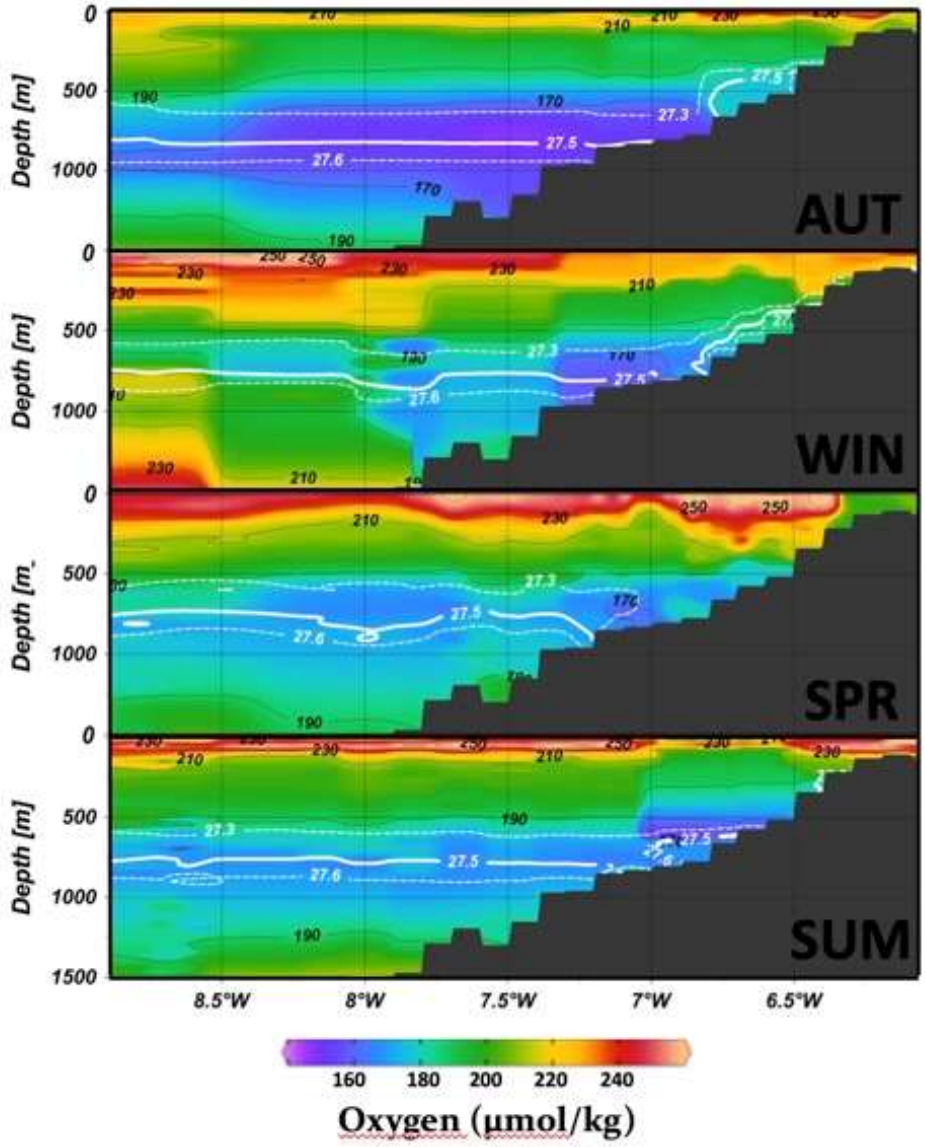

Figure 3.5. Vertical Oxygen concentration sections disposed zonally at a latitude of 36 ° N of observed variables for each season.

3.3.2 OMP analysis

The AAIW is present as an intermediate water mass extending along the middle slope from northern Morocco to the GoC year-round. There is a certain intra-annual variability, with

enhanced AAIW presence in autumn. To elucidate the pattern, we applied the OMP analysis to the dataset of vertical profiles in the target depth range (400-1000 m). Subsequently, we binned the results into 9 1ºx1º boxes (Fig. 3.6). As suggested before, the highest AAIW percentages are found in autumn. Only boxes G (the closest to the continent) and C (the farthest from the coast) show always AAIW percentages below 40 %. The SAIW shows its lower percentages (less than 10 %) in boxes closer to the Iberian coast (from E to I) during autumn while the higher values are found in winter in these boxes. The ENACW in the closer to coast boxes (G and H) shows its higher values in spring and summer while the MW shows these in winter and autumn. These results show the relationship among the different water masses. On one hand, in autumn the AAIW displaces the SAIW while the reverse situation occurs in winter. On the other hand, the alternation in predominance of these two water masses seems to be related to (i) a major confinement of the MW toward the coast in autumn (by the enhanced AAIW presence) and winter (by the SAIW) and (ii) a displacement toward offshore of the ENACW in the same seasons.

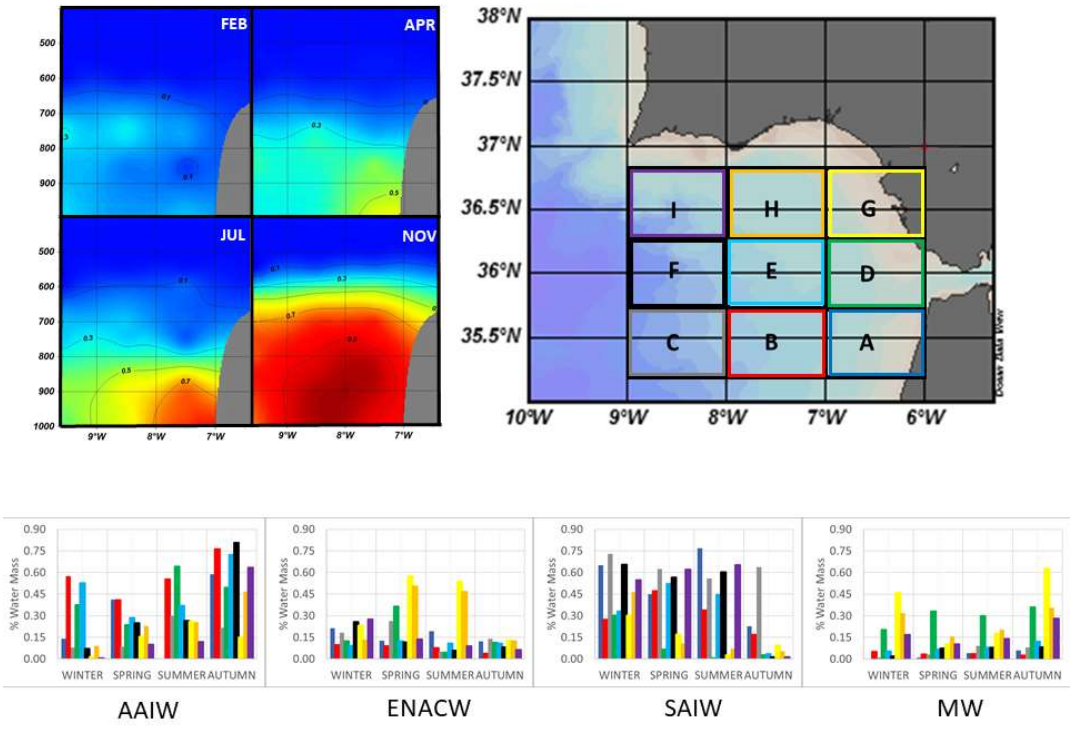

Figure 3.6. Values of percentages of each water mass resulting from the OMP analysis in each of the boxes shown in the map in the right hand lower corner, for each season. In the left hand lower corner, the resulting percentages are shown from the OMP analysis applied on the WOA data base for a zonal section at 36 ºN in selected climatological months. The data selected for OMP analysis are those in the depth range of 400-1000 m.

Regarding the OMP analysis on the WOA data, we have selected data located around a zonal section at a latitude of 36 º N (Fig. 3.6) in order to assure a clear identification of the AAIW coming from the Canary Islands latitude where this water mass has been previously identified

close to the African coast (Louarn and Morin, 2011; Machín and Pelegrí, 2016, 2009). Similar to the case of the observed profiles only data in the depth range of 400-1000 m have been considered. The water mass percentages have been computed for each month along the climatic year. Figure 3.6 shows the vertical sections of computed percentages of AAIW for February, April, July and November. The stronger AAIW presence occurs in November, when it is found near the African continent. We observe a weaker AAIW presence from February to April. The OMP results indicates that the autumn increase of the AAIW goes along with a reduction of the SAIW fraction, hence illustrating a sort of competitive seesaw between the two water masses. Figure 3.10a shows the climatic monthly values of the averaged percentages over the vertical section percentages of the four water masses. It can be seen that the SAIW is the most predominant water throughout most of the year, namely greater than 70 % for all months, with the exception of November when the AAIW rises to 40 %.

3.3.3 PC analysis

In order to carry out a better assessment of the seasonal variations of water mass percentages and the interrelation between the different water masses, we have applied a PC on the set of computed percentages. As explained in section two, this technique will allow us to identify common patterns in the seasonal variations of these percentages in the nine boxes located in the GoC shown in Figure 3.6.

In Figures 3.7 and 3.8, the results of this analysis are shown. The first PC (Fig. 3.7) shows a clear interaction between the AAIW and SAIW. In autumn a greater presence of the AAIW, coming from lower latitudes, seems to be related to a reduction in the presence of the SAIW coming from higher latitudes. In addition, this first principal component also reflects a significant increase in the presence of the MW in the box closest to the continental slope. The second PC (Fig. 3.8), picks up another clear interaction between the four water masses, but now it seems to be caused by a greater presence of the SAIW in winter that produces a displacement of the AAIW and ENACW and again a confinement of the MW against the continental slope.

The interpretation of these results is sketched in Figure 3.9, which shows the likely preferential tracks of the different intermediate waters along the GoC in the different seasons. In autumn the AAIW penetrates closer to the continental slope while the SAIW runs more displaced southward. Also, the ENACW and MW are found near the coast. In winter the situation is reversed regarding AAIW and SAIW behaviour. Now the SAIW is flowing closest to the continental slope, the AAIW is displaced southward and once again the ENACW and MW are confined toward the continental slope. The situation in spring and summer is similar

to the one in winter exception made for the increased transport of AAIW, close to the African coast, in summer.

3.3.4 Wind forcing in the north Atlantic and intermediate water presence in the GoC

Variability of the meridional transport in the North Atlantic is linked with two important wind driven mechanisms (Barrier et al., 2014; Machín and Pelegrí, 2009):

The meridional Sverdrup transport:

$$M_y = \frac{1}{\rho_0 \beta_0}\left[\frac{\partial \tau_y}{\partial x} - \frac{\partial \tau_x}{\partial y}\right] \quad (7)$$

and the Ekman pumping:

$$w_E = \frac{1}{\rho_0}\left[\frac{\partial}{\partial x}\left(\frac{\tau_y}{f}\right) - \frac{\partial}{\partial y}\left(\frac{\tau_x}{f}\right)\right] \quad (8)$$

Where τ_x and τ_y are, respectively, the zonal and meridional components of wind stress; ρ_0 is sea water density; $f=f_0 + \beta_0 y$ is Coriolis parameter, where β_0 is the variation with latitude of f in the β plane.

We computed both magnitudes from wind velocity data provided by ERA-Interim reanalysis spanning the period 1979-2018.

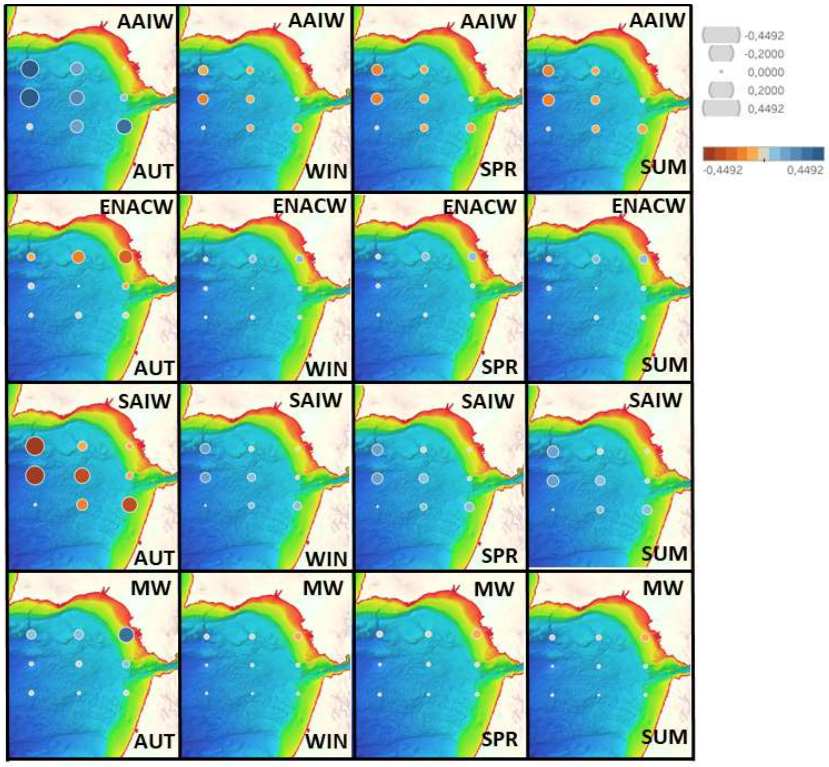

Figure 3.7. Seasonal variation of the percentages of each water mass given by the first principal component resulting from the PCA on the percentages previously estimated in the nine boxes considered in the GoC. Values are deviations from the averaged, through the different seasons, percentage at each location.

Figures 3.11 and 3.12 show, respectively, the meridional Sverdrup transport and the Ekman pumping for January and July, the two seasonal opposites in a climatological year. They are shown for the region of the North Atlantic spanning the latitudes 10º N to 70º N and for the zoomed region focussed on the GoC.

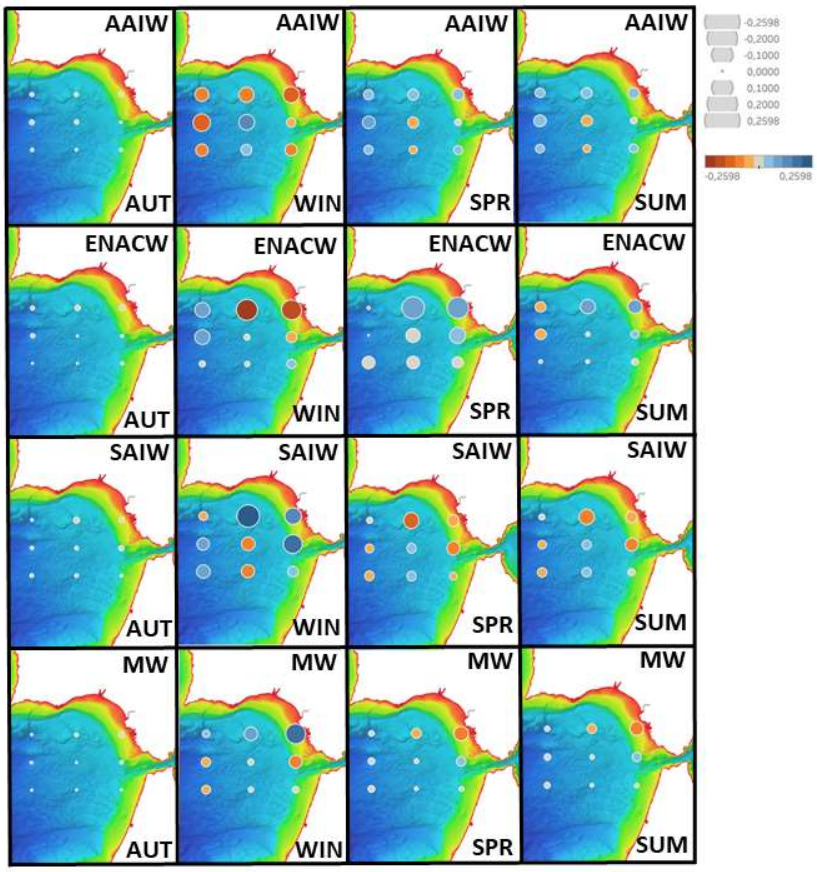

Figure 3.8. As figure 3. 7 but for the second principal component.

The meridional Sverdrup transport peaks close to the eastern coast (Figure 3.11). This suggests small-scale horizontal wind stress gradients near the continent. The Sverdrup transport along the eastern coast of Portugal is southward year-round, with highest (lowest) values in January (July). Along the African coast this transport is northward year-round, with highest (lowest) values in July (January). More detailed information about the seasonal variations of these transports can be found in Figure 3.10b where the mean monthly climatological values of Sverdrup transport are shown at three points close to the coast, namely at latitudes 30º N, 35.5º N and 40º N. At 30º N meridional transport is positive (northward) all year showing an increase in summer with a peak in July. This northward transport close to the African coast may contribute to the northward progression of the AAIW from latitudes as low as 10º up to at least 30º N. In contrast, the transport at 40º N is southward year-round, peaking in winter. Therefore, this behaviour could explain a special progression of the SAIW close to the Portuguese coast from high latitudes down to the GoC during this season.

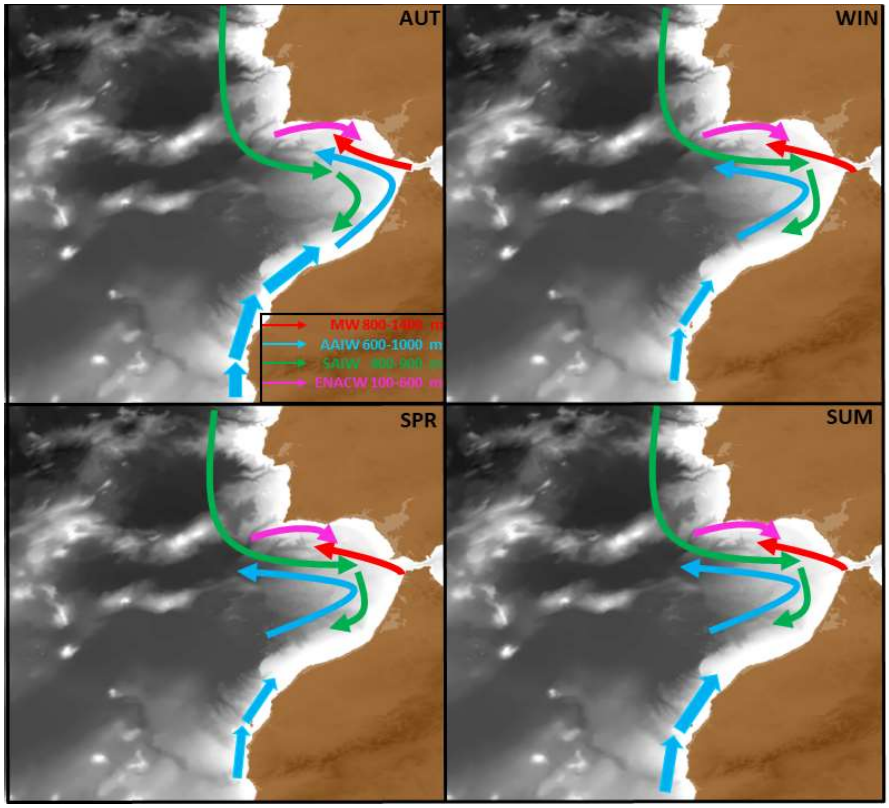

Figure 3.9. Illustration of the preferential tracks of the different intermediate water masses throughout the different seasons. Increased thickness of the arrows closer to the African coast point out the likely increase in the transport of AAIW in Autumn and Summer.

Concerning the Ekman pumping, Figure 3.12 shows its spatial distribution in the same two months of the climatological year, January and July, in the same domains considered in Figure 3.10. Note that the zones with negative values of the Ekman pumping roughly depict the location of the gyres within the basin. In winter (i.e. January) the zone where convergence (negative Ekman pumping) is more important within the subtropical gyre reaches latitudes as high as 48º while in summer (i.e. July) this zone is more reduced and displaced to latitudes lesser than 36º. Therefore, in winter, a more developed subtropical gyre may favour the increasing transport of high latitude intermediate waters toward the GoC while, in summer, a displaced towards the south gyre is not able to transport these high latitude intermediate waters toward the GoC.

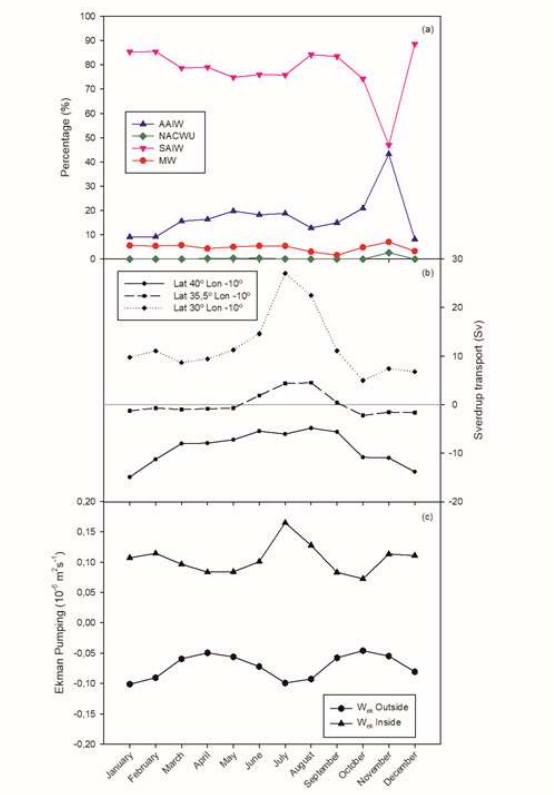

Figure 3.10. a) Averaged percentages of each water mass resulting from the application of OMP analysis on WOA data, for each climatological month, at 35.5 °N in the GoC. b) Sverdrup transport at three locations close to the continental borders: south of GoC (30 °N, 10 °W), in the GoC (35.5 °N, 10 °W), north of GoC (40 °N, 10 °W). c) Monthly Ekman pumping in two zones: Outside the GoC (between 35°-36° N and 19°-20° W) and Inside the GoC (between 35°-36° N and 7°- 8° W).

Besides the small scale variations in Ekman pumping, we observe generalised divergence (positive Ekman pumping) near the eastern ocean margins all year-round. As the Ekman pumping is implicitly accounted for in the Sverdrup transport, we expect that divergence near the continents may be held responsible for the local intensification of the meridional Sverdrup transport.

In order to present more detailed information about the time variability of the Ekman pumping at the latitude of the GoC, Figure 3.10c shows the monthly climatological averages of this variable, inside the GoC, in a box limited by latitudes 35º and 36º N and longitudes 7º and 8º W, and outside the GoC, in a box limited by latitudes 35º and 36º N and longitudes 19º and 20º W. Inside the GoC there is permanent divergence (positive pumping) in the Ekman layer caused by a small-scale cyclonic wind pattern existing in this area. This divergence, which is more intense during summer, would favour the displacement of the water masses underneath the Ekman layer toward the GoC, exerting a suction effect on them. So, intermediate waters that arrive at a latitude close to the GoC could continue progressing northward thanks to this effect. Outside the GoC there is a permanent convergence (negative pumping), which is more intense during winter and summer. It is expected that during these

seasons the dominant downwelling existing in the Ekman layer of this zone would not favour the transport of intermediate waters in that direction. However, in spring and autumn the intensity of these convergences decrease significantly, which could diminish the capacity of blocking the transport of intermediate waters in that direction.

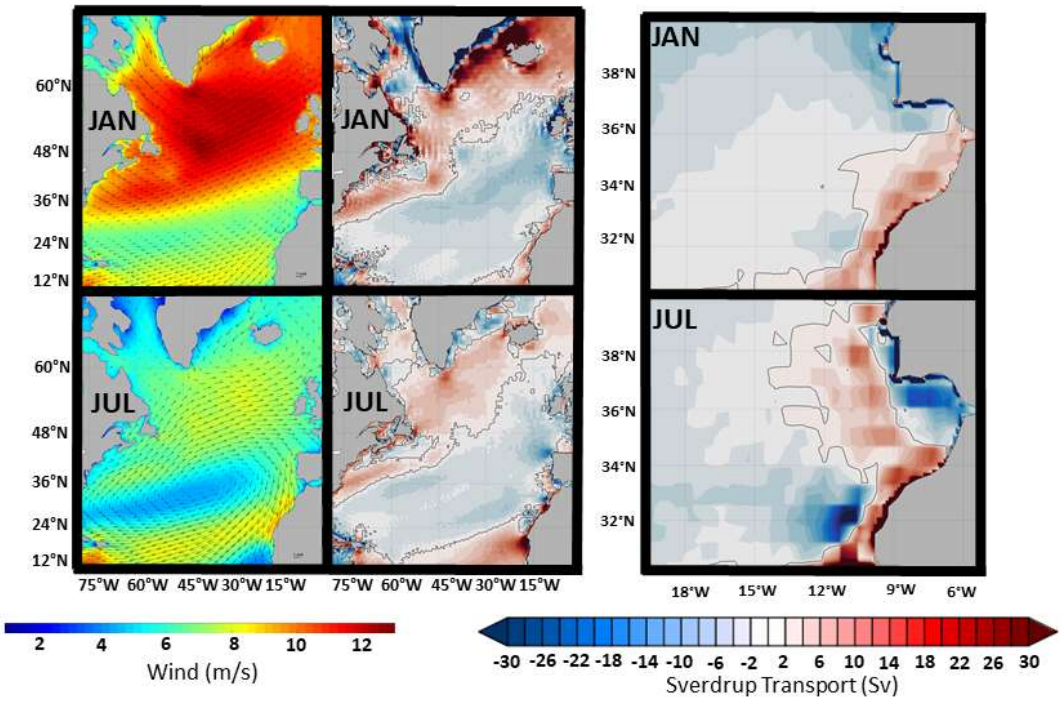

Figure 3.11. Maps of surface winds and Sverdrup transport in January (upper) and July (lower). Right maps are a zoomed study region of surface Sverdrup transport.

In the following section we discuss all these preliminary results as well as the results attached in the related references in order to depict a conceptual model that allows explanation of the mechanisms that control the fluctuation of intermediate water masses in the GoC.

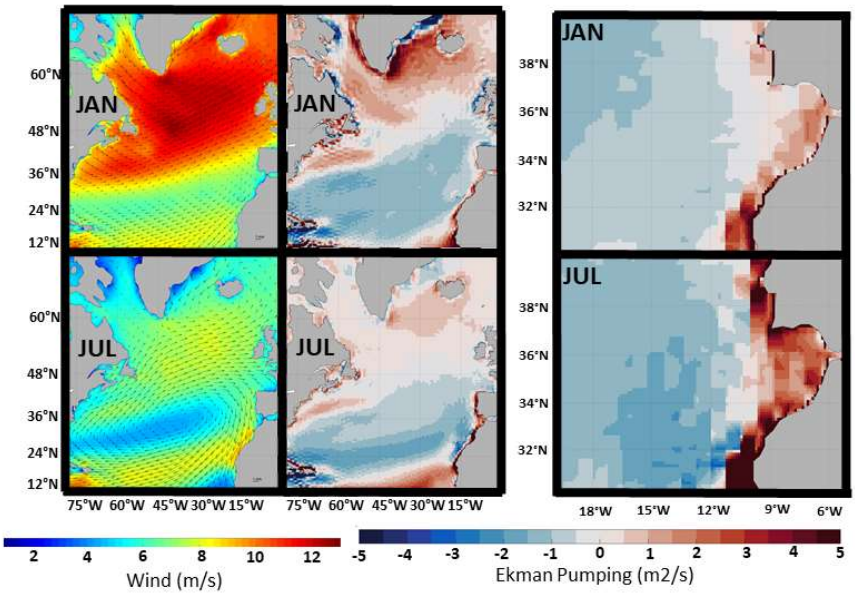

Figure 3.12. As figure 3.11 but for Ekman pumping.

3.4 Discussion

3.4.1 Extension and variability of the AAIW and its interrelation with other intermediate water masses

Presence of the AAIW in the GoC has been reported before (van Aken, 2000; Brogueira et al., 2004; Cabeçadas et al., 2002; Hernández-Molina et al., 2014; Louarn and Morin, 2011; Preu et al., 2013). There is also evidence of greater autumn AAIW presence near the African margin at least up to 32 °N (Knoll et al., 2002; Machín and Pelegrí, 2009; Tsuchiya et al., 1992). Thus far, we remain uncertain whether this seasonal variability extends into the GoC.

In section 3 we confirmed AAIW presence year-round along the middle slope from the northern Moroccan margin and into the GoC. We inferred certain seasonal AAIW variability featuring an autumnal approach to the continent, summer horizontal spread and offshore separation. Winter and particularly spring are characterized by a weaker AAIW presence.

Moreover, the results of the PCA on the water mass percentages allow the identification of clear interactions between the four water masses. In autumn a greater presence of the AAIW, coming from lower latitudes, seems to be related to a reduction in the presence of the SAIW and ENACW. This interaction also affects the MW, which is pushed by the AAIW toward the

continental slope. In winter, the SAIW is the predominant water mass reducing the presence of the AAIW and ENACW and once again pushing the MW toward the continental slope. Note that in autumn a less dense MW entering the GoC (Millot et al., 2006), may be settled closer to the slope making easier the AAIW penetration into the GoC.

The next step now is to investigate the physical mechanism that triggers these seasonal variations in the water masses presence.

(Machín and Pelegrí, 2009) explained the arrival of the AAIW to latitudes around the Canary Islands in terms of the divergences produced by the Ekman pumping close to the African coast, and the subsequent stretching of the water column below, which promotes a northward movement of the intermediate waters in order to conserve its potential vorticity. However, the identified divergence regions were located too far from the African coast to explain the observed confinement toward the coast of the observed AAIW core. Perhaps the spatial resolution of 1º of the wind data used was too coarse to capture the small scale variation of winds close to the continent. The importance of these small scale variation of winds has been recognised in several studies (Kanzow et al. 2010; Machín et al. 2010; Pérez-Hernández et al. 2013; Velez-Belchi et al., 2017) in connection with the generation of baroclinic Rossby waves that propagate toward the interior ocean and may affect the Atlantic meridional overturning circulation (AMOC).

(Barrier et al., 2014), who have analysed the response of the North Atlantic subtropical gyre to the North Atlantic Oscillation (NAO) and other atmospheric regimes, conclude that this response involved important changes in meridional transport of water masses in this basin. For instance, a positive/negative NAO displaces the subtropical gyre to a higher/lower latitude. A gyre centred at a higher latitude favours a southward meridional transport of high latitude water masses by the eastern boundary while a gyre centred at lower latitude does not favour this southward transport of water masses from higher latitudes. In terms of the intermediate water masses we are dealing with, a positive NAO would prevent the entrance of the AAIW toward the GoC in favour of a greater SAIW arrival here, while a negative NAO would weaken the southward transport of the latter and favour the spread of the AAIW toward the GoC. While in our case we are not dealing with the NAO variability, it is worth noting that the effect on the subtropical gyre dynamics of a positive/negative NAO are fairly similar to the effects that a winter/summer wind forcing produces.

Keeping these previous results in mind and referring to the results presented in section 3.3, we will propose a mechanism based on the seasonal variation of wind forcing in the North Atlantic that could explain the variations in the presence of the intermediate water masses in the GoC. Focussing on the greater presence of the AAIW in autumn, it seems that the following two types of processes are required:

a) Processes that promote the transport of intermediate waters (AAIW and SAIW) from high latitudes toward the GoC.

b) Processes that may favour the northward transport of intermediate waters when these have arrived at latitudes close to the GoC.

Regarding the first type of processes, we detach the small scale variability of the wind stress curl close to the continents and its implications in the near continent meridional Sverdrup transport. As shown in Figure 3.10b, these transports southward along the Portuguese coast and northward along the African coast, maintain a permanent direction during the whole year but become more intense from June to September along the African coast and from October to February along the Portuguese coast. Therefore, during summer the conditions for a decisive northward progression of the AAIW along the African coast are met and this mechanism could be responsible for bringing the AAIW up to the Canary Islands region. However, since these transport processes diminish considerably in September, they may not be able to sustain the subsequent northward progression of the AAIW that could explain the observed maximum in the percentage of the AAIW along the slope of northern Morocco and the GoC attached in November. Therefore, it is then necessary to find additional processes that help sustain this northward progression up to the GoC. This leads us to the second type of processes.

Regarding the second type of processes, we will consider the seasonal variations of the Ekman pumping within GoC and in the zone of the subtropical gyre closest to GoC. Figure 3.10c shows these values for the different climatological months. Note that when the Ekman pumping becomes less negative to the west of the GoC, southward transport on the eastern branch of the gyre weakens and this could favour a greater spreading of the AAIW towards the north. On the one hand, this weakening of the negative Ekman pumping in this zone is more pronounced during March-June and September-November. On the other hand, the Ekman pumping inside the GoC is positive during the whole year. As previously described, this permanent divergence in the Ekman layer caused by a small scale cyclonic wind pattern existing in this area and more intense during summer, would favour the displacement of the water masses underneath the Ekman layer toward the GoC, exerting a suction effect on them. Therefore, intermediate waters that arrive at a latitude close to the GoC could continue progressing northward inside the GoC thanks to this effect. Note that this Ekman pumping experiences a significant increase in November after having reduced its intensity during September and October.

3.4.2 Implication of the AAIW on the morphology of the continental margin

Intermediate water masses have been shaping the morphology along the northern Moroccan coast, the GoC and the Atlantic Iberian continental margins (see compilations in (Hernández-Molina et al., 2011, 2016)). During the last decades numerous researchers and institutions have analysed the influence of both the MW and ENACW on the sea floor morphology with great detail, particularly within the GoC ((García et al., 2009; Hans Nelson et al., 1993; Hernández-molina et al., 2014; Hernández-Molina et al., 2011, 2016; Hernández-Molina et al., 2003; Llave et al., 2007; Madelain, 1970; Nelson et al., 1999; Roque et al., 2012; Sánchez-Leal et al., 2017), among many others). These authors identified large depositional and erosional (contourite) features along the middle and upper continental slopes due to the vertical and lateral variation of the aforementioned intermediate water masses. The results obtained in the present study reveal clear seasonal variations of the AAIW and its interrelation with the SAIW, MW and ENACW. Nevertheless, changes in distribution of these intermediate water masses and the implications in particular of the AAIW for shaping the morphology and controlling sedimentation along the northern Moroccan coast, GoC and the Atlantic Iberian margins have not been considered so far and two new questions may arise: Is there any influence of the AAIW along the continental slope at present? Was there any influence of these intermediate water masses in the past?

Some recent papers have described the occurrence of bottom current features along the middle slope of the northern Moroccan margin, which do not fit well with present circulation of the ENACW and the MW and its associated interphases (pycnoclines). The onset of these features has been related both to the action of deep tides or a branch of upper MW veering southwards off the Strait of Gibraltar along the Moroccan margin (e.g., (Lebreiro et al., 2018; Vandorpe et al., 2014, 2016). Deep (barotropic and baroclinic) tides are important secondary processes amplifying the background water mass circulation generating local and smaller features but are not relevant for large regional depositional or erosional feature formation along continental slopes (Hernández-Molina et al., 2016; Rebesco et al., 2014). In contrast, a branch of upper MW veering southwards off the Strait of Gibraltar along the Moroccan margin is apparently against the Coriolis forces in the area (Baringer and Price, 1999, 1997) as well as the reported MW regional circulation(Sánchez-Leal et al., 2017). Northward flowing of a vigorous AAIW close to the margin, as reported here, could be considered as a plausible regional control factor in developing those features. However, this would require more detailed sedimentary, morphologic and paleoceanographic work in order to confirm this hypothesis.

Vertical variations of the MW and ENACW have been reported at short (seasonally) scales (e.g., (Borenäs et al., 2002; M.J. Bellanco and R.F. Sánchez-Leal, 2016) and in longer

geological cycles ((Hernández-Molina et al., 2016; Llave et al., 2006; Lofi et al., 2016; Rogerson, 2012; Voelker et al., 2006) among other). The Pliocene and Quaternary (last 5.3 Ma) sedimentary evolution of the slope has been related to those vertical changes. For example, in glacial periods some authors have reported that the MW was flowing approximately 700 m deeper than today with associated changes in both East North Atlantic Deep Water (ENADW) and North Atlantic Deep Water (NADW) (Rogerson, 2012; Schönfeld et al., 2003; Schönfeld and Zahn, 2000). An open debate about the relationship between the variation in the paths of these water masses and the sedimentary evolution along the northern Moroccan coast, GoC and the Atlantic Iberian continental margins has been ongoing since the recent Integrated Ocean Drilling Program (IODP) Expedition 339 in the GoC (Expedition 339 Scientists, 2012; Stow et al., 2013;Hernández-Molina et al., 2013, 2016) . However, in this debate the influence of the AAIW in the past has not been taken into account.

The AAIW represents a cold intermediate water mass formed at the ocean surface in the Antarctic Convergence Zone/Antarctic Polar Front (between 50° to 60°S), mainly at the southwest of the southern tip of South America (Tomczak and Godfrey, 2003). After its formation the AAIW flows north as an intermediate water mass as far as 20°N, with trace amounts as far as 60°N. It continues northward until it encounters other intermediate water masses (Talley, 1999). This is the case for the AAIW in the Atlantic Ocean (and similar in the Indian Ocean) where this water mass has higher influence and is denser in comparison with the Pacific Ocean where the AAIW is comparatively less important (Bostock et al., 2013). The formation and circulation of the AAIW is an important component of the upper branch of the AMOC that is associated with the transport of heat and salt within the Southern Hemisphere subtropical gyre (Stramma, 1999). Different authors have reported enhanced AAIW circulation during colder periods at different scales (e.g., (Curry and Oppo, 2005; Jung et al., 2010; Makou et al., 2010; Muratli et al., 2010; Oppo, 2000; Pahnke et al., 2008a; Wainer et al., 2012) among others). For example, during the last glacial, there is increased formation of intermediate water and the production of NADW is significantly weakened, and the NADW is replaced in large extent by enhanced AAIW (Wainer et al., 2012), which circulated lightly with a main core ~1100 m in a depth range between 900 and 1270 m (Makou et al., 2010). Therefore, vertical and lateral variations of the AAIW during glacial vs interglacial periods have been reported (e.g.: (Bozzano et al., 2011; Preu et al., 2012, 2013; Viana et al., 2002; Voigt et al., 2013), and some authors demonstrated that during the last decades the AAIW has been reduced, significantly warmer (0.058–0.158°C / decade) and shoaling (30–50 dbar / decade) since becoming less dense [up to 20.03 (kg/ m3) / decade], due to global warming (e.g., (Downes et al., 2010; Shmidtko and Johnson, 2012).

Therefore, based on all the above considerations we can conclude that the paths of the AAIW had to vary throughout the geological past at different scales, increase during cold periods and decrease and shoal during warmer periods. The results presented in this paper are important

and any future discussion on this subject should consider the lateral and vertical interaction of intermediate water masses in general and evaluate the role of AAIW in the past in particular, since its influence could be important, especially related to colder periods, in controlling the sedimentation along the slope. For example, in contributing to higher siliceous production in determinate time periods as has been described with Expedition 339 in the GoC (Expedition 339 Scientists, 2012; Stow et al., 2013;Hernández-Molina et al., 2013, 2016).

3.5 Conclusions

The analysis of the seasonal variation of the intermediate water masses carried out in the GoC and adjacent areas has determined remarkable changes of the Antarctic Intermediate Water (AAIW) and the Subarctic Intermediate Water (SAIW). During autumn a greater presence of the AAIW, coming from lower latitudes, seems to be related to a reduction in the presence of the SAIW and the ENACW. This interaction also affects the Mediterranean Water (MW) which is pushed by the AAIW toward the upper continental slope. In the rest of the seasons, the SAIW is the predominant water mass reducing the presence of AAIW.

This seasonal variability in the interchange between these intermediate water masses can be explained based on the concatenation of several wind-driven processes acting during the different seasons. The summer intensification of the Sverdrup transports near the African coast makes the progression of AAIW possible from low latitudes up to latitudes above the Canary Islands. Subsequently, once the AAIW has reached latitudes close to the GoC, its northward transport is sustained due to a decrease in the intensity of negative Ekman pumping within the subtropical gyre west of the GoC, which presents its minimum intensity during autumn. This transport toward the GoC is also favoured by the permanent cyclonic wind system that dominates locally in the GoC, although it shows its highest intensity in the months of July to August. In November it again experiences a significant increase. The high percentage of the SAIW during winter, spring and summer could be explained by the permanent southward Sverdrup transport that occurs near the coast of the Iberian Peninsula which favours the arrival of the SAIW to the GoC. From September onward this transport begins to weaken due to the arrival of the AAIW from the south and the deviation of part of the SAIW transport toward the eastern side of the subtropical gyre (west the GoC), where the intensity of the negative Ekman pumping is reduced between September and November.

Our results are important for a better understanding of intermediate water mass variability along the northern Moroccan coast, GoC and the Atlantic Iberian margins but further paleoceanographic, sedimentary and morphological research is needed in order to decode changes in the geological past and determine how these water masses, in particular the AAIW,

have been shaping the morphology and controlling the sedimentation along the northern Moroccan coast, the GoC and the Atlantic Iberian margins.

Capítulo 4

TIDAL DYNAMICS ON THE UPPER CONTINENTAL SLOPE OF THE EASTERN GULF OF CÁDIZ: THE INTERPLAY BETWEEN WATER MASSES AND ITS EFFECTS ON THE SEAFLOOR MORPHOLOGY

Roque D., Gomiz-Pascual J.J., Bruno M., Sánchez-Leal R., González C.J., García M., Fernández-Salas L.M., Hernández-Molina F.J.

Abstract. Although the effects of tidal dynamics have been studied in shallow marine environments and morphologically restricted straits, the impact of these processes on deep-water marine environments remains to be studied in depth. This study highlights the influence of tides on the seafloor morphology of the eastern Gulf of Cádiz, near the exit of the Strait of Gibraltar. Two moorings, one with an Acoustic Doppler current profiler (ACDP) and another one with a thermistor chain, and local and regional profiles of salinity, temperature, and ADCP reveal the water mass distribution in the study area and associated oceanographic processes. The intermediate water masses flowing along the continental slope are the Eastern North Atlantic Central Water (ENACW) and the Mediterranean Outflow Water (MOW), bound by an interface located regionally at depths greater than 300 m, but identified locally at much shallower depths (up to 150 m) in the studied upper slope. The hydrodynamics of the area is governed by barotropic tidal currents, the MOW upper core, and the internal tides, which act at different time and spatial scales shaping the local sea-floor terraced morphology and determining the dominant sedimentary processes. The obtained results allow a better understanding of how secondary oceanographic processes are modulating the water mass circulation in this particular hot spot and their importance in explaining the formation and evolution of morphological depositional and erosional features. tides effect are associated to shallow marine environments or within straits and the effect of those processes on deep-marine environments is only taken in account by few specialists and their effects on controlling sea floor morphology do not consider. In this contribution the importance of tides is demonstrated. on the continental slope of the eastern Gulf of Cadiz, close to the exit of the Strait of Gibraltar. This work is based on two moorings, one with an Acoustic Doppler current profiler (ACDP) and another one with a thermistor chain as well as on local and regional profiles of salinity, temperature and ADCP. The Eastern North Atlantic Central Water (ENACW) and the Mediterranean Outflow Water (MOW) are intermediate water masses flowing along the slope and although the ENACW-MOW interface is regionally located in depths greater than 300 m, it become much shallower (up to 150 m wd) in the studied upper slope. Its vertical and lateral variation is modulated by the barotropic and internal tides and other shorter than tidal periods internal waves, which are acting at different time and spatial scales focussing on this area for determining the local sea-floor terraced morphology and the dominant processes. Obtained results allow to a better understanding of how secondary oceanographic processes are modulating the water masses circulation in some particular hot spot and their importance to explain the formation of morphological depositional and erosional features.

Key words: water masses, tides, internal waves, sea-floor morphology, continental slope, Gulf of Cadiz

4.1 Introduction

During the last decades a myriad of studies have been published about the influence of water masses, bottom currents and associated processes on deep-water sedimentation (e.g., Rebesco et al., 2014: Thran et al., 2018). These oceanographic processes include barotropic tidal currents, internal tides and other shorter period internal waves (e.g., Yin et al., 2019) and are key in locally modulating and controlling the direction, velocity and the duration of bottom currents (Shanmugan, 2006, 2012, 2020), although their real effect on controlling sedimentation and the sea-floor morphology remains uncertain. There are some particular areas (hot spots) where these processes are particularly active (e.g., Quaresma and Pichon 2013), one of them being the eastern Gulf of Cádiz (GoC) offshore the southern Iberian Peninsula, in the area close to the Strait of Gibraltar. Here, the exchange between the Mediterranean Sea and the Atlantic Ocean, as well as the geological and morphological conditions of the Strait of Gibraltar determine the setting for active circulation with converging barotropic tides, internal tides, and the Mediterranean outflow (e.g., Baringer and Price., 1997; Sanchez-Leal et al., 2017), which interact with each other and the sea-floor (Hernandez-Molina et al., 2014a; de Castro et al., 2021). This interaction controls the final balance of warm and salty water which in turn has important consequences on the global ocean, affecting the supplies of water masses to the north Atlantic Ocean (Khélifi et al., 2011;2014; Rogerson et al., 2012; Sánchez-Leal et al., 2017). Nevertheless, there is a lack of information about how tidal dynamics and associated internal waves modulate the lateral and vertical position of the water masses and their boundaries along the continental slope. Therefore, the main aims of this study are: 1) to identify the tidal dynamics and the variability of the interfaces between water masses along the upper and middle continental slope in the eastern GoC (Fig. 4.1 and 4.2) and 2) to analyse the possible link between tidal dynamics and seafloor morphology.

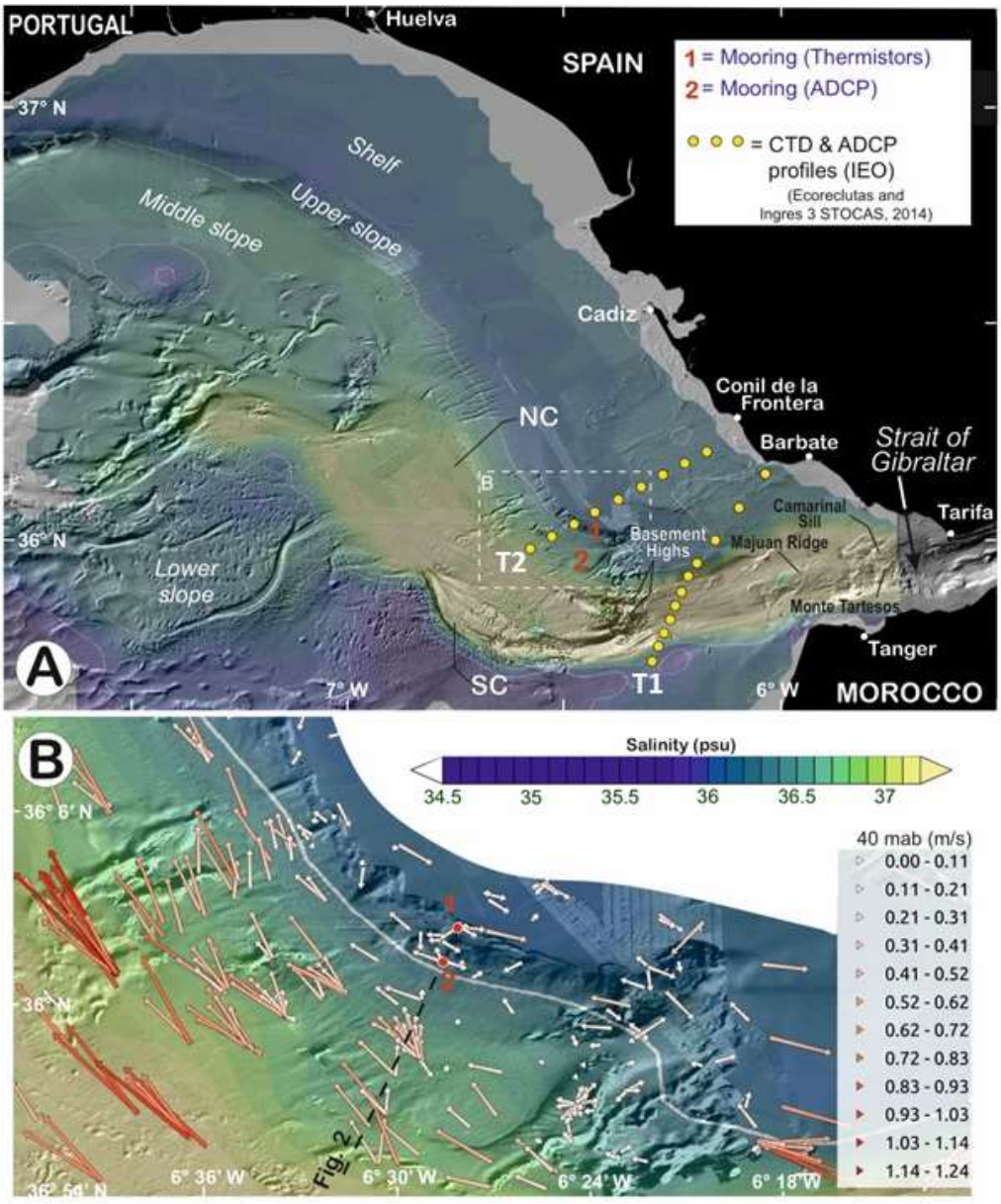

Figure 4.1. A) Regional bathymetric map of the Gulf of Cadiz (GoC) with the distribution of the Mediterranean Outflow Water (MOW) from Sanchez-Leal at al. (2017), observing the salinity distribution on the seafloor as a differential factor to identify the MOW, with salinities values over 36.5, in both figures, and including the sites where data were collected. Red Stars indicate the location of the two moorings: 1) mooring with a thermistors chain at 186 m water depth and 2) mooring with the Acoustic Doppler current profiler (ACDP) at 235 m water depth. Yellow points indicate the sections with salinity, temperature and ADCP collected during two oceanographic cruises in the same area (Ecoreclutas October 2014 and Ingres 3 STOCAS October 2014), they are organized into the two transects T1 and T2 also shown. NC is North Channel and SC is South Channel B) Zoom in on the study region with superimposition of lines indicating the intensity and direction of bottom currents collected by the IEO Cádiz and published by Sanchez et al. (2017).

4.2 Oceanographic and morphological settings

The eastern GoC has a very active circulation determined by the exchange of water between the Atlantic Ocean and the Mediterranean Sea through the Strait of Gibraltar (Fig. 4.1 and 4.2). Here, the Mediterranean Outflow Water (MOW) flows out into the Atlantic as a result of density driven circulation, the pressure gradient, the Coriolis force and the bottom friction with the slope (Gasser et al. 2017). In contrast, the Atlantic waters [Surface water (ASW) and Eastern North Atlantic Central Water (ENACW)] flow into the Mediterranean Sea (Ambar and Howe., 1979a,b; Price et al., 1993; Baringer and Price., 1997; Sanchez-Leal et al., 2017). The ASW flows east between the surface and 100 m water depth (wd), and the ENACW has a cyclonic circulation along the eastern continental shelf moving to the east toward the Strait of Gibraltar between the ASW and the MOW. The MOW circulates northwest along the middle slope between 300/500 and 1200 m wd (Fig. 4.2), interacting with both the ENACW and the modified Antarctic Intermediate Water, AAIW (Ambar and Howe., 1979a,b, Baringer and Price, 1997, Criado-Aldeabuena at al., 2006; García-Lafuente et al., 2006; Hernandez-Molina et al, 2014a; Bellanco and Sanchez-Leal, 2016; Sanchez-Leal et al., 2017; Roque et al., 2019). The upper boundary between the MOW and the ENACW is recognised with a salinity of 36.3 (Sanchez-Leal at al 2017), and is located at an average depth of about 250 m wd (Bellanco et al 2016).

Tidal forcing is a very important factor to explain the way in what the MOW spreads in the Gulf of Cadiz as indicated by several authors (Gründlingh 1981, Quaresma and Pichon 2013, Izquierdo et al. 2019). The greater effects occur in the area closest to the Strait of Gibraltar (Candela et al 1990). The semidiurnal constituent M2 is dominant over the region. The S2 is the second most important constituent, and together are responsible for the Spring-Neap tidal modulation along the continental shelf (Quaresma and Pichon, 2013).

Within the Strait, the tide flow interacts with the Camarinal sill and other morphological highs forming an internal bore and triggering remarkable internal waves in the presence of the strong stratification between the Mediterranean and the Atlantic waters (e.g. Brandt et al., 1996; Bruno et al., 2002; Farmer et al., 1988; Izquierdo et al., 2001; Sánchez Garrido et al., 2008; 2011; Tsimplis, 2000; Vázquez et al., 2006, 2008; Vlasenko et al., 2009). Solitons with amplitudes in the range of 50 to 100 m, wavelengths of 1 to 3 km and phase speed from 1 to 2 m/s are produced regularly and travel eastward. There are also less common, weaker, internal waves that propagate westward into the deeper Atlantic Ocean. They have been observed primarily during the summer, when solar heating produces a well-defined thermocline in the upper layer of the Atlantic Ocean (Brandt et al., 1996; Farmer et al., 1988; Farmer and Armi, 1985). In addition, the sea floor irregularities along the continental margin also generate other internal waves (Bruno et al, 2006; Quaresma and Pichon, 2013) and create residual currents (Meddies) by the interaction between the bottom topography and the

MW cores (Chérubin et al., 2003). Further westward from the Strait the influence of the tides and internal waves decreases.

The continental margin along the GoC west of the Strait of Gibraltar is very complex due to the geodynamics of the area and the interaction between the seafloor topography and the oceanographic dynamics, resulting in the development of large depositional and erosional features including large channels and valleys (García et al., 2009). The upper slope is located from 120-140 to 500 m wd (Fig. 4.2), the middle slope between 500 and 1200 m wd, and the lower slope extends to depths of about 4300-4800 m where it connects with the abyssal plains. The upper and middle slopes have been shaped by the action of water masses, especially the MOW (Nelson et al., 1999; Llave et al., 2007; Hernandez-Molina et al., 2014a). West of the Camarinal sill, two large channels (South (SC, Fig 4.1) and North (NC) channels trending west and north-west respectively forming the pathways for the main cores of the MOW (Fig. 4.1 and 4.2), that are on average of 2-6 km wide, 150 km long and about 30 to 50 m deep (Hernandez-Molina et al., 2014a). Smaller features such as furrows and erosional surfaces (Fig. 4.2) result from the activity of five branches within the main (Mi) MOW flow, where M1 and M2 flow along the southern channel and the others (M3, M4 and M5) move along the northern channel (Sanchez-Leal at al 2017, Figure 4.1).

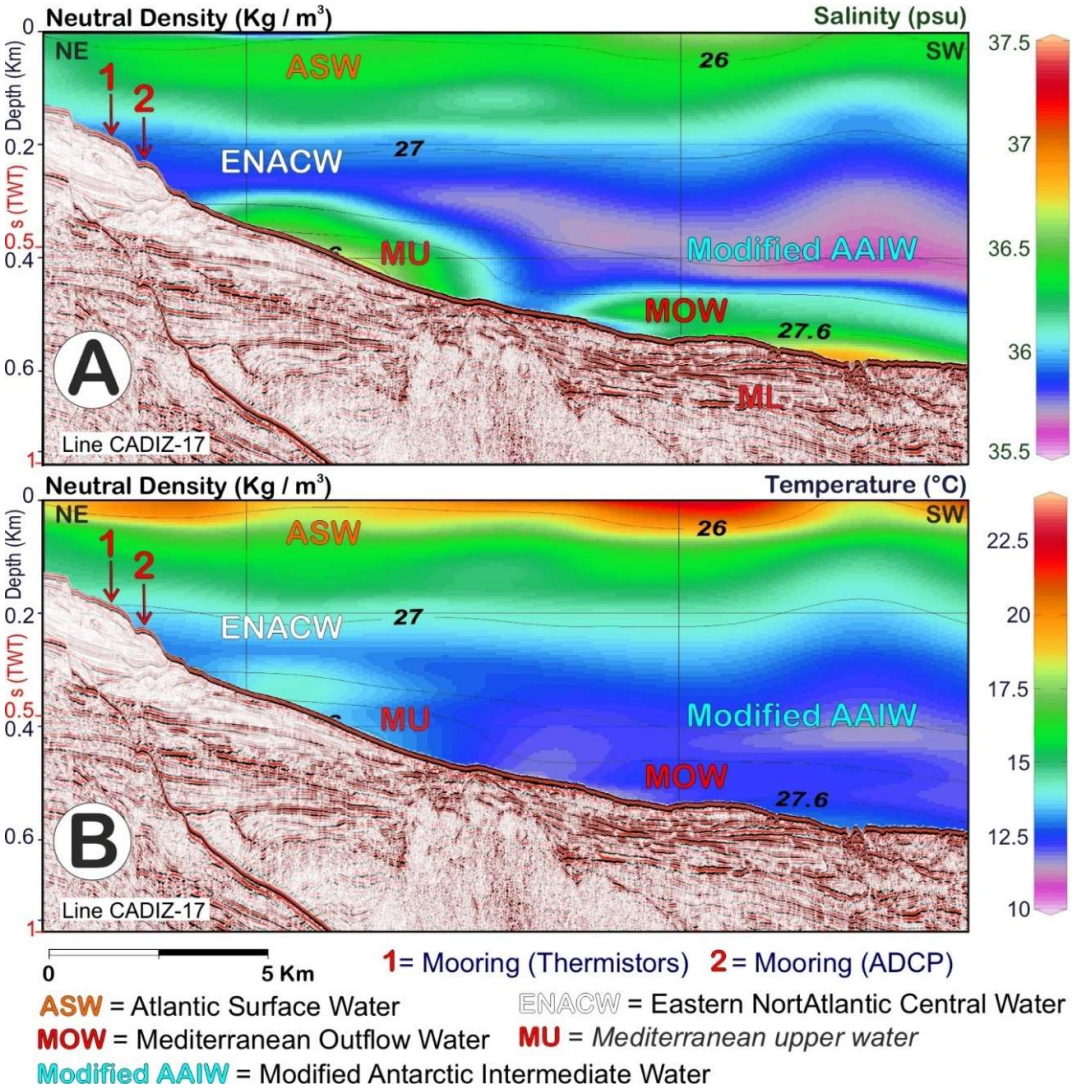

Figure 4.2. Seismic and hydrographic vertical sections from the continental shelf to the middle slope (from Hernandez-Molina et al., 2014a). The location of the two moorings is included. Water column colors indicate salinity (A) and temperature (B). Regional water-masses are shown. Profile locations are in Figure 4.1B. TWT—two-way travel time.

4.3 The data set

The observations to analyze the tidal dynamics in the study area come from two moorings (Fig. 4.1 and Table-4.1), one with an Acoustic Doppler current profiler (ADCP, a Workhorse 75 kHz, RDI) at 235 m wd. It was emplaced 10 m from the seafloor, and the cell size of the profile was 4 m with a blanking distance of 7.0 m, covering the water column.

The other mooring was performance with a thermistors chain at 186 m wd recording at very high temporal sampling rate. From these moorings, a three-week long time series of

temperature and current velocity was acquired. The sampling interval for the ADCP was 2 minutes, each recorded value is made of an average of 17 raw measurements spread over the two minutes intervals. The sampling interval of the thermistors was 1 minute.

	Initial Date	Final Date	Sample interval
Thermistors chain (36.0393 N 6.4690 W)	11/09/2014 10:00	20/10/2014 09:25	1 minute
ADCP moorings (36.0022 N 6.4847 W)	11/09/2014 10:40	29/09/2014 01:43	2 minutes
INGRES-STOCAS (T1)	06/10/2014 06:30	06/10/2014 17:13	Every cast, 24 samples/sec
ECORECLUTAS (T2)	16/10/2014 19:22	16/10/2014 23.52	Every cast, 24 samples/sec

Table-4.1 Descriptive information of data source.

The thermistor chain was 100 m long and occupied a water depth range between 75 and 175 m, porting 50 NKE S2T thermistors spaced 2 m apart from each other. The depth range was chosen in order to capture the possible excursions of the interface between the MOW and ENACW in the mooring site. In the uppermost part of the mooring, a pressure sensor Aquatec Aqualogger 520 PT was attached to track the possible vertical excursion of the instruments.

In addition, profiles of salinity, temperature (CTD) and Acoustic Doppler current profiler (ADCP) were acquired by the Spanish Institute of Oceanography (IEO) during three oceanographic cruises (Fig. 4.1) in the same area (Ecoreclutas October 2014 and Ingres 3 STOCAS October 2014) very close in time to the period of the mooring recording (Table-4.1). CTD data were collected with a Seabird Scientific SBE 911plus CTD while ADCP data were collected by a Lowered Acoustic Doppler Current Profiler (LADCP) system fixed to the rosette-CTD frame.

Finally, bathymetric, acoustic and seismic data from the IEO within the Indemares and Contouriber projects provided details on the sea floor morphosedimentary character along the upper slope of the studied area at different resolutions. For this study, the 1×1 km resolution grid domain covers the GoC and the Strait of Gibraltar (E -8.83º to -5.34º, N 32.95º to 37.23º), the bathymetry obtained from ETOPO-1 data (www.ngdc.noaa.gov) and nautical charts published by the Marine Hydrographic Institute of the Spanish Navy. The local bathymetry from Figures 4.3 and 4.13 from the Indemares and Contouriber projects was gridded at a resolution of 100 m. Visualization and interpretation of bathymetric data were achieved using Fledermaus and Global Mapper. Airgun profiles were acquired during the CONTOURIBER cruise, acquired using different arrangements of 610–910 cu.in GI-airguns adapted to the water depth and quality of the signal. Shot frequency was 6 s and sampling rate of 0.5 ms. During the cruises navigation was controlled by the EIVA NaviPac and the vessel was positioned with a GPS dynamic system. The data were acquired with a three-channel (40 receivers/ channel), 250 m long SIG streamer and recorded with a DELPH system. The

vertical resolution of the seismic profiles is less than 10 m. Processing was performed with the Hotshots software and followed standard procedure, including equalization, low frequency filtering, band-pass filtering, stacking, and resampling to 1 ms. Sub-bottom profiles were acquired using the Parasound P-35 parametric sounder during the CONTOURIBER cruise which worked with a primary frequency of 18 kHz and a secondary frequency of 4 kHz and the recorded signal. It was processed with the Parasound software, and the vertical resolution of these high-resolution seismic profiles is less than 1 m. The entire seismic data set has been visualized and interpreted using the Kingdom Suite software.

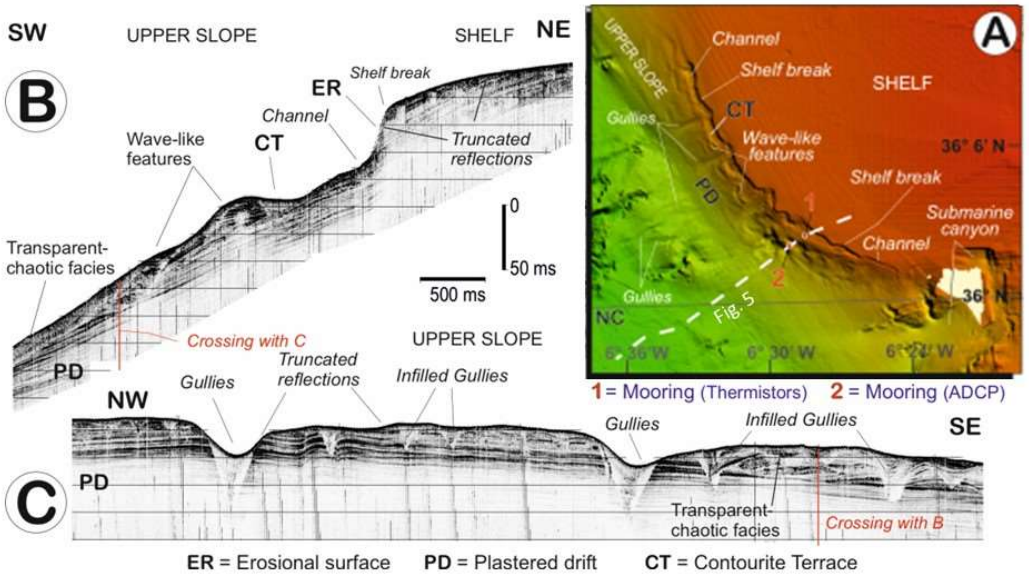

Figure 4.3. A) Regional bathymetric map from the continental shelf to the middle slope indicating the main depositional and erosional features. The location of the two moorings is included. B) and C) Sub-bottom profiles B and C with the main depositional and erosional features in the upper slope (Profiles location in A). ER, PD and CT are defined in figure C.

4.4 Methodology

The analysis methodology combines a descriptive analysis of the across slope distribution of the different water masses, based on the CTD and ADCP data taken during cruises, with more detailed analysis of time series collected from the moorings emplaced right over the sea floor morphological features of interest. Moreover, determination of vertical baroclinic modes, empirical orthogonal function and hydrodynamic modelling are used to aid in the physical discussion of the results. In the following paragraphs the main methodological aspects related to each of those elements of the analysis will be described.

4.4.1 Pre-processing of collected data

CTD data quality was checked by using both automated and manual quality procedures following the SeaDataNet protocols to eliminate the anomalous data (https://www.seadatanet.org/content/download/596/file/SeaDataNet_QC_procedures_V2_%28May_2010%29.pdf). LADCP data were processed using the Common Ocean Data Access System (Visbeck 2002). After their quality control, a graphical representation of salinity, temperature and current velocity along the selected transects (Fig. 4.6) was performed.

Before the analysis of the data from the moored thermistor chain and ADCP, a moving average filtering of 6 points (12 minutes) was applied to the recorded time series of temperature and current velocity to remove unnecessary noise. Due to remaining noise, an additional vertical moving average of 6 points (6 cells) was applied to ADCP data. Temperature series were subsampled at a 2-minute interval in order to be synchronized with the ADCP series. Finally, to obtain a characterization of the barotropic current at the measurement sites a vertical average at each time instance was applied throughout the entire profile.

4.4.2 Vertical dynamical modes

In order to obtain a suitable identification of the origin of the internal tide arriving at the mooring sites it is important to distinguish certain important behaviours of the internal tide propagation. The internal tide perturbations, propagate their energy from the generation places (over near-critical bottom) following beams oriented at given angles with the horizontal (as illustrated in Fig. 4.11), and progressing at both upwards and downwards directions. At certain distances from the generation sites the upwards progressing beams used to be travelled on the pycnoclines now propagating the energy horizontally to places far from their generation region. In the latter situation the vertical structure of the internal tide oscillations is organized into a set of different vertical modes of oscillation often called vertical dynamical (or baroclinic) modes (Marchuk et al., 1970; Kundu et al. 1975; Siedler et al., 1991; Bruno et al. 2000).

The determination of these vertical modes is performed in the frame of the hydrodynamic equations for the rotating case, with the additional assumptions of Boussinesq and horizontally unbounded fluid, negligible non-linear and dissipative effects, flat bottom and horizontal homogeneity of the background stratification. The set of equations of motion, conservation of density and continuity that governs the perturbations are then,

$$\frac{\partial u}{\partial t} - fv = -\frac{1}{\rho_0}\frac{\partial p}{\partial x} \qquad (1a)$$

$$\frac{\partial v}{\partial t} + fu = -\frac{1}{\rho_0}\frac{\partial p}{\partial y} \qquad (1b)$$

$$\frac{\partial w}{\partial t} = -g\frac{\rho}{\rho_0} - \frac{1}{\rho_0}\frac{\partial p}{\partial z} \qquad (1c)$$

$$\frac{\partial \rho}{\partial t} - \frac{\rho_0 N^2 w}{g} = 0 \qquad (1d)$$

$$\frac{\partial u}{\partial x} + \frac{\partial v}{\partial y} + \frac{\partial w}{\partial z} = 0 \qquad (1e)$$

where *u* and *w* are the horizontal and upward vertical component of the perturbation velocity in the Cartesian co-ordinate system (*y,z*); p and ρ are the perturbations of pressure and density, respectively; ρ_0 is the mean sea water density; $N(z) = \sqrt{-\frac{g}{\rho_0}\frac{d\bar{\rho}(z)}{dz}}$ is the buoyancy frequency; $\bar{\rho}(z)$ is the undisturbed density profile.

Assuming normal mode solutions to the set of equations (1a-1d) of the form:

$$(u, v, p/\rho_0) = \sum_{n=0}^{\infty} [\hat{u}_n, \hat{v}_n, \hat{p}_n]\psi_n(z)e^{i(\omega t - k_n x - l_n y)} \qquad (2)$$

$$w = \sum_{n=0}^{\infty} \left[\int_{-H}^{z} \psi_n(z)\, dz\right] \hat{w}_n e^{i(\omega t - k_n x - l_n y)} \qquad (3)$$

$$\rho = \sum_{n=0}^{\infty} \hat{\rho}_n \frac{d\psi_n}{dz} e^{i(\omega t - k_n x - l_n y)} \qquad (4)$$

where k_n an l_n are the wave numbers in the *x* and *y* directions, ω is the angular frequency and $(\hat{u}_n, \hat{v}_n, \hat{v}_n, \hat{p}_n, \hat{\rho}_n)$ are constants. By substituting (2-4) into equations (1a-1e) we obtain the following equation for $\psi_n(z)$

$$\frac{d}{dz}\left[\frac{\omega^2}{N^2}\frac{d\psi_n}{dz}\right] + k_n^2\psi_n = 0 \qquad (5)$$

which along with the boundary conditions at the surface (*z=D*) and bottom (*z=0*)

$$\frac{d\psi_n}{dz} = 0 \qquad (6)$$

constitute a Sturm-Liouville problem with eigenvalues k_n^2. The solution for a given ω is a linear superposition of a set of eigenfunctions $\psi_n(z)$, or vertical modes, satisfying the orthogonality condition

$$\int_0^D \psi_n(z)\,\psi_m(z)dz = \delta_{nm} \qquad (7)$$

where δ_{nm} is the Kronecker delta.

Focussing attention on density and horizontal velocity perturbations, changing the exponential expressions of equations (2) and (4) by cosine functions and particularizing for internal wave modes progressing in the 'x' direction, neglecting (as a first approximation) the earth rotation effects (i.e. f=0), we can write the following simplified expressions

$$\rho(x,z,t) = \sum_{n=1}^{M} \Gamma_n(z)\cos(\omega t - k_n x) \qquad (8)$$

$$u(x,z,t) = \sum_{n=1}^{M} U_n(z)\cos(\omega t - k_n x) \qquad (9)$$

where $U_n(z)$ *and* $\Gamma_n(z)$ are the vertical modes for the amplitude of the density and velocity perturbations; M is the number of the considered baroclinic modes. An example of these vertical functions for the study area is shown in Figure 4.4. For the first baroclinic mode the maximum amplitude of density perturbation locates its maximum in the middle of the upper pycnocline, right where the stratification is maximum, about 40 m wd. That the function keeps the same sign throughout the whole water column is meaning that the isopycnic oscillations occur in the same direction (up and down) in all depths. The first baroclinic mode for the horizontal velocity changes its sign at a depth of about 80 m wd, meaning that when a horizontal velocity maximum is reached in the upper half of the water column a corresponding maximum is happening in lower half in the opposite direction. The prevailing orientations in the horizontal plane of these horizontal current oscillations are rather aligned (with slight variations in direction due to earth rotation effects) with the orientation of the given internal wave front.

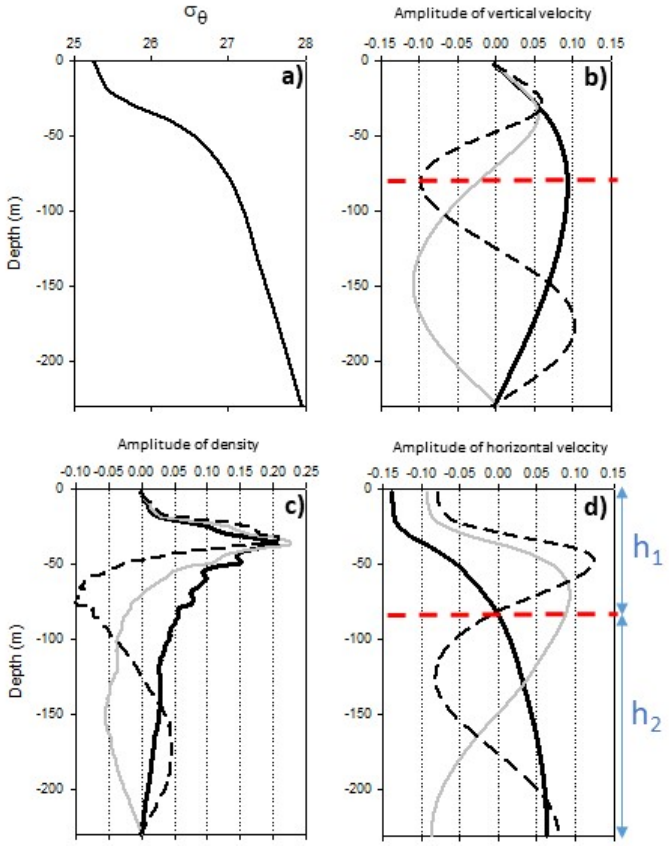

Figure 4.4. Vertical distribution of the amplitude of perturbations induced by the first four baroclinic modes corresponding to a density profile close to mooring site. a) taken close to the mooring site (Fig. 4.1); b) for vertical velocity, c) for density perturbation and d) for horizontal velocity perturbation. First baroclinic mode (solid black line), second baroclinic mode (grey line), third baroclinic mode (dashed black line) and fourth baroclinic mode (solid blue line). Horizontal dashed red line in b) and d) indicates the location of the maximum amplitude of the first baroclinic mode of vertical velocity and the location of the zero crossing of the first baroclinic mode for the horizontal velocity. It would locate the kinematic interface for a two-layer approach to the actual stratification. In this case, h_1 and h_2 would be the upper and lower layer thicknesses respectively.

This behaviour, which is extensive to every baroclinic mode, will be used in next sections to infer the orientation in the horizontal plane of the internal tide propagation by knowing the prevailing orientation of the baroclinic horizontal currents created by the former. Note that this inference does not specify what point is the internal wave advancing towards. For instance, if a prevailing baroclinic current oscillation is being manifested with a E-W orientation, we can infer that the internal tide creating that current is propagating in a line oriented E-W but it is unknown if propagation goes eastward or westward.

Figure 4.5 illustrates the relationship between the vertical displacements of the isopycnics and the tidal current perturbation induced by the propagation towards the right of the first three baroclinic modes. As indicated, for the first baroclinic mode, with the arrival of the crest

created by the isopycnic undulation all the isopycnics are rising in the whole water column and horizontal current velocities reach their maximum intensities above and below the pycnocline, but being directed leftward or rightward, depending if it is above or below the mean depth of the pycnocline. Therefore, a crest of a first internal baroclinic mode propagating rightward would induce leftward currents in the upper layer (above the pycnocline) and rightward current in the lower layer (below the pycnocline). The reversed situation would be met with the propagation of the internal wave trough. Similar reasoning can be argued for the relation expected for the second and third baroclinic modes. For a second baroclinic mode a crest of isopycnics above the mean position of the pycnocline is accompanied by a trough of isopycnics below it. In this case, a rightward propagating second baroclinic mode develops a rightward/leftward horizontal current below an isopycnic crest/trough in the near-bottom layer.

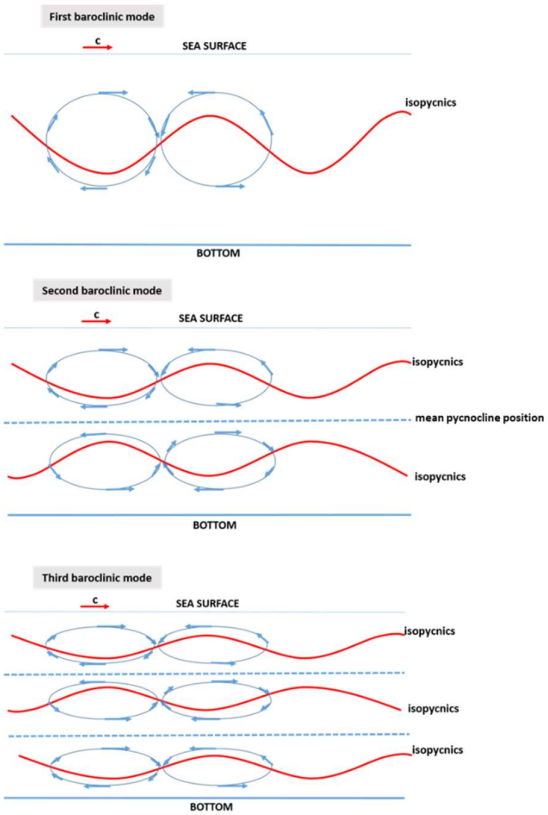

Figure 4.5. Sketch illustrating the pattern of particle circulation and vertical displacement of isopycnals induced by the first three baroclinic modes.

Finally, for a third baroclinic mode we have to consider three layers; an upper layer, a middle layer centered at the mean pycnocline position and a lower layer. An isopycnic crest in the upper layer is accompanied by an isopycnic trough in the middle layer and another isopycnic crest in the lower layer. Therefore, the arrival of a third baroclinic mode crest develops a rightward horizontal current in the near-bottom layer. This relationship between current velocity oscillation and isopycnic undulations has allowed us to infer the preferential

orientation of the multimodal internal tide propagation using the observed baroclinic currents, isolated as described in subsection 4.5.3.4.

4.4.3 Empirical orthogonal function decomposition

The empirical orthogonal function decomposition (EOF) (Wallace and Dickinson, 1972) has been described as a useful technique for separating the barotropic and baroclinic variability of currents (i.e. tidal currents) (Candela et al., 1990; Bruno et al., 2000, 2006). Once these common patterns are determined, the signal of an analysed current velocity components can be expressed as:

$$u(z,t) = \sum_{j=1}^{M} e_j^u(z) a_j^u(t) \qquad (10a)$$

$$v(z,t) = \sum_{j=1}^{M} e_j^v(z) a_j^v(t) \qquad (10b)$$

Where $u(z,t)$ and $v(z,t)$ are the current velocity component in the East and North direction respectively; z denotes the spatial position (i.e. vertical coordinate), t is time, $e_j^u(z)$ and $e_j^v(z)$ are the EOFs (also known as spatial coefficients), $a_j^u(t)$ and $a_j^v(t)$ are the temporal amplitudes of the EOFs, and M is the number of EOFs (equal to the number of time series included in the analysis).

In addition, this technique has been applied on the temperature time series recorded in the thermistor mooring. In this case, the temperature signal at each thermistor depth may be expressed as:

$$T(z,t) = \sum_{j=1}^{M} e_j^T(z) a_j^T(t) \qquad (11)$$

The application of this technique on the current and the temperature has helped to find a common pattern of oscillation between isotherms (as tracer of isopycnals) and current. Also, these patterns can be identified with the vertical baroclinic modes associated with the internal tide dynamics of the measurement site.

4.4.4 Barotropic hydrodynamical model

To complement the analysis of the relevant hydrodynamic mechanisms we have used the barotropic hydrodynamic model UCA2D (Álvarez et al., 1999). It is a two-dimensional (depth-averaged), nonlinear, finite-differences, high-resolution UCA2D hydrodynamic model that numerically solves the vertically-integrated equations of conservation of mass and momentum, by means of a Crank-Nicolson semi-implicit scheme on an Arakawa-C staggered grid (Álvarez et al., 1999). Bottom and wind drags are parameterized by the so-called 'law-of-the-wall'. At the open boundaries, the system is forced with the harmonic constants of elevation and currents for the given tidal constituents. The model was forced at the western and eastern open boundaries by the mean barotropic flow (Z0) and the main semidiurnal M2 tidal constituent, inferred from the IBI_REANALYSIS_PHYS_005_002 reanalysis data (www.copernicus.eu) and model results by González et al. (2013), and run for 10 M2 tidal cycles with a time-step of 5 s. Data from the last 5 cycles were used for the harmonic analysis, once numerical stability and energy conservation was assured.

Validation was performed by comparison of the model simulations with observed data taking from different sources: Puertos del Estado (tide stations), Le Provost et al. (1995), Álvarez (1999), Álvarez et al. (2003), García Lafuente (1986), and Candela (1990). It provides rms-errors of 4.6 cm and 3.6º for the amplitudes and phase-constants of tidal elevation, respectively; and 7.3 cm/s and 4.9º for currents (Gomiz-Pascual et al., 2021). The use of this model is intended to simulate the tidal barotropic current and to compute the barotropic forcing (BF) of internal tides (Quaresma and Pichon, 2013) using the formula:

$$BF = \frac{Ucos(\omega t - \phi_u)}{D}\frac{\partial D}{\partial x} + \frac{Vcos(\omega t - \phi_v)}{D}\frac{\partial D}{\partial y} \qquad (12)$$

Where for a given tidal component of frequency ω, U and V are the amplitudes of the corresponding barotropic zonal and meridional tidal current; ϕ_u and ϕ_v their corresponding phase lags; D is the bottom depth.

4.5 Results

4.5.1 Morpho-sedimentary characterization of the study area

The study area presents a 40-43 km wide continental shelf that turns from a E-W orientation at the Strait of Gibraltar to almost NW-SE orientation at the easternmost part of the Gulf of Cádiz (Fig. 4.1 and 4.3). Truncated reflections in sub-bottom profiles indicate the erosive

character of the outer continental shelf. The shelf-break in this area presents an abrupt change in gradient, from the <1° in the continental shelf to an up to 10° steep upper slope, that forms the NE (landward) wall of a 1-1.5 km wide terrace at depths of 150 to 190-200 m wd. Towards the NW, a channel-like feature is incised parallel to the shelf-break in the shallowest part of the terrace. It is 1-1.5 km wide, about 22 km long and up to 5 m deep with a U-shaped thalweg profile. Sub-bottom profiles show reflections truncated at the NE wall of the terrace and channel (Fig. 4.3). The upper slope is narrower (about 2 km wide) and concave-upwards in the SE area, where it connects with the middle slope at depths of 200-250 m. The upper slope turns to a convex-upwards shape towards the NW, as it increases its width to about 4.5 km and its deepest limit at the connection with the middle slope occurs at depths of up to 420 m. Sub-bottom profiles of the upper slope show parallel stratified facies, that correspond to the southern extreme of the contouritic plastered drift defined by Hernandez-Molina et al. (2014a), Brackenridge et al. (2018) and García et al. (2020).

In the study area the topography is irregular, with wave-like features below the outer rim of the channel. These sediment waves are characterized by highly undulated reflections forming mounded elongated reliefs about 1.5 km long and with crests oriented parallel to the shelf-break (Fig. 4.3). They are interrupted by downslope-trending U-shaped gullies, up to 25 m deep and 1 km wide. These gullies (Fig. 4.3 and 4.13) extend from the outer rim of the terrace down to the middle reaches of the upper slope, at around 400 m wd, and their location coincides with semi-circular escarpments in the shelf-break. Sub-bottom profiles show that these gullies, with truncated reflections along their flanks, are the few active ones among many other inactive, smaller gullies that have been infilled and cannot be distinguished in the present-day bathymetry (Fig. 4.3). Transparent-chaotic deposits are also locally identified overlying the parallel layered reflections

4.5.2 Vertical transects near the mooring site

Figure 4.6 shows the vertical sections of salinity, potential temperature and current velocity components along the two hydrographical transects near the mooring sites. The salinity profile in the transect T1, located furthest from the moorings, shows that the core of the MOW reaches bottom depths along the upper slope as shallow as 150 m wd, therefore very close to the shelf break. The current velocity section shows that the mean flow associated with the T-S properties averaged bottom current (spatially averaged the cells of the ADCP data for each water mass) velocities obtained for the MOW is ~0.30 m/s flowing NW and ~0.16 m/s for the ENACW flowing SE (Fig. 4.6C and 4.6D). Note that these values must not be understood as mean current intensity since the effects of the possible tidal current contribution has not been removed. However, the current directions agree with the expected mean flows directions within the upper core of MOW and ENACW.

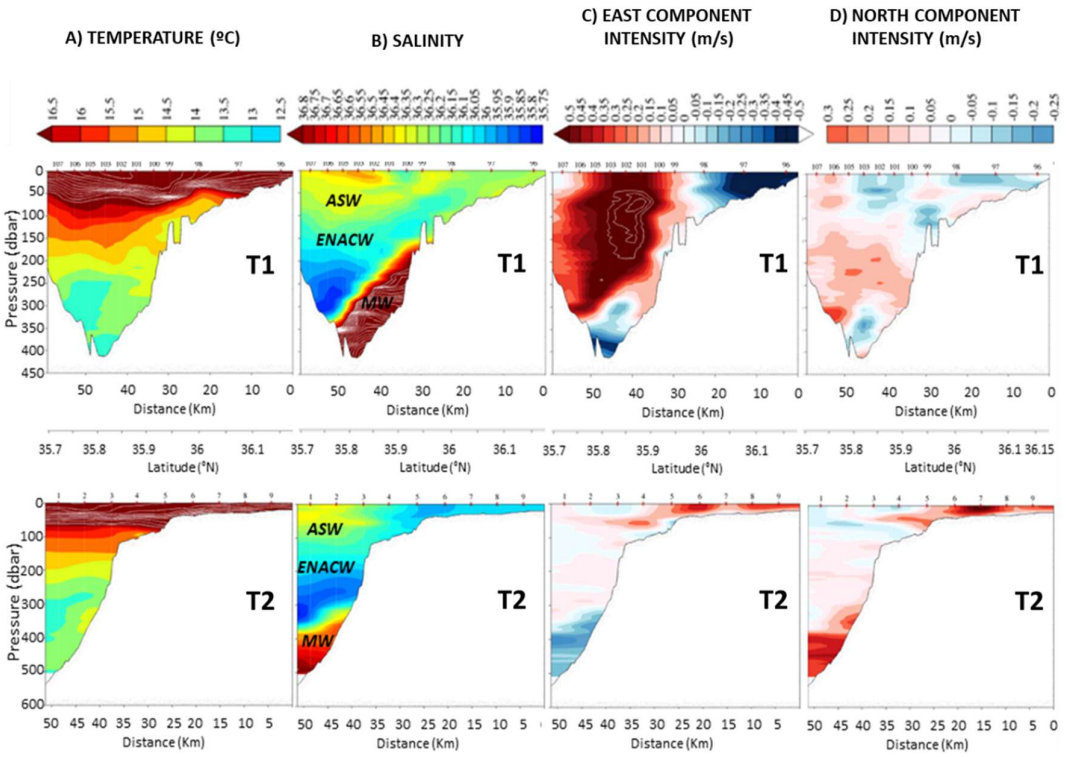

Figure 4.6. Vertical sections of temperature (A), salinity (B) and instantaneous current velocities along the transects T1 and T2 indicated in the Figure 4.1.

In transect T2, the one that lies closest to the mooring site, the MOW core is found farther south and deeper (below 300 m) moving in a northwest-ward direction (Fig. 4.6C and 4.6D). Here the ENACW is above the upper core of the MOW throughout the section and moving southeast-ward with intensities 0.10-0.15 m/s. The interface between the MOW and ENACW cores cut the continental slope bottom in a range of 300-350 m wd.

The ASW (with higher temperature and salinity) is occupying the upper 100 m wd and below this depth is located an interface where the ASW is gradually mixed with the ENACW which is extended down to about 300 wd, the mean depth of this interface is located about 200 m wd in the two transects (T1 and T2) (Fig. 4.6B). This position corresponds to previous observations (Criado-Aldeabuena et al 2006; Bellanco and Sanchez-Leal 2016).

4.5.3 Temperature and ADCP profiles recorded at the mooring sites.

The temperature record of the deepest thermistor in mooring 1 (Fig. 4.7), reveals that the arrival of colder and deeper water at tidal frequencies.

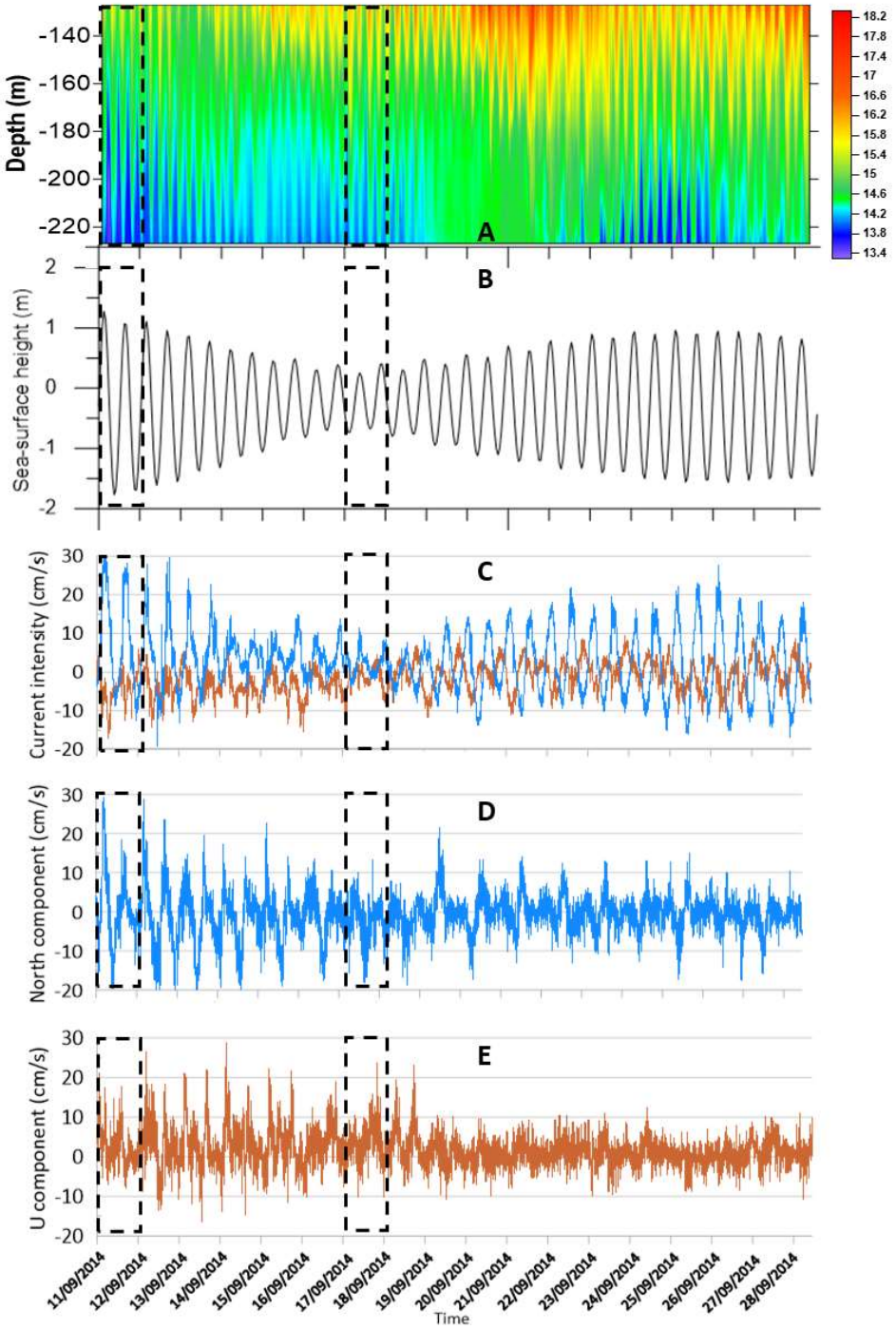

Figure 4.7. Time series of different variables: A) time evolution of temperature profiles by the moored thermistors chain (1 in Fig. 4.1); B) sea level tidal prediction in the Port of Cadiz; C) barotropic current velocity recorded by the moored ADCP (2 in Fig. 4.1), north component and east component; D) and E) are the time series of north and east components at the deepest ADCP bin. The first rectangle indicates the spring tide analyzed in Figure 4.9 and the second rectangle is the neap tide analyzed in figure 4.10.

In order to determine the origin of these colder waters, the temperature and salinity profiles taken in the INGRES-STOCA campaigns (the closest in time to the mooring records) nearest to the mooring places have been considered (Fig. 4.8a). At intermediate depths, the temperature and salinity decrease downward to minimum values at about 325 m wd and then increase, gently in the case of temperature, and abruptly for salinity (Fig. 4.8a). This change of tendency in both values denotes the limit between the ENACW and the MOW and can be used as a key indicator for the ENACW-MOW interface. It is worth noting that although farther seawards from the continental slope a more pure ENACW may be found within a concrete water depth range, in our study area (over the continental slope) the ENACW is gradually mixed with the ASW and with the MOW and it does not appear in a clear-cut way throughout the water column.

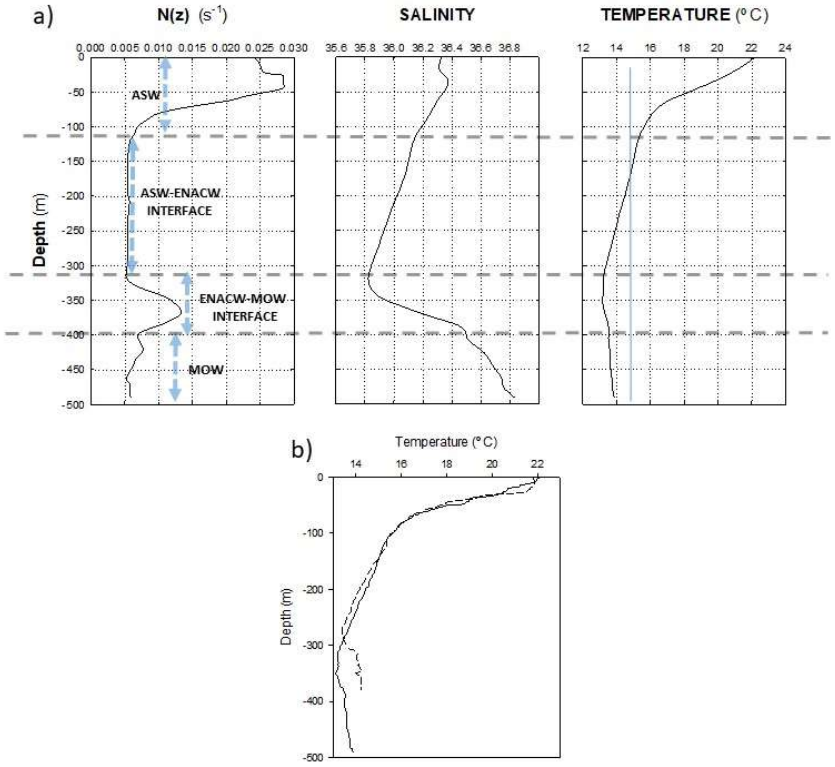

Figure 4.8. A) N(z), salinity and temperature profiles close to the moored thermistor chain showing the location of the layers resulting from the confluence of the different water masses in the studied zone. The ENACW-MOW interface can be seen and the details of the temperature and salinity variation around this interface. The location of the ASW-ENACW is also shown. It must be noticed that the ENACW-ASW interface is characterized by a roughly constant N(z) extended throughout a thickness of about 200 m. B) Temperature profiles at the two westernmost stations on the transect T2 (shown in Fig. 4.1), the more seaward in solid line and the another in dashed line.

The temperature profiles recorded the shallowest depth for the colder water at 135 m (*profile 1*) during spring tides (Fig. 4.9). In this profile, it is identified the arrival of the upper part of

the ENACW-MOW interface over the terrace, note the temperature increase shown by the profile 1 between the 135 and 155 m wd. Note that the minimum temperature of the profile recorded by the thermistor chain is about 13.9 º C while the minimum temperature of the EANACW-MOW interface recorded in the CTD cast (shown in Figure 4.8a) is about 13.2. However, when we progress shoreward over the slope the interface rises and the characteristic ENACW minimum of temperature increases. This latter fact probably due to more intense mixing with the ASW. In the figure 4.8b shown are two profiles of temperature corresponding to the two first casts (from the most seaward position) on the transect T2 (shown in Fig. 4.1). It can be seen this shoaling of the minimum temperature and its increase when progressing over the continental slope landwards.

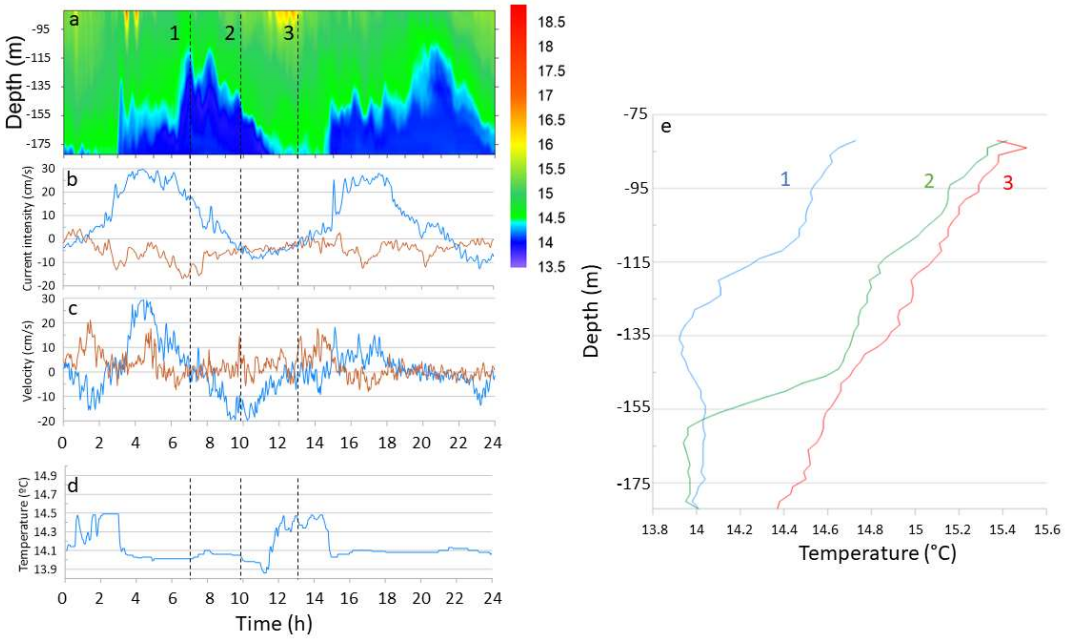

Figure 4.9. Short record (24 hours) of time variations in temperature and horizontal current velocity during a spring tide period. On the left are, a) the time evolution of temperature profiles; b) the barotropic current intensity for north (blue) and east (brown) components; c) the current velocity recorded at the deepest ADCP bin for north (blue) and east (brown) components; d) temperature record at the deepest thermistor; e) are the temperature profiles at time indicated in a.

Only another clear arrival of this interface, happening twenty-four hours later, was recorded during the whole recording period. In the light of these results, the arrival of the upper part of this interface to the mooring site seems to be quite occasional. Evidently, during neap tides the ENACW-MOW interface was never recorded in the mooring site. In the selected period corresponding to neap tides (Fig. 4.10) we cannot see any increase of temperature in the deepest levels. Therefore, it seems quite clear that the origin of the cold water arriving at the mooring is the ENACW, which is responsible for a temperature minimum located in average within the 300-350 m wd range shown in Figure 4.8.

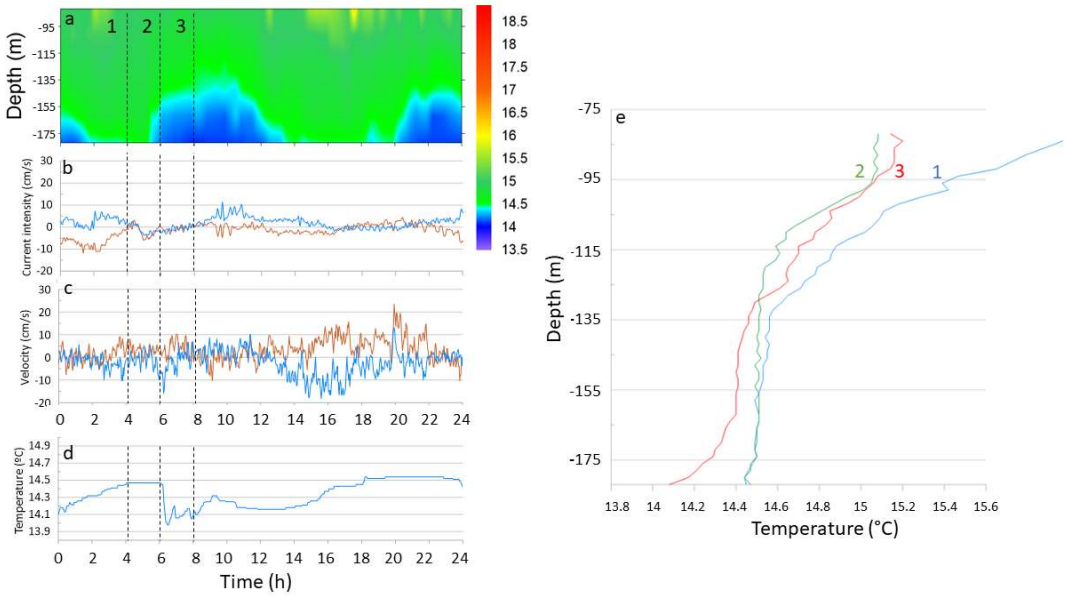

Figure 4.10. The same as Figure 4.9 but for a neap tide situation.

During the spring tide period (Fig. 4.9), the arrival of colder water starts when the peak of the barotropic tidal current is reached. However, the coldest water (in this occasion accompanied with the arrival of the ENAWC-MOW interface) is recorded three hours later. Nevertheless, during the neap tide, with a clearly less intense barotropic current, colder water occurrence has smaller amplitude and, in this case, occur three hours before the barotropic tidal current peak.

The barotropic current shows intensities ranging between 5 and 30 cm/s and show a time average value directed towards northwest (Fig. 4.7d). The peaks towards southeast hardly surpass 10 cm/s. However, if the total current (barotropic and baroclinic tidal current) is considered, current peaks close to the bottom of about 20 cm s^{-1} are recorded in that direction. During spring tides bottom current velocities could reach up to 30 cm/s, coinciding with a cold-water intrusion of about 60 m above the seafloor (Fig. 4.9). Nevertheless, during neap tides bottom current intensities are only 10 cm/s with a cold-water intrusion of about 30 m above the seafloor (Fig. 4.10). Therefore, the intensity of bottom currents has a marked dependence on the tidal conditions, and it seems fairly evident the existence an important contribution of the internal tide in the time variability of current and temperature at the measurement sites.

4.5.4 Internal tide dynamics

4.5.4.1 Local effect of a barotropic flow over a two layer flow.

A common manifestation of the internal tide is that associated to the local effect of a barotropic tidal current on a two-layer water column when those current opposites or favors the mean flow in the upper or lower layer. Thus, when the barotropic current point at the same direction of the upper layer mean current, the interface between the two layers deepens while when the barotropic current points at the opposite direction the interface rises. This kind of kinematic pattern of internal tide is observed, for instance, at Camarinal Sill in the strait of Gibraltar (Bray et al. 1990).

The arrival of cold water peaks are not on phase with the peaks of barotropic tidal currents (Figures 4.9 and 4.10). Vertical displacements of isopycnic surfaces are not affecting by local barotropic currents, so it is indicating that others factors as internal tides generated in other locations can generate these movements. This aspect will be treated in the next subsections.

4.5.4.2 Generation of internal tide by the effect of tidal currents acting on critical bottom

The generation of internal tides over the sea floor requires: (i) an appropriate density stratification close to the bottom, (ii) sufficiently intense bottom current, and (iii) a bottom slope so that the bottom current can produce the necessary vertical velocity for generating internal waves.

In order to explore if the density stratification close to the bottom and the bottom slope would favour the local generation of the internal tide it is necessary to assess the quotient

$$\gamma = \frac{\alpha}{\beta} \qquad (13)$$

Where α is the slope of the bottom and β is the slope of the internal wave beams close to the bottom which is given by:

$$\beta = \pm\left(\frac{\sigma^2 - f^2}{N^2 - \sigma^2}\right)^{1/2} \qquad (14)$$

σ is the internal wave frequency (i.e. 1.4 10^{-4} s^{-1} for the main semidiurnal tidal constituent M_2); f is the local Coriolis frequency at a latitude φ=36 º (representative of the Gulf of Cádiz),

where $f=2\,\Omega\sin(\varphi)$, Ω being the modulus of the angular frequency of earth rotation; and N is the local Brunt-Väisälä (or buoyancy) frequency.

The value given by (14) allows us to analyse the slope criticality (i.e., how generated internal wave beams are oriented with respect to the slope) according to the ratio between the seafloor slope angle (α) and the slope of the internal wave beams (β). We have transmissive or subcritical conditions when $\beta < \alpha$, critical or near critical conditions when $\beta \approx \alpha$; and reflective or supercritical conditions when $\beta < \alpha$ (Cacchione et al., 2002).

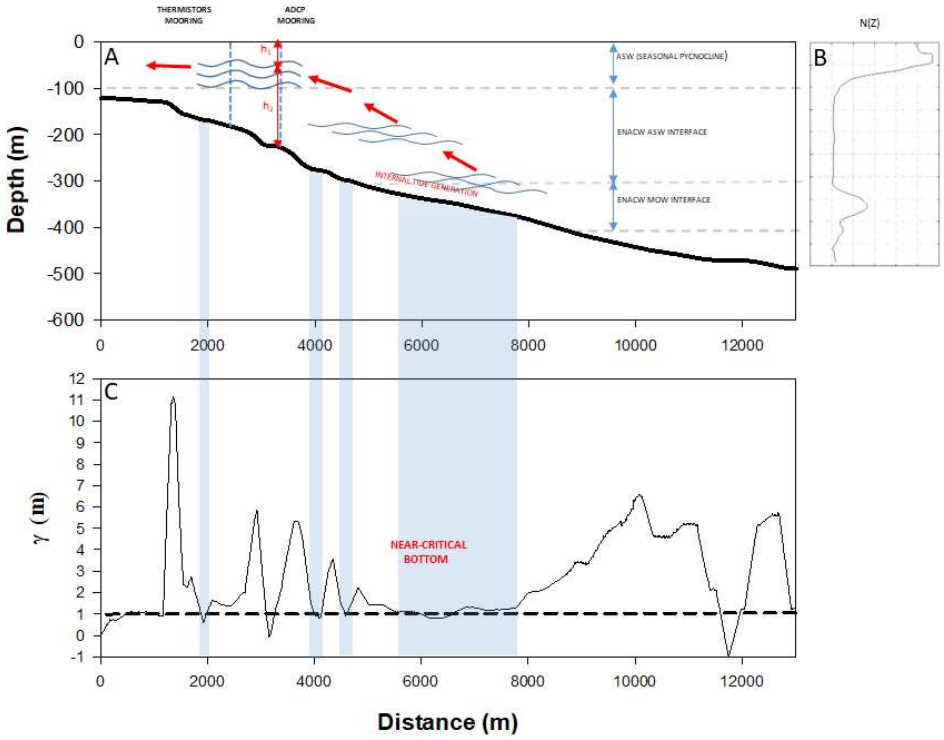

Figure 4.11. (A) White dashed transectof Figure 4.3 which comprises part of the continental shelf and slope. Wavy lines illustrate the water particle displacement induced by the barotropic tidal current; red arrows are the internal wave beams; h_1 and h_2 are the the upper a lower layer thicknesses. (B) Buoyancy frequency profile. (C) Gamma coefficient corresponding to the .The blue shaded vertical bars locate the strips over the continental slope where near critical conditions for the internal tide generation (gamma close to 1) are met.

In the following paragraphs we will explore the field of barotropic tidal current in the analysed region and, subsequently, we will explore the possibilities for local generation of internal tides in the vicinity of the mooring sites.

Figure 4.12 shows modelled barotropic current ellipses of the main semidiurnal M_2 constituent over the eastern GoC and the Strait of Gibraltar. The tidal current intensities around the mooring site are in good agreement with the observed barotropic tidal current intensities (Fig. 4.7). The barotropic tidal current intensity is reduced westward, being almost

zero about 25 km westward of the mooring site (Fig. 4.12c). Based on these observations the tidal barotropic current dynamics where the mooring sites are located is in a transition zone throughout which the tidal barotropic current undergoes a sharp reduction.

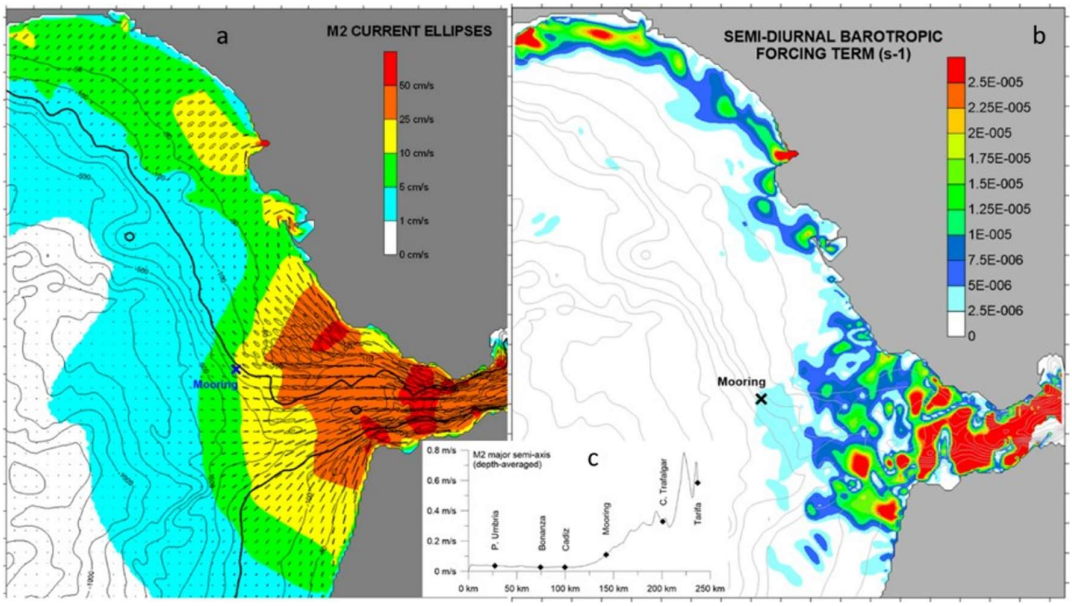

Figure 4.12. Numerical simulations from the UCA2D model. a) map of amplitudes of tidal current (major semi-axis) due to the main semidiurnal tidal constituent M2; b) map of Barotropic forcing due to M2 semidiurnal constituent (eq. 12); c) M2 major semi-axis along the 200 m isobath (dark contour line in figure a).

As shown in the previous section a clear internal tide has been recorded at the mooring sites. However, at this moment, the place where this internal tide is coming from remains unknown. Is it being generated locally close to the mooring site? Is it coming from remote places? Is it coming from remote and local generation places together? In order to give answers to these questions, the barotropic forcing of internal tide has been computed using the equation (12) and shown in Figure 4.12b. The highest values of this forcing are met within the Strait of Gibraltar close to the Camarinal and Spartel sills and close to the westernmost side of the Morocco coast. Therefore, it must be considered that the internal tide generated in these remote places could arrive at the mooring sites contributing to the observed vertical variations of isopycnics and horizontal currents at this site.

In the vicinity of the mooring sites, the barotropic forcing is not as high as in the abovementioned places, on the western side of the Strait of Gibraltar. However, this forcing could still be high enough to locally generate internal tides if the bottom slope there accomplishes a coefficient $\gamma \approx 1$ (near-critical bottom). Figure 4.11 shows the γ coefficients computed along the bottom profile of Figure 4.13b using the angular frequency of the main semidiurnal constituent M_2 (ω=1.4 10^{-4} rad s^{-1}).

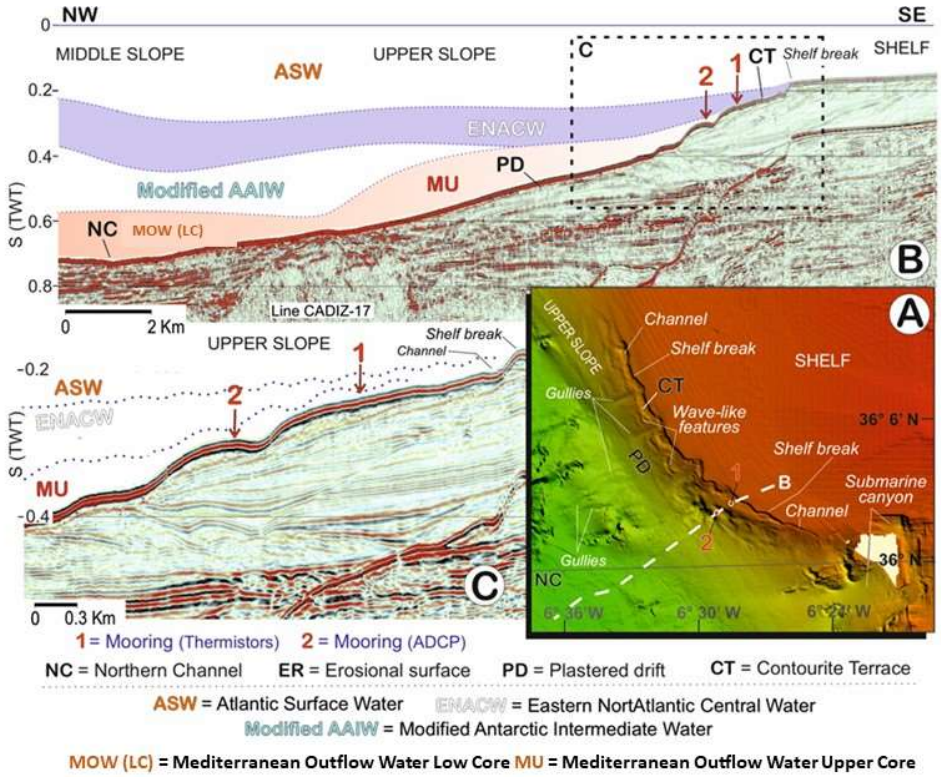

Figure 4.13. A) Seismic profile (Cadiz-17) sections from the continental shelf to the middle slope indicating the main depositional and erosional features, and the regional water masses. The location of the interfaces between the different water masses are depicted, showing as the upper core of the MOW (MU) is able to eventually invade the location of the two moorings is included. TWT—two-way travel time. B) Detail of the upper slope where the two moorings were located. The vertical and lateral variations the upper slope terrace under the action of the internal tide.

As can be seen, there is a wide strip (located between 300 and 400 m wd) where the bottom slope yields near-critical values ($\gamma \approx 1$). The computed slope of the Internal tide beams generated in this near-critical bottom zone along the water columns, indicates that this internal tide would be able to reach the upper slope where the moorings are deployed without being reflected further seawards, as explained in Figure 4.11. It is worth considering the narrower strips of near-critical bottom located landwards, which are bounded by supercritical bottom zones. Here the generated internal tide could propagate landwards over only limited distances and would be reflected towards open sea or broken over the sea floor of adjacent supercritical bottom regions. The mooring sites are located in the middle of them.

Depending on the distance of the observations location with respect to the generation region the horizontal current oscillations produced by the internal tides are not generally in phase with the local barotropic tidal current in the observation site. On the one hand, the tidal barotropic current in the generation region may be out of phase with respect to the local barotropic current, the larger the distance from the generation region, the greater the delay. On the other hand, even when this delay between barotropic tidal currents between the

generation region and the observation site be small, another source of delay is always assured due to the time needed by the internal tide in travelling the distance separating the generation region and the measurements point.

It is worth noting that the used barotropic model does not consider other likely sources of internal wave generation that arrives at the observations site such as, for instance, the tidal dynamics of the MOW upper core close to the near-critical bottom strips (Fig. 4.4b). The upper core of MOW could be channeling part of the internal tide generated in other remote places, for instance Camarinal Sill. This internal tide could, in turn, generate new internal tides over the critical bottom regions south of the moorings, which could propagate towards the moorings location. Note that this MOW-associated internal tide has nothing to do with the local tidal barotropic current and this contribute again to an arbitrarily varying phase lag between the local tidal barotropic current and the internal tide.

4.5.4.3 Inferring the internal tide origin by analysing baroclinic current roses.

As a first step to gain insight into the origin of the internal waves arriving at the observation site it will be worthwhile to determine which are the predominant directions of the baroclinic current associated to the internal tide here. This information may be achieved by analysing the current rose of this baroclinic current along the water column which has been obtained after:

(i) Removing the barotropic current from each of the original current components (zonal and meridional). Barotropic current is computed as the depth-average of each current component at each time instant.

(ii) Removing from the signal of the previous step the time averaged current at each cell depth. It is worth noting that the obtained baroclinic signal must be explained by the internal wave activity in the observation site. This step is intended to remove the effect of long term baroclinic currents from the current roses and to enhance, instead, the effect of shorter period baroclinic oscillations as those promoted by the internal tides.

Figure 4.14 shows the current roses at 12 m above the bottom and 28 m depth for spring and neap tides. During spring tides, from both roses we can infer that current with the highest intensity are oriented in the northeast-southwest (NE-SW) direction although some events of high current intensity may occur in the northwest-southeast (NW-SE) direction. In the mooring sites, the NE-SW direction is roughly perpendicular to the continental shelf break while the NW-SE is roughly parallel to it (see map of Figure 4.1). During neap tides, as described, the tidal current intensities are weaker. The highest current intensities are

manifested in the NW-SE directions although some frequent peaks of currents may be associated to the NE-SW directions.

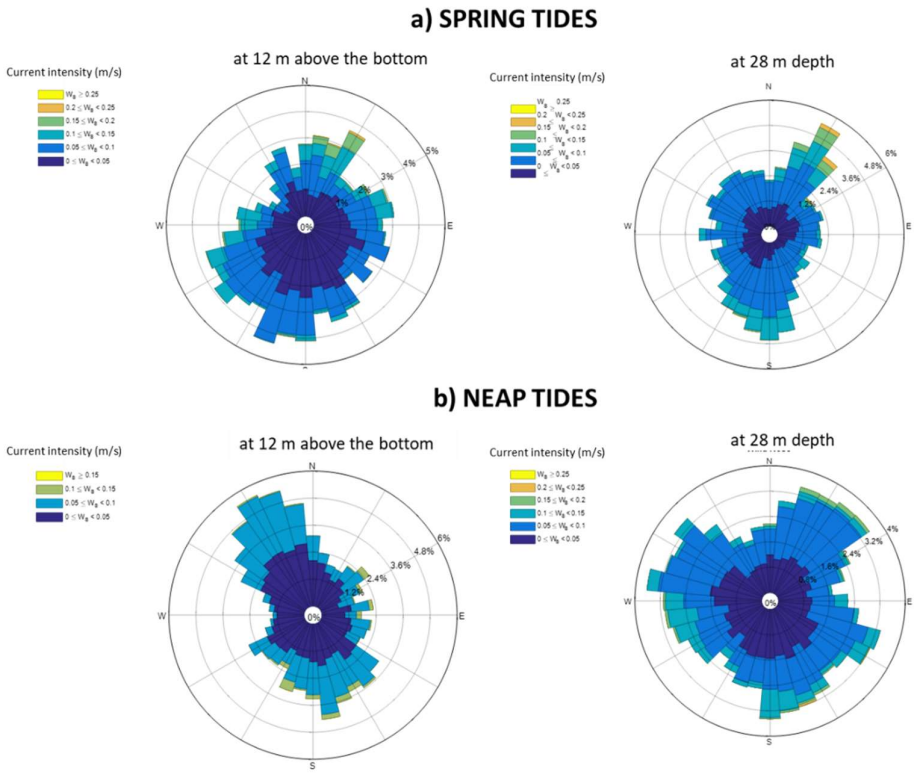

Figure 4.14. Current roses for the baroclinic signal associated to internal waves activity. The represented signals have been obtained after subtracting first, the barotropic current (the instantaneous depth averaged value of current) and second, the mean (time-averaged) current profile.

Independently of the spring-neap cycle, using the association between baroclinic current direction and orientation of internal waves propagation explained in section 4.4.2, these current roses reveal two different patterns of internal tides arriving at our observation sites, one with waves propagating with a NE-SW orientation and another one with waves oriented NW-SE.

At this point of the analysis, it is not fully clear where these internal tides are coming from. However, for the NE-SW type a generation place further north-east from the mooring is unlikely since subcritical bottom slopes, not favourable to internal wave generation, are found there. Therefore, NE-SW internal waves should proceed from some place further southwest. A more than likely place could be found in the previously identified stretch along the continental slope (Fig. 4.11) where near critical bottom would favour the internal tide generation there. However, the internal waves moving with a NW-SE orientation could originate at some remote places further west or east from the mooring sites as suggested in previous paragraphs. As mentioned in section 4.4.2 the internal tide, coming from places of generation that are far enough away, arrives at the observing stations organized into a set of

vertical baroclinic modes. The identification of this multi-modal character of the internal tide in our observations will be dealt with in the following subsection.

4.5.4.4 Baroclinic modes.

Figure 4.4 shows the first three vertical baroclinic modes of the M_2 internal tide corresponding to the density profile taken at the station of section T2 closest to the mooring site (Fig. 4.1). Although this cast was performed 17 days after the end of the analysed recording period (Table-4.1), it is representative of the vertical variability pattern which will be useful to quantify their presence (or not) in the current velocity and temperature observations during data acquisition at the mooring site.

The presence of these baroclinic modes in our observations has been identified using the EOF analysis. This was made possible by comparing the vertical profiles of spatial weights yielded from the analysis with the theoretical baroclinic modes profiles (shown in Fig. 4.6). The first four EOFs resulting from the analysis of temperature series explain more than 90% of the variance of the temperature series in the whole sampled water column (Fig. 4.15d). The first EOF which explains the majority of the variance (68 %), shows a spatial weight distribution that resembles the amplitude distribution of the first baroclinic mode of density variations (Fig. 4.6c), indicating that the amplitude of the temperature oscillations increases from bottom to the middle of the water column.

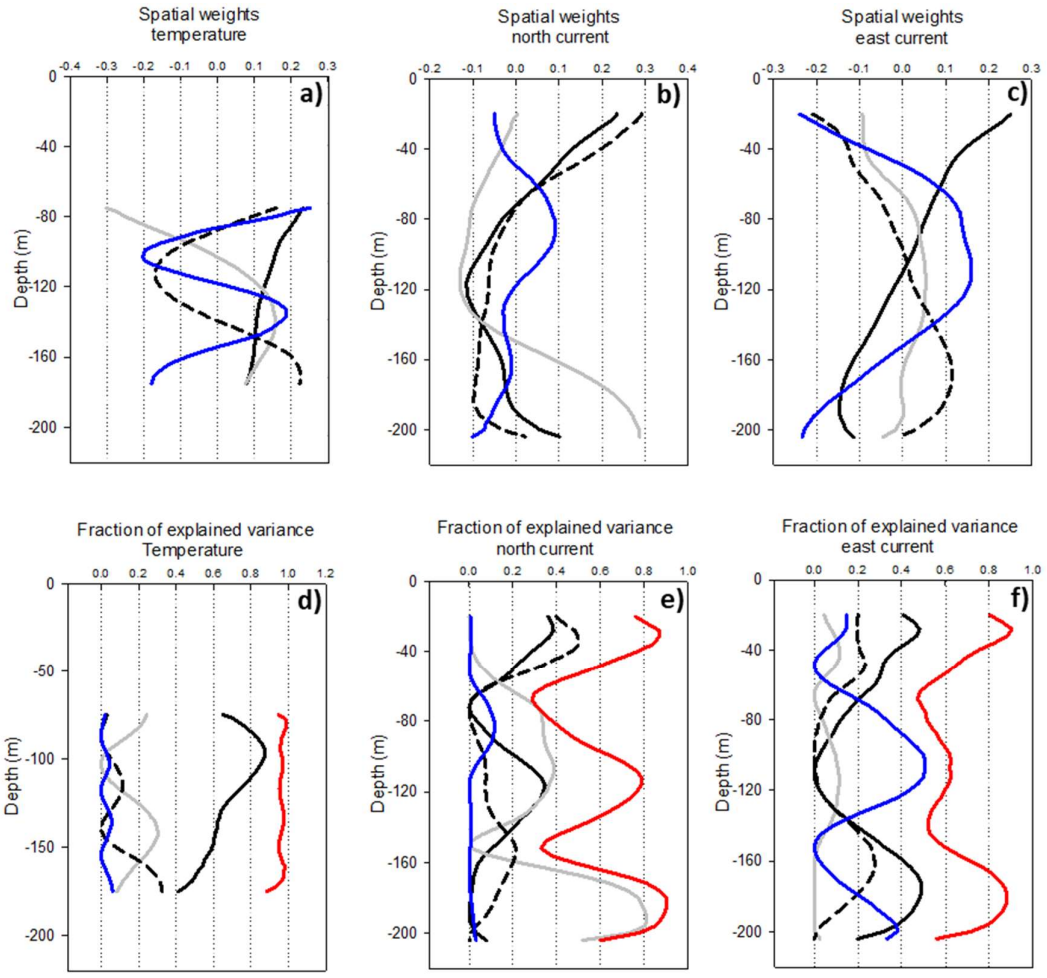

Figure 4.15. Results from the EOF decomposition on temperature and baroclinic horizontal current velocity time series. In a), b) and c) are shown, for temperature and horizontal components of the current, the spatial weights corresponding to the first (solid black line), second (solid grey line) and third (dashed black line) EOF modes. In d), e) and f) is shown, for the temperature and horizontal components of current, the fraction of variance explained by each mode throughout the water column sampled, for the first EOF mode (solid black line), the second (solid grey line), the third (dashed black line), the fourth (blue line) and the joint contribution of all three modes (solid red lines). e) and f) the same as c) and d) but for the east component of the current.

The second and third EOF modes, explaining about 28 % of variance, do not offer an easy association with the second and third baroclinic modes; this association is not always straightforward, and is caused by an incomplete coverage of the sampled water column or the possible linear correlation among the time variations of some baroclinic modes. As described in Bruno et al. (2000), EOF decomposition is not able to separate two correlated baroclinic modes into two different EOF modes. Anyway, the existence of the second and third EOF modes is clearly indicating the involvement of baroclinic modes higher than the first, in the explanation of the temperature variations associated with the internal tide at the mooring site and, in turn, in the internal tide dynamics in the area. In addition, it must be considered that these higher baroclinic modes are more important near the bottom (120-180 m) where they

account for almost 30% of the temperature variance. Figure 4.16a shows the reconstruction of the time series of temperature recorded at the deepest thermistor using the first three EOF modes. It can be seen that the first EOF mode reproduces quite well the basic oscillation patterns. The next two modes must be considered in order to explain some important features of the temperature observations here. For instance, without the participation of the second and third EOF modes it is impossible to reproduce the sustained cooling in time shown by the observations.

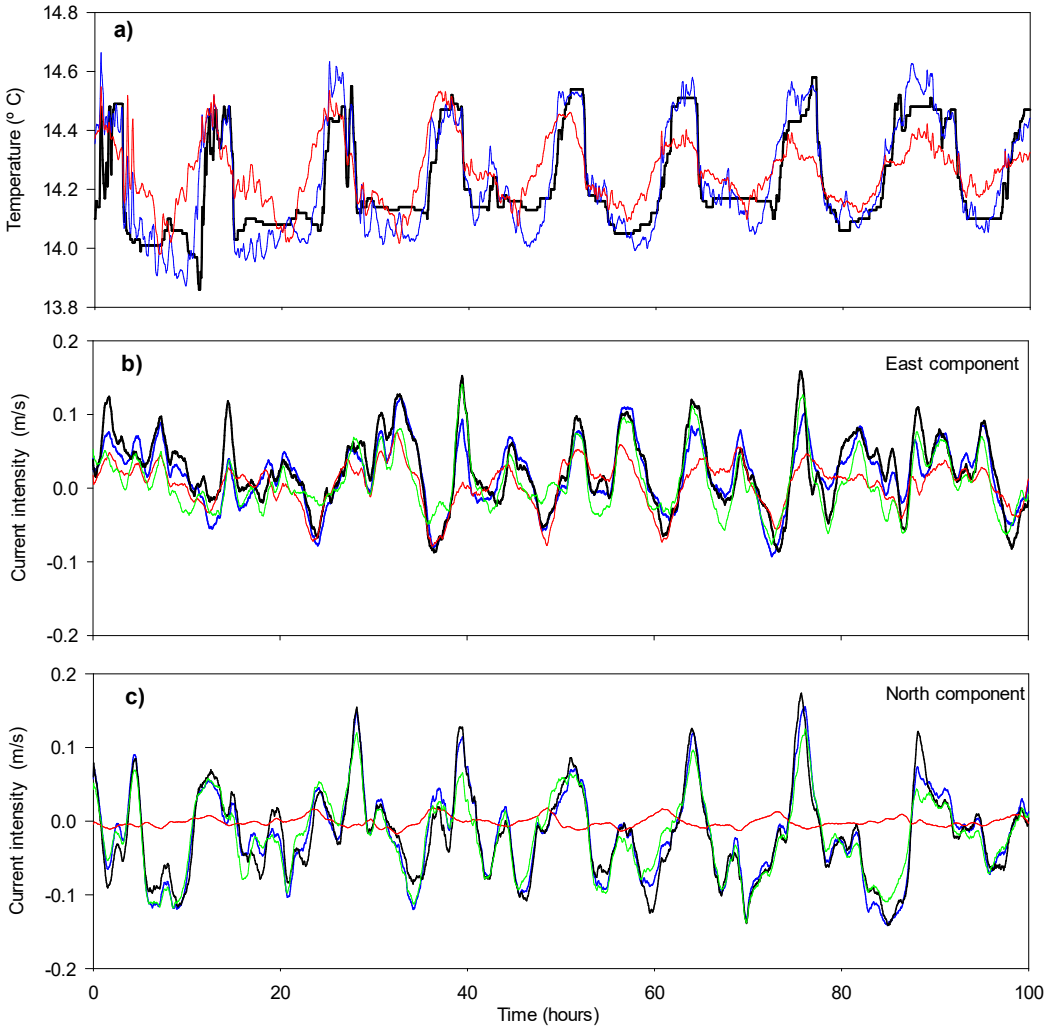

Figure 4.16. a) Temperature series recorded at the deepest thermistor depth (thick black line), time series of the first EOF mode contribution to temperature variations (red line) and time series of the contribution due to the first three EOFs (blue line). b) and c) the same as in a) but for the East and North components of the baroclinic horizontal current velocity, respectively, at the third ADCP cell (at 25 m from bottom). The observed baroclinic current (black line), the contribution of only the first EOF (red line), the joint contribution of the first and second EOFs (green line), the joint contribution of the first four EOFs (blue line).

Concerning the EOF decomposition of current velocity series, the corresponding results (Fig. 4.15b, 4.15c, 4.15e and 4.15f) show that the first four EOFs explain 66% and 65 % of variance, for east and north components of the current velocity respectively, throughout the whole water column.

The first EOF resembles for the east component, the vertical structure of a first baroclinic mode while for the north component it seems to be made of a first baroclinic mode (more dominant) with certain additional contribution of a second baroclinic mode. It is present at similar intensity in both current components. Considering that the spatial weights for the two horizontal components of the current in the upper layer have the same sign. This is meaning that an increase in the east(west) component is accompanied by an increase in the north(south) component and this results in a oscillatory current oriented along a NE-SW axis. As explained in section 4.4.2 the propagation of the involved internal tide should show the same orientation.

The second EOF seems to be made of a superposition of a first and second baroclinic mode. It is present above all in the north component of the current being almost inexistent in the east component. Based on the latter, the propagation of the involved internal tide must have a N-S orientation.

Moreover, the third EOF seems to be composed of a superposition of a first and second baroclinic mode, with predominance of the first one. It is present at similar intensity in the two current components. The different sign of the spatial weights for the two components in the upper layer indicates an oscillatory current oriented in the NW-SE axis. Consequently, the involved internal tide is propagating as in the case of the first EOF with a NW-SE orientation.

Finally, the fourth EOF resembles the behaviour of a second baroclinic mode and is present, above all, in the east component of the current. Consequently, the involved internal tide must propagate with a W-E orientation.

These propagation patterns identified with the first four EOFs are in good agreement with the information shown by the baroclinic current roses in Figure 4.14, where the existence of two different propagation patterns, one following a NW-SW orientation and the another a NE-SE orientation were initially suggested.

The time behaviour of the horizontal baroclinic currents based on the sum of the resolved EOF modes superimposed is shown in Figures 4.16b and 4.16c. For the east component, a suitable fit is only achieved when the first three EOFs are used. In the case of the north component, the contribution of the first EOF is insignificant, and the suitable fit is achieved by adding the second EOF.

Therefore, the basic characteristics of the baroclinic tides in the observation site are quite well reproduced by the four first EOFs. In order to reproduce several peaks in the east and north

current components (Fig. 4.16b and 4.16c) the involvement of EOFs are needed in which the presence of the second baroclinic mode is evident, which demonstrates a decisive participation of at least this baroclinic mode in the internal tide description.

It is important to note that there is not a clear visual correspondence between the temperature oscillations at the deepest thermistor (Fig. 4.16a) and the baroclinic current components (Figs. 4.16b and 4.16c), despite the proximity between the thermistors and ADCP moorings. This may be due to the fact that the amplitude of density perturbations (and temperature) depends inversely on the wave number k_n (Kundu, 1993). It implies that two baroclinic modes with similar current velocity amplitudes, but different wave numbers could show fairly different density amplitudes. The baroclinic mode of less wave number (larger wavelength) will show greater density amplitudes. Also, lower k_n values are corresponding with lower wave frequency (greater wave periods). Because of this, it is hard to visualize a clear relationship between the current velocity perturbations and their corresponding density perturbations above all when different internal tide patterns are contributing jointly to the density (and temperature) oscillations at a unique observation point.

4.6 Discussion

4.6.1 Internal tide generation

4.6.1.1 Near-mooring generation

An observational evidence of internal tide generation near the observation sites is that contained in the internal tide pattern oriented in a NW-SW axis and associated to the first EOF determined in section 4.5.4.4. It must be coming from the SW, since there is no other plausible generation places further NE of the moorings. This first EOF is also the most important for explaining the baroclinic current variance at the observation site. More concretely, this internal tide could have been generated over the near-critical strip on the middle part of the slope (see Fig. 4.11), as explained in section 4.5.3. In addition, Figure 4.11 also shows the narrower strips of near-critical bottom located landwards, which are bound by supercritical bottom zones. In these localized portions of the slope, the generated internal tide could propagate landwards over only limited distances close to the bottom (Dauxois et al., 2004) and would be reflected towards open sea or broken over the sea floor of the adjacent supercritical bottom regions (Hall et al, 2013). Note that the internal tide signal associated with these latter processes, more erratic and transient, is not expected to be captured by any

EOF and likely it is contributing to the baroclinic current variance not explained by the four EOFs considered.

It is worth noting that the buoyancy frequency value that determines the near-critical-bottom strips through Equation (13) are those characteristics of the ENACW layer located in the depth range of 110-300 m. This layer is characterized by a roughly constant value of N=0.005 rad s^{-1} (see N(z) profile in Figure 4.8a). Therefore, these near-critical-bottom regions for the internal tide generation are related to the presence of the ENACW laying on that portion of the bottom slope. However, the presence of these strips of near-critical bottom seems to be extended along the slope to the westernmost limit of the terrace, coinciding roughly with the sharp decrease of the barotropic tidal current intensity (see Fig. 4.12). It is then expected, that over the part of the slope located further westwards from the terrace, internal tide generation is enabled while it is not over the slope further west of the terrace, where neither near-critical bottom nor intense barotropic current forcing are present. Even when the ENCAW is bathing the latter slope floor and yields a near-critical bottom strip, the local internal tide generation would not take place because of the absence of an intense barotropic tidal current. In addition to the barotropic current, the vicinity of the MOW upper core to the near-critical bottom strip in the studied area provides another plausible source for tidal-driven vertical displacements that can give rise to internal tide generation over that strip (as illustrated in Fig. 4.17a). In this sense, passing the easternmost tip of the along-slope channel the upper MOW core deepens, lying over rather subcritical bottom ($\gamma < 1$), which does not favour the internal tides generation close to the core.

These particular dynamics of the internal tide generated in places near to the observation sites seems to be crucial for understanding some singularities of the bottom morphology existing here, as will be discussed in section 4.6.2.

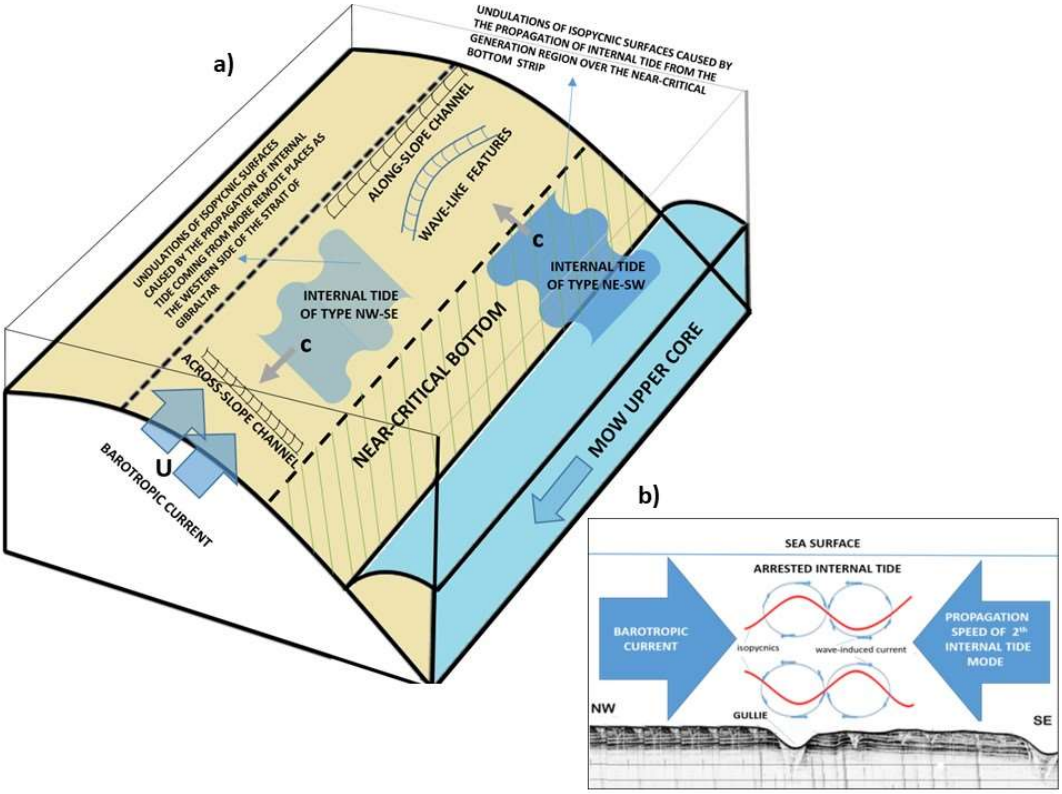

Figure 4.17. a) Illustration sketching of the two main types of internal tides acting in the studied region and their involvement in explaining the along- and across-slope channels formation. b) Illustration of across-slope channel formation due to the arresting of a second mode internal tide by the barotropic tidal current. This happens when the propagation speed of the baroclinic mode is equal in magnitude, but in the opposite direction, to the barotropic current. The channel is expected to be formed where the wave-induced bottom current matches the barotropic current direction since here the two currents are in phase producing a more localized and intense net bottom current in the place where the channel is situated.

4.6.1.2 Remote generation

The internal tide patterns coming from remote generation places seem to be those associated to the second, third and fourth EOFs. The second and third EOFs could be associated to internal tide patterns that come from S and SE, respectively, since the more plausible nearby generation places point at the western part of the Strait of Gibraltar or the continental slope along the north-western coast of Morocco (see Fig. 4.12). However, these two EOFs could contain some contribution from internal tide coming from Portimao Canyon and Gorringe Bank (located respectively south and southwest of the southern Portuguese coast) with high values of the barotropic forcing term (Quaresma and Pichon, 2013; Izquierdo and Mikolajewicz, 2019) and even from some other interaction of the MOW cores with bottom topography singularities that could be met along its pathways. These latter sources may also be behind the internal tide associated to the fourth EOF which seems to come from W.

4.6.2 Effects of the internal tide dynamics on the seafloor geomorphology

The results of our analysis suggest a direct link between the hydrodynamics and the particular morphological characteristics of the study area. The interfaces between the ENACW and the MOW and between the ENACW and the ASW in the study area affects the seafloor on the upper slope (Fig. 4.2 and 4.13). The ENACW-MOW interface is identified regionally at depths around 350 m wd (see Fig 4.9) but in the study area it is able to reach depths of around 150 m. On the other side, the ENACW-ASW interface occupies the depth range between 100 and 300 wd, thus bathing the seafloor of the two major along-slope morphological features, the terrace and the along-slope channel. The two features disappear to the NW coinciding with the deepening of this interface. Terraces are often identified in zones affected by intense currents, and constitute the proximal part of plastered drifts, affected by weaker flows (Cattaneo et al., 2017; Miramontes et al., 2019b). Terraces often show an erosive character (Hernández-Molina et al., 2009; 2017; Preu et al., 2013; Thiéblemont et al., 2019), due to the activity of intense flow, represented in the study area by the truncated reflections identified in the TOPAS profiles (Fig. 4.3).

The wave-like features identified just basin-ward from the outer rim of the terrace on the upper slope are also interpreted to have a genetic link with oceanographic processes. The activity of internal tides generated in nearby places over the near-critical bottom slope strips (see Figures 4.5 and 4.17a) seems to be the best likely responsible for the incision of the along-slope channel on the proximal part of the terrace and of the secondary features as the wave-like features (Fig. 4.13), as it was proposed for the South China Sea (Yin et al., 2019).

To investigate some of the effects on the sea floor that could be produced by the internal tide hydrodynamics it will be worthwhile the use the two-layer approach to the actual continuous stratification (Lynett and Liu, 2004). In this approach, which reproduces the main behavior of the first baroclinic mode, the interface separating the upper and lower layers would be located at the depth where the maximum amplitude of the first baroclinic mode for vertical velocity is located (Camassa and Tiron, 2011), which in our case it is at around 80 m wd (as indicated in figure 4.4b). Now we can determine the thicknesses of the upper (h_1) and lower (h_2) layers as the vertical distances from that maximum to the surface and bottom, respectively. Roughly, h_1 encompass the ASW layer while h_2 extends throughout the ENACW-ASW and ENACW-MOW interfaces.

Taking into account that if the channel is placed at around 140 m wd, the quotient between the upper and lower layer thicknesses (h_1/h_2) is greater than one, the isopycnic undulations of the internal tide will suffer a rather abrupt transformation from undulations of depression(elevation) to undulations of elevation(depression) (Keulegan, 1953), once the

shelf break is reached. Considering that the internal tide is coming from the lower slope, it would propagate as a depression wave, since there the quotient h_1/h_2 is lower than one, and would change to an elevation wave when the shelf break is reached. The later change occurs together with a current velocity intensification in the lower layer and a more than likely breaking of the wave close to the shelf break (Lauton et al., 2021). These abrupt changes close to the shelf break could be behind the channel formation right along the shelf break. Also, as shown in Figure 4.11, the proximal part of the terrace shows narrower strips of near-critical bottom located among strips of supercritical bottom. The internal tide generated over the near-critical bottom strips and propagating landwards, is expected to be reflected basin-ward or broken once reaching the adjacent supercritical bottom. Both processes have been proven to be very energetic and able to affect considerably the seafloor morphology (Dauxois et al, 2004) and could be responsible for the wave-like features on the terrace seafloor morphology.

The westward limit of the terrace also coincides with the strip where the barotropic tidal current intensities are sharply reduced (Fig. 4.12) and also where the MOW upper core is weaker in intensity, deepens and separates from the near-critical bottom. Without barotropic current or MOW core close to a near-critical bottom the local internal tide generation and its hydrodynamic effects on the upper slope would disappear.

In addition, once the arrival of high order baroclinic modes in the study zone is clear, the barotropic flow could be able to trap them, if barotropic current intensity equals the propagation speed of one of these modes (Miramontes et al, 2020; Vázquez et al., 2006; Vázquez et al., 2008). A similar process has been claimed to explain the location of a channel excavated along the proximal part of a contourite terrace in Mozambique by Miramontes et al (2020). An illustration of this mechanism is shown in Figures 4.17a and 4.17b.

Using the density profile close to the mooring site shown in Fig. 4.6a, we have determined that these speeds are 0.74, 0.35 and 0.25 m/s for the first, second and third baroclinic modes, respectively. Assuming that these values are representative of the studied zone, a second or third baroclinic mode would be susceptible to get trapped by the barotropic flow along the terrace, strengthening the local velocities of water masses. As described by Miramontes et al. (2020), the trapping of these baroclinic modes is followed by a growth of the isopycnic undulations and baroclinic current intensities below the arrested isopycnic crests or troughs, provoking the intense erosion along very localized strips of the seafloor which may lead to the formation of across-slope incised features, such as the gullies shown in Figures 4.3c, 4.13a and 4.17b.

The head of the gullies in the study area are incised in the outer part of the terrace, coinciding with indentations of the shelf-break. This location suggests a different origin than that proposed for the gullies identified NW of the studied area by García et al (2020), and explained by diffuse, sheet-like turbidity currents presumably originating on the shelf or alternatively low-density cascading water flows. The transparent-chaotic deposits identified

locally on the upper slope also suggest the occurrence of mass transport deposits originated in zones within the upper slope where intense hydrodynamic processes are actives. In that sense, we highlight the two following types of processes: (i) internal tides generated in nearby places downslope and (ii) the trapping by the barotropic flow of particular baroclinic modes that compose the given internal tide (i.e. second and third modes), arriving at the area from remote places, could trigger on the upper slope area, dominant gravitational processes (i.e. turbidity currents) which, in turn, contribute to maintaining and accentuating the pre-existing across-slope channels.

In addition, the variations related to ENACW, MOW and their interfaces are controlled by seasonal, longer-term sub-millennial, millennial and orbital climatic fluctuations associated to glacial/interglacial periods (Llave et al., 2006; Hernández-Molina et al., 2014b, 2016; Bellanco and Sánchez-Leal, 2016; Sánchez-Leal et al., 2017; Roque et al., 2019; Sierro et al., 2020). Consequently, the present-day upper slope morphology represents the final record of the long-term effect of both ENACW and MOW circulation and the fluctuation of the ENACW-MOW interface throughout time, as well as their modulation by secondary processes (barotropic tidal currents, internal tides and surely other shorter period internal waves). The inactivation and infilling of numerous small upper slope gullies, and the highly complex morphology of the study area reflects this variability.

4.7 Conclusions

The obtained results have determined the relevance of the secondary hydrodynamic processes related to barotropic tidal currents and internal tides hydrodynamics in shaping the sea-floor morphology. However, some important morphological features such as the terrace existence, along- and across-slope channels and wave-like features are found only over a limited along-slope distance from the western mouth of the Strait of Gibraltar. One the one hand, this seems to be related to a drastic weakening in the intensity of the barotropic tidal current and, on the other hand, the weakening of the intensity of the MOW upper core and its displacement to depths far from the near-critical bottom that favours the internal tide generation. The internal tides governing the hydrodynamics of the area are separated in (i) those generated close to the terrace over near-critical strips disposed along the slope, propagating preferentially from SW to NE and (ii) those generated in places further away and propagating preferentially along the slope from SE.

The near-critical strips giving rise to the generation of the first type of internal tides is determined by the presence of the ENACW layer in the area that provides the needed stratification in order to achieve that the slope of the internal tide beams matches with the bottom slope over these strips. Also, the vicinity of an intense MOW upper core close to these

near-critical strips would favour the generation of this type of internal tides. These internal tide dynamics seems to be responsible for the formation of the along-slope channel and wave-like features.

However, the second type of internal tides propagating along-slope seems to be responsible for the formation of the across-slope channels (gullies). The formation mechanism is based on the arresting of higher order baroclinic modes that make up the internal tide by the barotropic tidal currents.

The long-term effect of both ENACW and MOW circulation and internal tides affecting the ENACW-ASW and ENACW-MOW interfaces over time have been responsible for the onset and the evolution of an upper slope terrace. Additional similar studies and deeper knowledge of bottom currents above the seafloor and the modulation of different oceanographic processes are needed for a better understanding of its implications on sea-floor morphology, sedimentation and geo-habitats.

Capítulo 5

ROLE OF ATMOSPHERIC FORCING ON THE WATER MASSES ON THE CONTINENTAL SLOPE OF THE EASTERN GULF OF CÁDIZ

5.1 Introduction

The continental shelf and slope are the link between shallow coastal and deep waters in more regions of the different oceans. This area, whose average depth is usually 200 m depth, is of high scientific interest due to the presence of multiple interactions between physical, biological, and geological processes.

The continental platform of the Gulf of Cádiz (GoC) has been one of the most studied during the last three decades. It contributes to the border between Mediterranean and Atlantic waters (Maldonado & Nelson, 1999b; Hernández-Molina et al., 2014a; Sánchez-Leal et al., 2017). The continental shelf of GoC is divided into two parts, delimited by Cape Santa María and the Portimão canyon (Figure 5.1). In the western part, the shelf is 15-20 km wide while it is increased to 40 km near the Strait of Gibraltar (SoG). The circulation in the eastern part is quite active due to the proximity of SoG (Figure 5.1) and the Atlantic-Mediterranean interaction (Farmer et al., 1988; Price et al., 1993).

The deep outflow of Mediterranean water, towards the Atlantic Ocean, takes a main north-westerly direction as a result of the pressure gradient, Coriolis force, and bottom friction (Gasser et al., 2017). The lower-density Atlantic water is emplaced above the saltier Mediterranean water and it is directed towards the Mediterranean Sea through SoG (Ambar & Howe 1979, a,b; Price et al., 1993; Baringer & Price, 1997; Sánchez-Leal et al., 2017). Previous works in the area have detailed the surface circulation patterns within GoC (Criado Aldeanueva et al., 2006; García-Lafuente et al., 2006), identifying three main water masses located in the area: Surface Atlantic Water (SAW), Eastern North Atlantic Central Water (ENACW) and Mediterranean Water (MW).

The wind is a key factor in the circulation patterns of water masses on the Portuguese coast: Fiuza et al. (1982) observed that westerly winds (Ponientes) generate upwellings on the Portuguese coast, while easterly winds (Levantes) block them. Also, the wind has a great influence on modifying coastal dynamics within GoC as they generate counter currents during episodes of strong easterly winds (Relvas and Barton, 2002, Criado-Aldeanueva et al., 2006, Garel et al., 2016, Oliveira et al., 2021).

Cape Trafalgar (CT, Figure 5.1) is a region of relative cold waters and high chlorophyll values for almost the entire year (Navarro & Ruiz, 2006; Vargas-Yañez et al., 2002; Vargas et al., 1999; Sala et al., 2018), where the interaction between tides, winds, and bathymetry are the main modulating factor of upwelling processes (Bolado-Penagos et al., 2020; Sala et al., 2018; Vargas-Yañez et al., 2002). However, all these studies were focused on the surface area near the coastline, and the upwelling influences from circulation pattern change caused by winds and other factors such as bathymetry, tides, and river discharges.

Atmospheric forcing over the western Mediterranean Sea is the main modulator of subinertial fluctuations in SoG, with periods greater than 30 hours (Candela et al., 1989; García-Lafuente, 2002a). Other authors have observed that both remote atmospheric forcing, high pressure over the Ligurian Sea and local wind over the SoG and the Alboran Sea, modulate the input of Atlantic water through the Strait (Macias et al., 2016, Dastis et al., 2018, Bolado-Penagos et al., 2021) (blue square in Figure 5.1A).

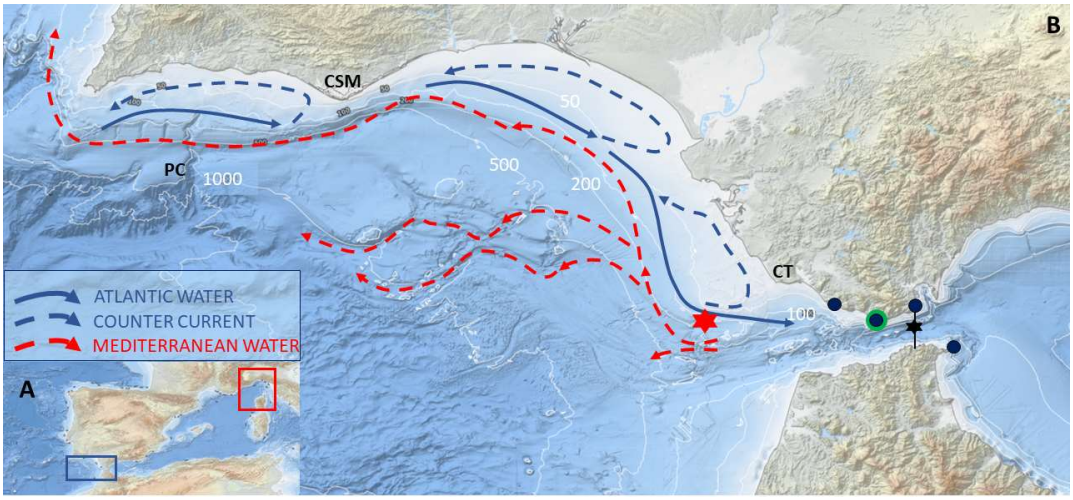

Figure 5.1. Study site. A, general image of the Strait of Gibraltar (blue frame) and the Ligurian Sea (red frame). B, detailed area of the Strait of Gibraltar showing bathymetry, main water masses circulation patterns, and locations of the experimental stations. Red star: mooring of a chain of thermistors; black circles: location of High-Frequency Radar antennas for measuring surface currents; green circle: Tarifa tide gauge; black line: cross-Strait section of radar-measured surface currents time series; black star: hydrodynamic model data point. CSM: Cape Santa Maria, PC: Portimão canyon; CT: Cape Trafalgar.

Tidal dynamics is essential to understand the interaction of water masses that takes place on the eastern platform of GoC and its geomorphological implications on the seabed (Ambar and Howe., 1979a, b; Price et al., 1993; Baringer and Price., 1997, Sánchez-Leal et al., 2017). Nevertheless, previous studies did not discuss the effect of the subinertial variability (with characteristic periods longer than 30 hours in this area) that can affect the interface between the different water masses in the water column and which could have geomorphological implications on the platform as well.

For all these reasons, the main objective of this work is to evaluate how atmospheric forcing (local and remote fluctuations of the atmospheric pressure and local wind) affects the dynamics of water masses on the continental shelf and slope in the southeastern area of GoC.

To achieve this objective, different data have been analyzed: (i) in situ observations of the water column (thermistors chain and Acoustic Current Doppler Profiler, ADCP), (ii) observations of surface currents obtained from the High-Frequency Radar (HFR) system placed in the SoG (Figure 5.1B), (iii) high-resolution numerical model, (iv) sea level

observations, and (v) reanalysis meteorological data in the study area, as well as within the SoG and the Ligurian Sea.

5.2 Data and Methodology.

To study the influence of atmospheric forcing on the water column of the eastern shelf area of GoC, it was necessary to analyze observations along the water column, as well other oceanographic and atmospheric variables with plausible influence on the study area according to previous studies.

Vertical fluctuations of the water column were evaluated from a chain of thermistors that was moored between September and October 2014 on the bottom of the continental slope of the GoC (36.0393ºN, 6.4831º W) (Figure 5.1B, red star). This mooring manoeuvre was carried out in the hydrographic vessel Malaspina of the Spanish Marine Hydrographic Institute (IHM). The mooring consisted of a chain of 50 NKE model S2T600 thermistors placed every 2 m, which allowed obtaining temperature values within a depth range between 75 and 175 m. The original sampling interval was 1 data per minute, although the observations were hourly and daily time-filtered for comparisons with the other variables. The chosen depth range was intended to contemplate the variations of the interfaces between the different water masses in the study area, especially that associated with ENACW and MW. The sampling period was 40 days (Table 5.1).

Observations of surface currents were acquired by the HFR system of SoG, operated by Puertos del Estado, which has 3 CODAR Seasonde antennas (Tarifa, Punta Carnero, and Ceuta; black circles in Figure 5.1B). Subsequently, in February 2019, this system was expanded with a fourth antenna placed at Cape Camarinal. This methodology allows obtaining hourly fields of surface currents of the eastern area of SoG, with a spatial resolution of approximately 1.5 km and a range that reaches up to 60 km from the coast, and they are accessible via OpenDAP (http://opendap.ports.es/thredds/catalog.html). HFR observations from this system were previously validated by Lorente et al. (2014), Soto-Navarro et al. (2016), and Chioua et al. (2017) among others. To identify possible connections between the observations recorded by the thermistors chain and the current dynamic in SoG, a transversal transect (W-5.4492°, N -35.9503°/ 36.0315°, black line in Figure 5.1B) was extracted from the HFR data for the same period (September-October 2014). Additionally, to determine the time-variability of the processes observed during 2014, the time series of the zonal velocity component for the entire year 2019 has been extracted for the same latitudinal transect. When HFR measurements were not available, linear interpolation was carried out.

Sea level data was obtained from the tide gauge at Tarifa (Figure 5.1B, blue circle), which belongs to Puertos del Estado Tide Gauge Network (REDMAR). In this case, the historical data was downloaded from the agency's website (http://www.puertos.es/es-es/oceanografia/). Hourly data has been downloaded for the period between September-November 2014.

An ADCP with an attached pressure sensor was moored near the bottom close to the thermistor chain location. The sampling period was 18 days, and the interval sampling was 2 minutes just to obtain the best resolution (Table 5.1). The ADCP mooring was accidentally released so it is sampling period only covers approximately the first half of that from the thermistor chain. The sea level height values inferred from the pressure sensor observations were used to validate such from the SAMPA hydrodynamic model, to complete the whole study period by using current and sea levels from this model (see Figure 5.2G). SAMPA is a regional circulation model, implemented in the area of the SoG, which comes from the global circulation model of the Massachusetts Institute of Technology (MIT-gcm, Marshall et al., 1997). The spatial domain covers GoC - SoG- Alboran Sea. Its horizontal resolution in the open borders is 8-10 km, densifying to its maximum within the Strait (300-500 m). Tidal and meteorological forcings at the boundaries come from the model described in Carrere and Lyard (2003) and from the HAMSOM model (Álvarez Fanjul et al., 2001). On the surface, the model is forced every 3 hours with wind values obtained by the Spanish meteorology agency (AEMET) through the HiRLAM model (Cats, 1996).

	Initial Date	Final Date	Sample interval
Thermistors chain (36.0393 N 6.4690 W)	11/09/2014 10:00	20/10/2014 09:25	1 minute
ADCP moorings (36.0022 N 6.4847 W)	11/09/2014 10:40	29/09/2014 01:43	2 minutes

Table 5.1. Descriptive information of moorings. ADCP: Acoustic Doppler Current Profiler.

For the analysis of the wind regime in the area, data from the MM5 meteorological model (Penn State/NCAR Fifth Generation Mesoscale Model, Grell et al., 1994) was used. A high-resolution, nested-grid downscaling of this model was implemented for the Andalusian region, centered on the SoG with a maximum resolution of 3.3 km (Reyes, 2015). The MM5 outputs were compared with historical data obtained from Puertos del Estado open-sea buoy at GoC, obtaining an excellent fit (Reyes, 2015). In this study, we used hourly horizontal wind data at 10 m above sea level.

Ekman pumping was derived from horizontal wind data (Eq. 1), which gives an estimation, under certain assumptions, of the vertical speed w_E during upwelling/downwelling processes related to divergence/convergence of currents due to Ekman transport in the area:

$$w_E = \frac{1}{\rho_0}\left[\frac{\partial}{\partial x}\left(\frac{\tau_y}{f}\right) - \frac{\partial}{\partial y}\left(\frac{\tau_x}{f}\right)\right] (1)$$

where τ_x and τ_y are the wind-stress components in the x (zonal) and y (meridional) directions, respectively; ρ_0 is the mean density of the seawater in the study area (1028 kg/m3); and f = $2\Omega\sin\varphi$ is the Coriolis parameter, Ω and φ being, respectively, the angular velocity of Earth's rotation and latitude.

Finally, atmospheric pressure at mean sea level (mean sea-level pressure, MSLP) data in the Ligurian Sea area was obtained from the ERA5 atmospheric reanalysis Copernicus Climate Change Service (https://cds.climate.copernicus.eu/cdsapp#!/dataset/reanalysis-era5-single-levels?tab=form), since Bolado-Penagos et al. (2021) found a clear relationship between the variations of atmospheric pressure in this area and the currents and water masses transport in SoG. The spatial and temporal resolutions of the ERA5 product are 0.25°, and 1 hour respectively. The so-called inverse-barometer effect of MSLP, which causes the sea level to rise (fall) as MSLP decreases (increases) and was removed from the analyzed sea level series in order not to mask other possible sources of variability.

A low bandpass fast Fourier transform, (FFT) filter was applied to all analyzed variables, with a cut-off period of 30 hours, to remove aliasing from the tidal signal that could remain after a simple daily averaging. In this way, the low-frequency (subinertial) signal forced by other than the tide is isolated, allowing to analyze how the dynamics of the water masses developed in the study area.

5.3 Results.

5.3.1 Observations

Thermistors chain allowed to observe variations in temperature through the water column in the continental slope of GoC (red star in Figure 5.1B). These temperature observations (Figure 5.2A) show an oscillation related to the arrival of cold water (<14.0 – 14.5 °C) at the lower part of the water column (about 160 m depth), which could be related to the presence of the interface between ENACW and MW water masses (Bellanco & Sánchez-Leal, 2016).

Meanwhile, the presence of warmer water (> 15 ºC) is observed in the upper part of the column (above 100 m depth).

The amplitude of the isotherms performs, a direct relationship with the cycle of spring/neap tides during the first two weeks of the recording period (Figures 5.2A and 5.2G), as previously commented by Roque et al. (2022). However, around October 2nd (neap tide), water temperatures become warmer in the deepest part of the water column. This situation is being extended up to October 8th (spring tide).

A low-pass filter was applied to the thermistor chain time series (Figure 5.2B) so periods shorter than 30 hours were removed, suppressing the tidal signal and avoiding the aliasing due to the main tidal constituents. As observed in Figure 5.2A, the filtered series show smoothed temperature variations, and the coldest values at the lower water column present in the original series are not present.

The relation between these low-frequency vertical excursions of water masses and the atmospheric forcing is analyzed. In this case, wind at 10 m height (Figure 5.2D) was considered at two locations: at the mooring point, and within the SoG itself. The presence of high-intensity easterly winds (~10 m/s) is observed by the time that the entry of colder waters at the lower water column disappears (October 2nd). The presence of cold water in this range coincides with the prevalence of westerly winds (Figures 5.2A, 5.2B, and 5.2D). Isotherms deepened up to 40 m in the water column during intense and persistent easterlies.

As indicated by previous studies (García-Lafuente et al., 2002; Bolado-Penagos et al., 2020), currents in the upper layer of the SoG are strongly conditioned by the presence of westerly and easterly winds in this region. While westerly winds enhance the surface Atlantic water input towards the Mediterranean Sea, the presence of intense and persistent easterly winds is even capable of reversing this surface current westward, as can be seen in Figures 5.2C and 5.2D.

Regarding MSLP over the Ligurian Sea (Figure 5.2E, red time series), higher atmospheric pressures (> 1013 hPa) are related to the presence of easterly winds over the Strait (Figure 5.2D). Also, lower MSLP took place during westerly episodes, and the transport of surface water intensified towards the Mediterranean Sea (Figure 5.2C). Similarly, the Ekman pumping and upwelling/downwelling processes are directly related to winds (Figure 5.2E, black and grey time series): downwelling (upwelling) occurs when blowing easterly (westerly) winds (Figures 5.2D and 5.2E). They are also related to variations in MSLP over the Ligurian Sea (Macias et al., 2008a; Bolado-Penagos et al., 2021).

In situations of strong and persistent easterlies, there is usually a weakening of the Atlantic jet (Bolado-Penagos et al., 2021) towards the Mediterranean Sea, which can cause, in turn, a rise in sea level in both the SoG that can extend to the coastal areas of GoC (Figure 5.2F).

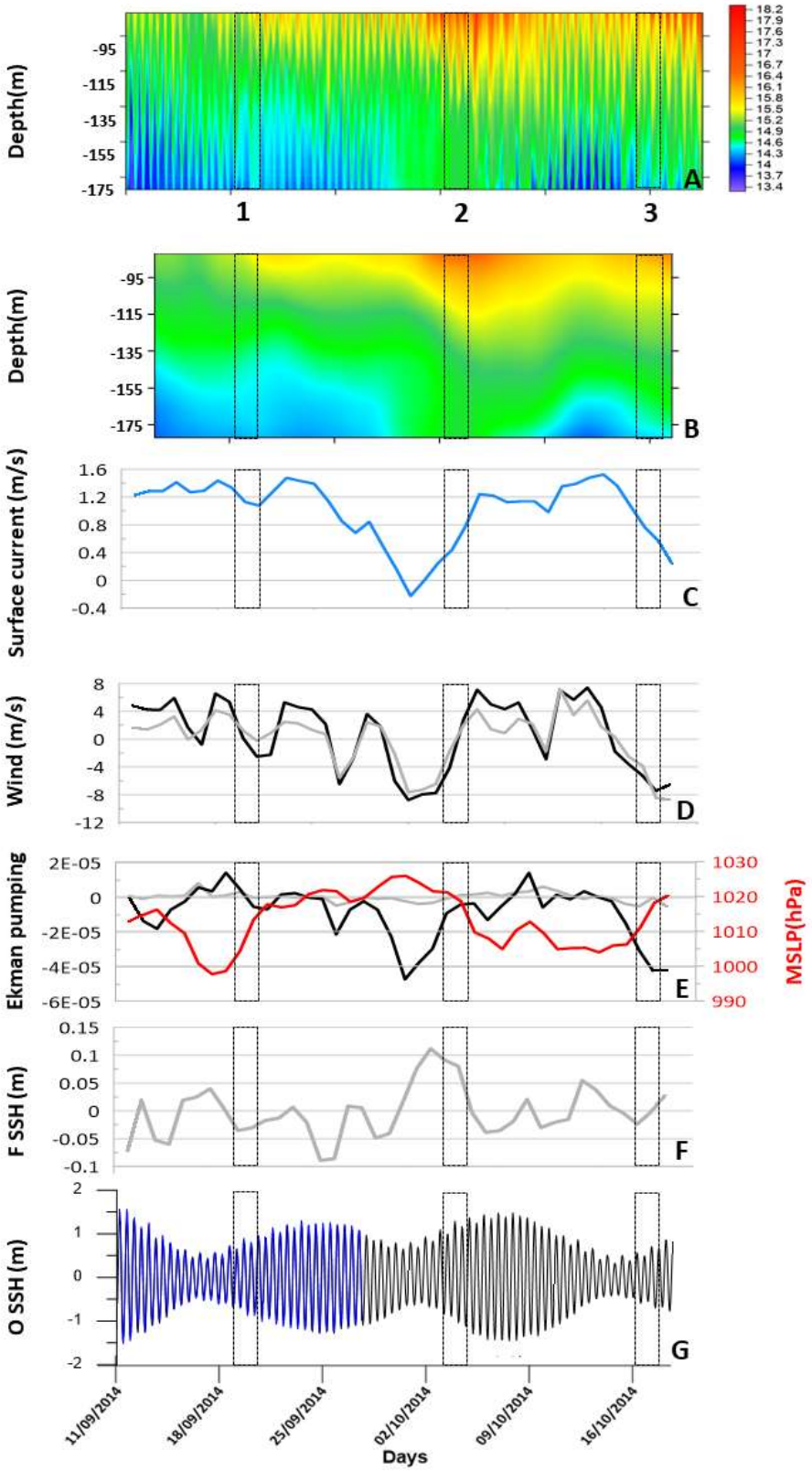
Depth(m)
-95
-115
-135
-155
-175
1
2
3
A
18.2
17.9
17.6
17.3
17
16.7
16.4
16.1
15.8
15.5
15.2
14.9
14.6
14.3
14
13.7
13.4
B
Surface current (m/s)
1.6
1.2
0.8
0.4
0
-0.4
C
Wind (m/s)
8
4
0
-4
-8
-12
D
Ekman pumping
2E-05
0
-2E-05
-4E-05
-6E-05
MSLP(hPa)
1030
1020
1010
1000
990
E
F SSH (m)
0.15
0.1
0.05
0
-0.05
-0.1
F
O SSH (m)
2
1
0
-1
-2
G
11/09/2014
18/09/2014
25/09/2014
02/10/2014
09/10/2014
16/10/2014
Days

Figure 5.2. Time series during the anchoring period of the thermistors. (a) the measured temperature in the water column (from 75 to 175 meters depth); (b) 30-hour low-pass-filtered temperature series; (c) zonal component of filtered surface velocity measured by the HFR system; (d) zonal component of the filtered 10-m wind (m/s) within the Strait (black line) and at the anchorage area (greyline); (e) Ekman Pumping at the anchorage area (grey line) and within the Strait (black line), and MSLP series in the Ligurian Sea (red line); (f) filtered (F) sea surface height (SSH, m); (g) original (O) SSH measured from the ADCP pressure sensor (blue line), and those obtained from the SAMPA model (black line) at the anchorage site, as indicative of the tidal phase and situation (spring/neap).

5.3.2 Correlation analysis

To quantify the possible relationship between the considered variables during the study period, mutual linear regression analyses were carried out between each pair of them (Table 5.2).

The temperature series show a significant correlation with the winds at both the mooring site and in the eastern part of the Strait (R=-0.56 and R=-0.54 respectively for the deepest thermistor). This indicates that easterly (westerly) winds are related to an increase (decrease) in the temperature of the water column at the mooring site.

As a representative for the upper and lower water column behavior, temperature records of the shallowest (75 m) and the deepest (175 m) thermistors were selected to investigate their relationship with atmospheric variables (i.e., zonal wind and MSLP). In the case of temperatures, the most significant (negative) correlation occurs between the surface current in the Strait (Pearson's correlation coefficient R equal to -0.60 and -0.80 for the shallow and deep thermistors, respectively). Having in mind the sign criterion for directions (positive eastwards), that means that the presence of an intensified zonal eastward (westward) flow in the Strait would be related to the presence of colder (warmer) temperatures at the mooring position. These temperatures also show a negative correlation with wind, both in the Strait and at the mooring position. Therefore, the presence of westerly (easterly) winds would be related to the presence of colder (warmer) temperatures in the study area.

Temperature time series and MSLP over the Ligurian Sea show positive correlations. An increase in MSLP over the Ligurian Sea corresponds to an increase in temperature in the water column of the anchorage site.

The Ekman pumping also shows some correlation with the temperature series deepest thermistor: R=-0.53 and R=-0.42, for the Strait and anchorage sites, respectively .

Meanwhile, the temperature series also show a positive correlation with the SAMPA-modelled SSH (the deepest thermistor showing a greater correlation). This relationship

indicates that when there is a rise in sea level at the anchorage site, there is an increase in temperature of water column.

	SSH SAMPA	SL TF	U10 (MM5) STRAIT	U10 (MM5) MOORING	We STRAIT	We MOORING	UHFR	TEMP SHALLOW	TEMP DEEP
SSH SAMPA	1								
SL TF	0.9797	1							
U10 (MM5) STRAIT	-0,4701	0,4514	1						
U10 (MM5) MOORING	-0,4666	0,4867	0,9248	1					
We STRAIT	-0,4392	0,5433	0,7567	0,8631	1				
We MOORING	-0,2400	0,6913	0,5045	0,6032	0,6351	1			
UHFR	-0,4350	0,6325	0,7159	0,6935	0,7189	0,4435	1		
TEMP SHALLOW	0,4913	-0,3498	-0,4623	-0,4981	-0,5386	-0,4210	-0,6029	1	
TEMP DEEP	0,5335	-0,4349	-0,5669	-0,5451	-0,5375	-0,3951	-0,8025	0,8100	1
MSLP LIGURIA	-0,3879	-0,7991	-0,5292	-0,5566	-0,5767	-0,4839	-0,6661	0,2901	0,4301

Table 5.2. Values of the Pearson's correlation coefficients of the different variables analyzed during the study period. SSH SAMPA is the mean sea level simulated with the SAMPA model at the anchor point. SL TF is the level recorded by the Tarifa tide gauge. U10 (MM5) corresponds to the wind series (at 10 m height) obtained from the MM5 model in the Strait and at the mooring point (Mooring). We, Strait and Mooring, are the Ekman pump variables for the same points as the wind data. UHFR is the zonal component of the surface current speed in the Strait obtained by radar data. Temp shallow and Temp Depth are the temperature value of the shallowest thermistor (75 m) and the deepest thermistor (175 m). MSLP Liguria is the atmospheric pressure data series in the Ligurian Sea area.

These correlation analyses pointed out plausible connections between many of the temperature-affecting variables during the mooring period, although its relatively short length does not allow for the analysis of their inter-relationships in the yearly timescale. Hence, analogue correlation analyses for the entire year 2019 were carried out by using the SSH series provided by the SAMPA model (there were not available SAMPA data for the study year 2014), once its representativeness had been validated for the mooring period.

Figure 5.3 shows data series of wind, surface current speed, Ligurian Sea MSLP, Ekman pumping, and variation in sea level (subinertial and tidal) for the entire year 2019, where marked, qualitatively, relationships between them can be visually appreciated, similar to those found in the analysis of the mooring period, especially at times of intense easterly/westerly winds.

During 2019, the highest easterly wind intensities are observed at the beginning and the end of the year, with values close to 10 m/s. There were also marked easterly wind periods during summer and autumn, although having less intensity (Figure 5.3A).

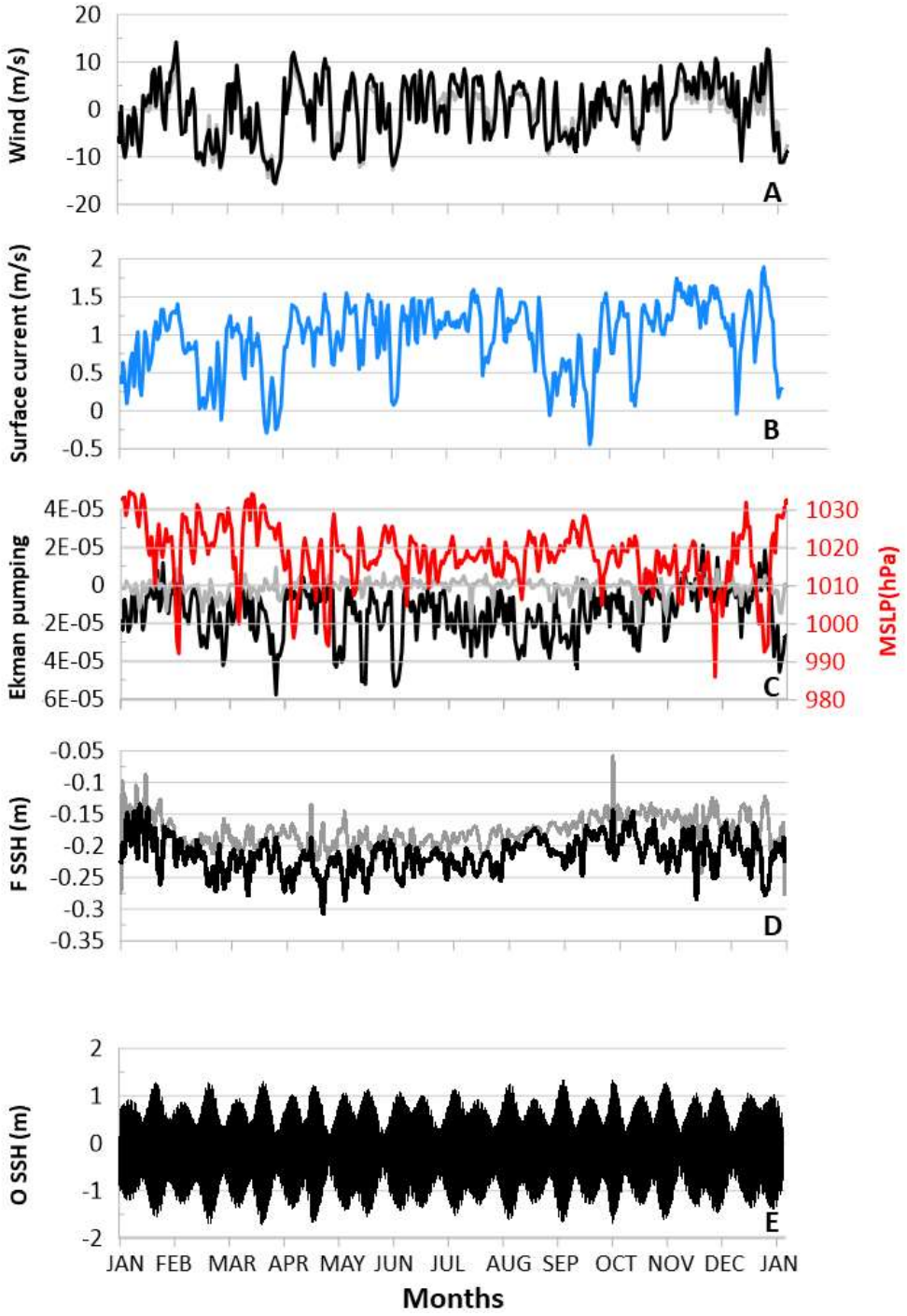

Figure 5.3. Time series throughout the year 2019. (a) 10-m zonal component of the wind at the anchorage site (grey line) and within the Strait of Gibraltar (black line) ; (b) filtered HFR surface current velocity; (c) Ekman Pumping at the anchorage site (grey line) and the Strait (black line), as well as MSLP in the Ligurian Sea (red line); (d) filtered SSH from the Tarifa tide-gauge record (black line) and the SAMPA model at the anchorage site (grey line); (e) original SSH from Tarifa tide-gauge.

Table 5.3 shows the correlation coefficients between all the variables during the year 2019, both for the entire year and seasonally discern. The highest correlation is observed between the surface current, and the wind, both at the location of the moorings (R = 0.78) and within the Strait (R= 0.77). Wind and Ekman pumping show a positive correlation, while it is a negative between wind and MSLP in the Ligurian Sea (i.e., anticyclonic conditions in the Ligurian Sea promote easterly winds within the study area, and vice versa). When attending to the seasonally- discerned analyses, it is remarkable that several correlation coefficients are sign-inverted during summe r.

The correlations for the mooring period and those made for the year 2019 show the same signs between variables, although the latter show lower values plausibly because of the strengthening of the interrelationships during periods of sufficiently intense and persistent easterly/westerly winds, while they weaken in other situations.

	SSH SAMPA BI	SL TF	U10 STRAIT	U10 MOORING	We STRAIT	We Mooring	U HFR	MSLP Liguria
SSH SAMPA BI	1							
SL TF	0,7956 0,3431 0,3559 0,2660 0,2560	1						
U10 Strait	0,4131 0,3099 0,3745 -0,0229 0,5448	0,1542 0,0859 0,0360 -0,4059 0,0922	1					
U10 Mooring	0,4282 0,2643 0,4120 -0,0359 0,5407	0,1798 0,0977 0,0421 -0,4503 0,1091	0,9533 0,9710 0,9509 0,9211 0,9635	1				
We Strait	0,2046 0,1674 0,2787 -0,1083 0,5009	0,0309 0,0437 0,0064 -0,0216 0,2045	0,6666 0,8258 0,7401 0,2833 0,7799	0,6973 0,8530 0,8385 0,4109 0,7821	1			
We Mooring	0,2961 0,2161 0,1409 -0,0636 0,4261	0,1844 0,0754 0,0691 -0,1501 0,0961	0,5266 0,4584 0,2253 0,5355 0,7641	0,5590 0,4951 0,1921 0,6084 0,7995	0,3387 0,3369 0,0364 0,2190 0,7479	1		
U HFR	0,2842 0,2888 0,3671 -0,2100 0,1778	-0,0431 -0,0570 -0,0925 0,7736 -0,2982	0,7765 0,8691 0,7845 0,6378 0,7702	0,7803 0,8914 0,7970 0,6713 0,7356	0,4823 0,7195 0,6629 0,0203 0,5548	0,3861 0,3423 0,0774 0,2868 0,5468	1	
MSLP Liguria	-0,5751 -0,4331 -0,4707 -0,4160 -0,6123	-0,5200 -0,4662 -0,4395 -0,0950 -0,3789	-0,5843 -0,5300 -0,5412 -0,3641 -0,6228	-0,5646 -0,4809 -0,5165 -0,3759 -0,5896	-0,3664 -0,2886 -0,3442 -0,1220 -0,5599	-0,3537 -0,3745 -0,1891 -0,1262 -0,4186	-0,4584 -0,3534 -0,3264 -0,2121 -0,4510	1

Table 5.3. Pearson's correlation coefficients between variables for the year 2019. From up to down: entire year, January to March, April to June, July to September, October to December periods.

Results from these correlation analyses could be physically interpreted as follows: high MSLP (anticyclonic) conditions within the Ligurian Sea promote intense easterly winds, which themselves weaken, or even reverse, eastward flow within the SoG and the study area on the continental slope of the GoC. This enhances the net Ekman transport towards the Iberian shelf, promoting water accumulation and subsequent sea-level rising, as well as negative Ekman pumping (downwelling). A plausible effect of that, as inferred from temperature profiles during the mooring period, is the increase of the SAW layer thickness and deepening of the ENACW-MW interface. During low MSLP (cyclonic) conditions within the Ligurian Sea, the situation would be quite the opposite.

From Figure 5.3, it can be deduced that the periods throughout 2019 where these processes could be activated correspond to the periods corresponding months of February-March-April and December.

5.3.3 Spatial variability of wind and atmospheric pressure fields at sea level

In this section, the MM5-modeled wind fields in a region covering the eastern GoC, the SoG, and the western Alboran sea are analyzed for three chosen days within the mooring period (dashed frames in Figure 5.1 ,with numbers 1,2 and 3), all during neap-tide situation but with different wind conditions: 4- 6 m/s north-westerly (09/18/2014), intense easterly (10/02/2014), and weak easterly (10/16/2014).

Daily averaged fields of winds, Ekman pumping, MSLP, HFR surface currents, and sea level for each situation are shown in Figures 5.4 and 5.5.

Analyzing the values of the Ekman pumping, for the different wind situations, it is deduced that the situations of intense easterly (westerly) would favor the sinking (upwelling) of the base of the Ekman layer on the continental shelf.

In the case of the atmospheric pressures in the three moments, there is higher pressure in the moment of intense easterly, while the atmospheric pressure is lower in moments of westerly. Focusing on the area of the Ligurian Sea, an increase in pressure can be observed as the wind changes in the Strait towards easterly.

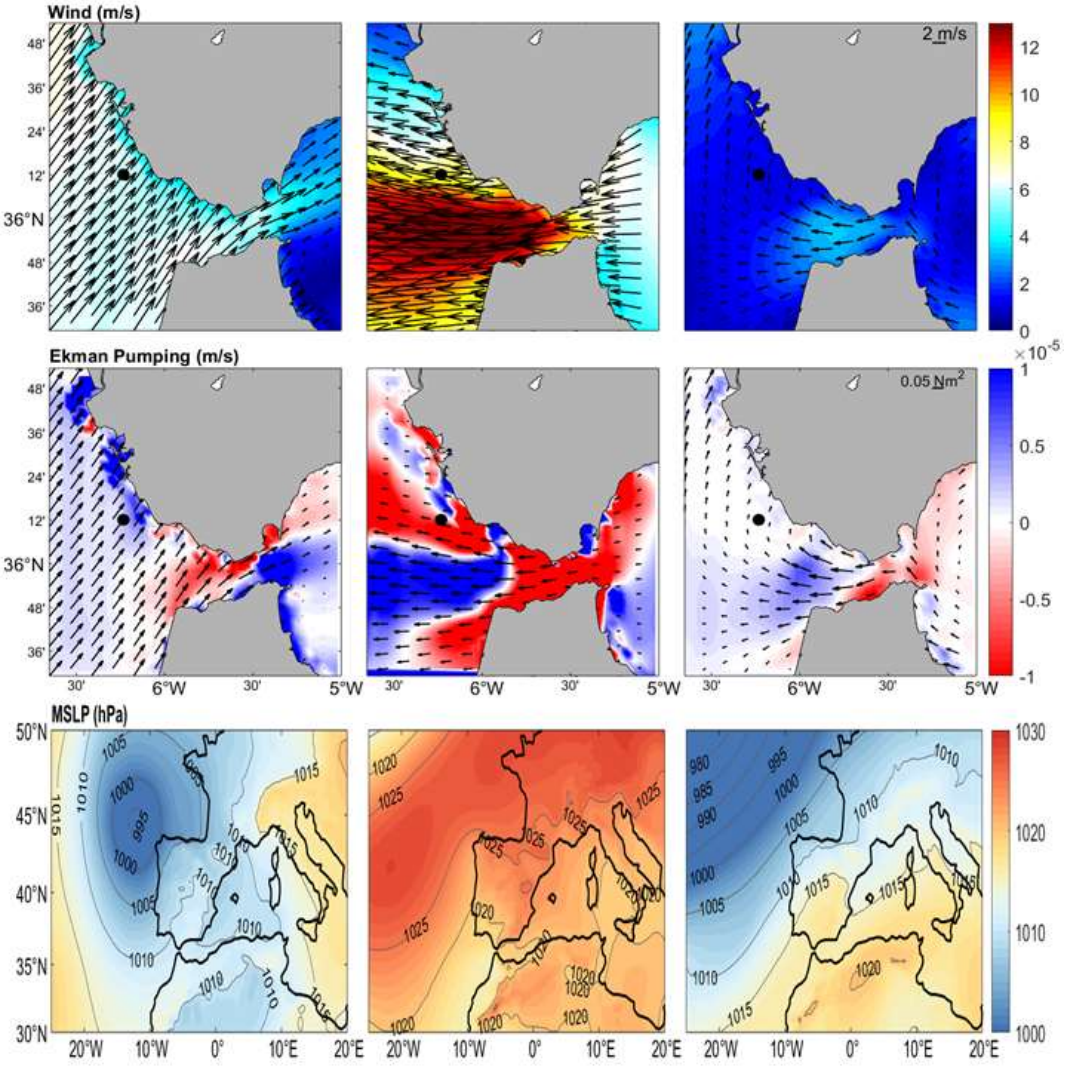

Figure 5.4. From top to bottom, daily averaged fields of wind (m/s), Ekman pumping (N/m²), and atmospheric pressure at sea level (hPa), from left to right: 09/18/2014, 10/02/2014, and 10/16/2014.

The surface currents for weak westerly and easterly winds, when the MSLP over the Ligurian Sea is relatively low, are east-directed towards the Mediterranean Sea, with a related mean sea level decrease over the Iberian shelf. On the contrary, in the case of strong easterlies and high MSLP over the Ligurian Sea, the direction of currents reverses (towards the Atlantic Ocean), coinciding with an increase in sea level on both sides of the Strait.

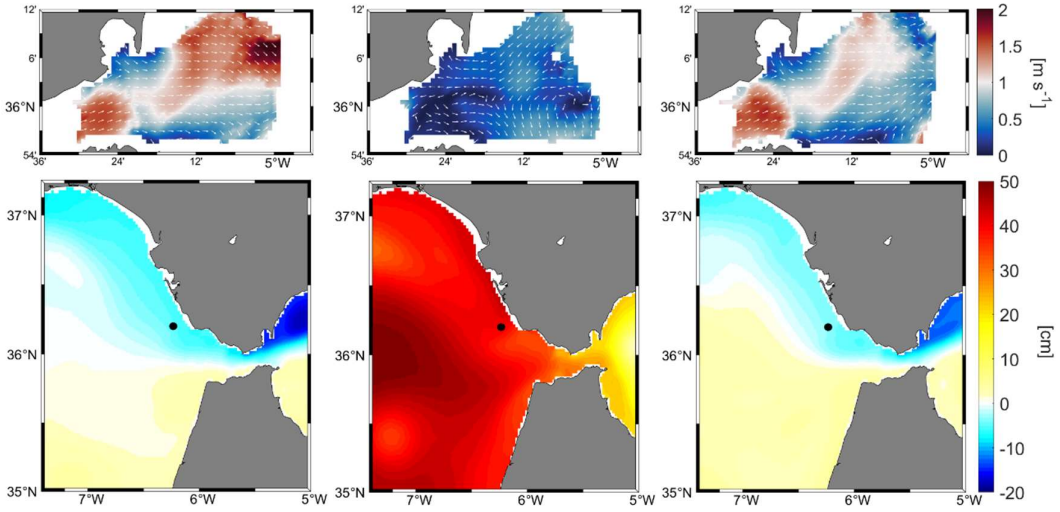

Figure 5.5. The same as in Figure 5.4 but for HFR surface currents (m/s) and SAMPA SSH (cm).

5.3.4 Response of flows thrugh the Strait to variations of MSLP in Liguria

The link between the variabilities of subinertial flows through the SoG and the atmospheric pressures in the western Mediterranean Sea has been established by previous works (Candela et al., 1989; García-Lafuente et al., 2002). Specifically, Dastis et al. (2018) and Bolado-Penagos et al. (2021) highlighted the importance of the pressure center over the Ligurian Sea as a modulator of the Strait's flow. Concluding that an increase in the Ligurian MSLP weakens the Atlantic through the narrowest part of the Strait, with related SSH rising. These results came from simulating the effects of a 20 hPa increment of Ligurian MSLP by a single-channel numerical model (Bolado et al., 2021) and they are complemented here by using the same model to simulate a -20 hPa Ligurian MSLP instead.

The idealized model domain consists of a single channel closed on the widest easternmost side and open on the narrower westernmost end (Figure 5.6A), with the along-channel depth variation shown in Figure 5.6B, to resemble the main morphological characteristics of the transition from the Atlantic Ocean to the Mediterranean Sea through the SoG.

Figures 5.6C and 5.6D show the results of this simulation. An increase in the eastwards current (red line) is present at the central sill of the idealized strait reaching 0.30 m/s, accompanied by the decrease in SSH (grey line). It is explained by the propagation of the SSH depression wave generated by the MSLP drop forced at the easternmost channel end (i.e., idealized the Ligurian Sea).

SSH fluctuation replicate in the model and shown in Figure 5.6 are barotropic (the model is not forced with the wind) and comes directly from the MSLP in the Ligurian Sea (from the depression wave propagated), and there are other indirect effects such as Ekman pumping from the MSLP effect that causes the continental winds (upwelling/downwelling). Winds also can affect the currents, and this is an additional contribution from MSLP. Changes in the SSH from wind-Ekman pumping are linked to vertical movements (downwelling/upwelling) in the water masses (i.e., temperature changes observed in the thermistor chain).

5.3.5 Analysis of temperature fields in the study area

In this section, SAMPA-simulated surface temperature and current fields within the eastern GoC are analyzed (Figure 5.7), focusing on the area of the thermistor chain mooring (black circle).

Figure 5.7 shows the model results for two days of different wind conditions weak westerlies (5 m/s 09/28/2014), and strong easterlies (12 m/s 10/02/2014).

The weak westerly case coincides with the presence of colder temperature values (18 °C) near the Spanish coast. At a depth of 14.5 m upwelling of colder waters in the Trafalgar area (Figure 5.1), as observed by Bruno et al. (2013). Outside the continental shelf, the surface values are higher (22-24 °C). Regarding the field currents, a cyclonic gyre is established in the mooring area directed northwards near the platform and southwards further away.

During the strong easterly case, a significant increase in temperature of 6 °C is observed on the shallow area near the Iberian coast. However, there is an upwelling of colder coastal waters all along the African coast of the Strait. Regarding the field of currents, a clear weakening of the Atlantic water input to the Mediterranean Sea is observed, with a reversion of currents near the African coast.

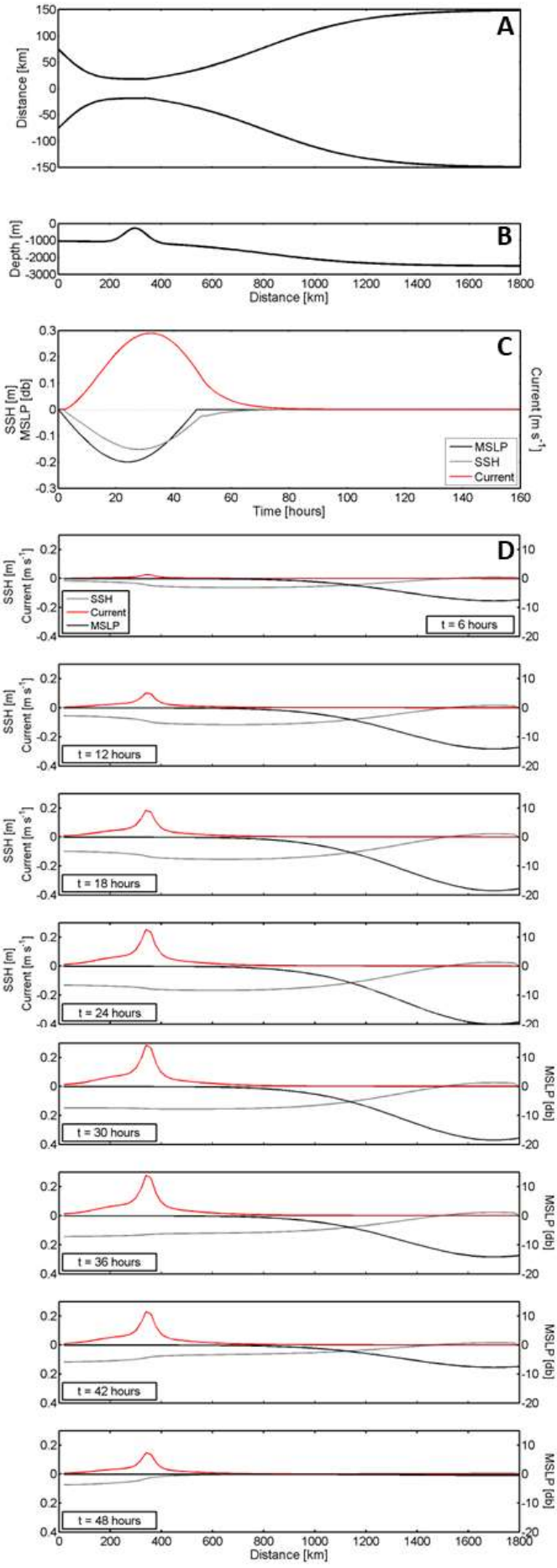
A
Distance [km]
B
Depth [m]
Distance [km]
C
SSH [m]
MSLP [db]
Current [m s-1]
MSLP
SSH
Current
Time [hours]
D
SSH [m]
Current [m s-1]
SSH
Current
MSLP
t = 6 hours
t = 12 hours
t = 18 hours
t = 24 hours
t = 30 hours
t = 36 hours
t = 42 hours
t = 48 hours
MSLP [db]
Distance [km]

Figure 5.6. (a, b) Horizontal and vertical geometry of the model idealized channel. (c) Time series of model-forcing MSLP (black line) at the rightmost side of the domain (see Figure 5.6A), together with SSH (grey line) and longitudinal current (red line) at the position of the sill central to the idealized strait (see Figure 5.6A as well) a. (d) Sequence (every 6 hours) of the along-channel distribution of the simulated variables.

5.4 Discussion

The analysis of the different variables during the mooring period carried out in the eastern part of the GoC platform indicates the influence between atmospheric phenomena and the changes produced in the water column (Figure 5.2).

The tidal cycle in the study area has a great influence on the water column. This variability is the one that has the greatest influence in this area. But in periods of neap tides and strong easterlies in the Strait, an increase in water temperature appears in the platform area for the entire water column, which could indicate a significant sinking of the ENACW-MW interface that prevents its arrival at this continental slope zone.

The changes produced by the atmospheric forcing in the area of the Strait are reflected in the eastern part of the GoC. The existence of strong easterlies in the Strait is normally related to the increase in atmospheric pressure in the Ligurian Sea (Macías et al., 2008; Bolado-Penagos et al., 2021). As indicated in Bolado-Penagos et al. (2021) the combined effect of uplifts surges arriving from the Ligurian Sea in response to the rise in atmospheric pressure there, reduces the intensity of the Atlantic jet causing a blockage of the entry of surface Atlantic water into the Mediterranean in the Strait area. This reduction in the intensity of the jet produces a decrease in the ability to dislodge water from the GoC through the Strait, which in turn causes an accumulation of SAW in the eastern part of the GoC that increases the thickness of these warmer waters, displacing ENACW waters at greater depth as can be observed in the Roque et al. (2022) definition of water masses in the study area. This accumulation effect is reflected in the rise in sea level experienced in the area in a situation of intense and persistent upheavals (Figure 5.5).

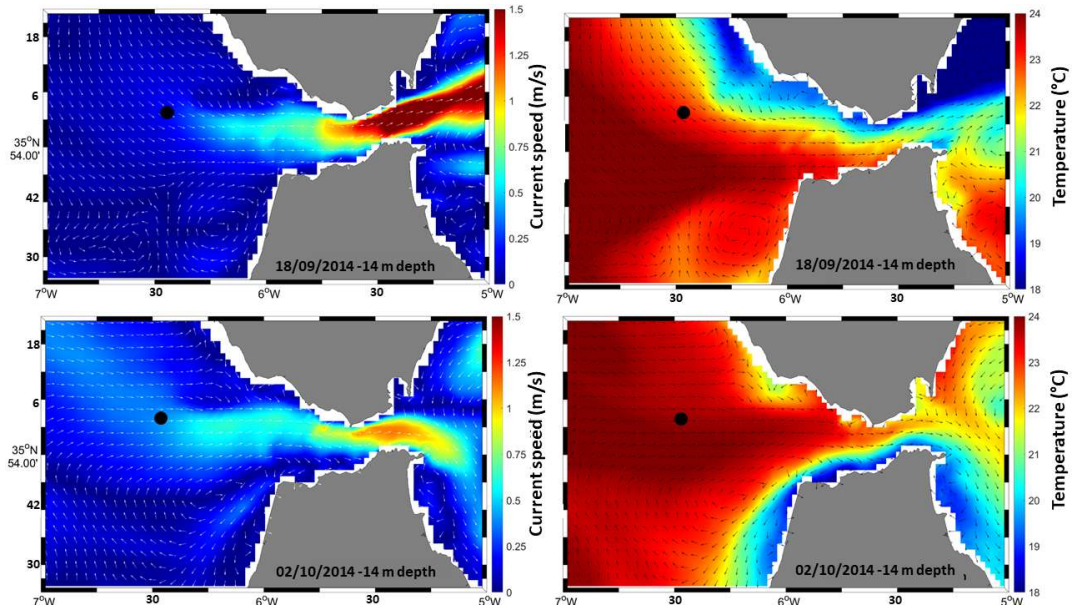

Figure 5.7. Temperature and current data in the surface SAMPA model. Weak west moment (top), strong lift (bottom). The black circle in the graphs is the point where the mooring is located.

The opposite effect occurs with westerlies situations. A decrease in atmospheric pressure in the Ligurian area favors the passage of Atlantic surface water toward the Mediterranean Sea. Therefore, westerlies produce a decrease in sea level on the eastern platform of the GoC, which in turn favors the ENACW and its interface with the MW to reach the area of the slope where the analyzed observations are located.

It is very difficult to distinguish the relative importance of direct-indirect effects from the MSLP in the Ligurian Sea as with the data set. Changes in the temperature profile registered by the thermistor chain cannot be associated with only the model mechanism recreated by the idealized model.

According to Sammartino et al. (2015), the outflow of Mediterranean water into the Atlantic has been maximum (minimum) during the spring (autumn) period, with the interface being shallower (deeper). This conclusion reinforces the hypotheses of this study since these fluctuations coincide in the mooring period (autumn), and that causes an increase (decrease) of periods with easterlies (westerlies) that block the entry of Atlantic water into the Mediterranean. and consequently, causes the ENACW-MW interface to go down.

From the geomorphological point of view, these changes in the vertical extent of this interface should help to delimit the extension on the slope of the hydrodynamic effects associated with it.

5.5 Conclusions

The main objective was to evaluate how atmospheric forcing affects the vertical distribution of water masses on the continental slope in the southeast of the GoC and the implications of the changes experienced.

It has been verified that there are significant correlations between the different variables proposed to characterize the possible mechanisms forced by meteorological variability both in the surroundings of the GoC – SoG –Alborán Sea and in the Western Mediterranean (Ligurian Sea).

The intense and persistent easterly winds block the entry of Atlantic water into the Mediterranean, as shown by the surface current fields recorded by the strait's HFR system. These wind situations are related to increases in atmospheric pressure in the Ligurian area, as has already been described by other authors (Macías et al., 2008; Bolado Penagos et al, 2021).

The blockage of the entry of Atlantic water into the Mediterranean causes an accumulation of Atlantic water in the GoC in its eastern part with the consequent rise in sea level. At the same time, there is an increase in temperature in the water column and in the thickness of the SAW layer, which forces the ENACW-MW interface to move deeper.

Vertical excursions in the depth of the isotherms can reach 40 m in amplitude. This may involve displacements of the ENACW-MW interface of the same order that may be important in determining the geomorphological features of the slope and terrace of the studied area.

In summarizing, we can say that an increase (decrease) in temperature in the water column at the mooring site, which is an indicator of the increase (decrease) in the thickness of the SAW layer, is related to:

a) An increase (decrease) of the SSH in the place of the mooring.

b) A situation of increase (decrease) of the MSLP in the Ligurian Sea.

c) A decrease (increase) in Ekman pumping, especially in the eastern part of the Strait.

Capítulo 6

CONCLUSIONES

A continuación, se resumen las principales conclusiones derivadas de los resultados de investigación que han ido describiéndose a lo largo de la presente Tesis.

1. La variación estacional de las masas de agua intermedias en el GoC incluye cambios notables en el Agua Antártica Intermedia (AAIW) y el agua Intermedia Subártica (SAIW). Durante el otoño hay una mayor presencia de la AAIW, proveniente de latitudes bajas estando relacionada con una reducción de la SAIW y la ENACW. Esta interacción también afecta al agua Mediterránea que es empujada por la AAIW hacia el talud continental superior. En el resto de estaciones, la SAIW es la masa de agua predominante reduciendo la presencia de la AAIW.
2. Esta variabilidad estacional en el intercambio entre masas de aguas intermedias se puede explicar en base a la concatenación de varios procesos impulsados por el viento que actúan durante las distintas estaciones. La intensificación de los transportes de Sverdrup en verano cerca de la costa africana hace posible la progresión de la AAIW desde latitudes bajas hasta latitudes por encima de las Islas Canarias. Posteriormente, una vez que la AAIW ha alcanzado latitudes cercanas al GoC, su transporte hacia el norte se mantiene debido a una disminución en la intensidad del bombeo de Ekman negativo dentro del giro subtropical al oeste del GoC, que presenta su intensidad mínima durante el otoño. Este transporte hacia el GoC también se ve favorecido por el sistema de vientos ciclónicos permanentes que dominan localmente en el GoC, aunque muestra su mayor intensidad en los meses de julio a agosto. En noviembre vuelve a experimentar un aumento significativo. El alto porcentaje de SAIW durante invierno, primavera y verano podría explicarse por el transporte permanente de Sverdrup hacia el sur que se produce cerca de la costa de la Península Ibérica y que favorece la llegada de SAIW al GoC. A partir de septiembre este transporte comienza a debilitarse debido a la llegada del AAIW desde el sur y la desviación de parte del transporte SAIW hacia el lado este del giro subtropical (oeste del GoC), donde la intensidad del bombeo negativo de Ekman es reducido entre septiembre y noviembre.
3. Nuestros resultados son importantes para una mejor comprensión de la variabilidad intermedia de la masa de agua a lo largo de la costa norte de Marruecos, GoC y los márgenes atlánticos ibéricos, pero se necesitan más investigaciones paleoceanográficas, sedimentarias y morfológicas para decodificar los cambios en el pasado geológico y determinar cómo estas masas de agua , en particular las AAIW, han ido modelando la morfología y controlando la sedimentación a lo largo de la costa norte de Marruecos, el GoC y los márgenes atlánticos ibéricos.
4. La dinámica de las mareas en el talud continental superior en la parte oriental del golfo de Cádiz es un factor clave para controlar las variaciones laterales y verticales de las masas de agua existentes en la zona, aumentando las velocidades locales de las corrientes de fondo.

5. Los resultados obtenidos han determinado la importancia de la circulación de masas de agua y los procesos secundarios asociados en la conformación de la morfología del fondo marino. La interfaz ENACW-MOW se discrimina por una temperatura mínima localmente menos profunda en el talud superior porque se ve afectada por la combinación de mareas barotrópicas, baroclínicas y ondas internas que determinan un punto de salto local donde estos procesos se amplifican y disipan más energía contra el fondo del mar.
6. El efecto a largo plazo de la circulación ENACW-MOW y su fluctuación a lo largo del tiempo de esta interfaz han sido las responsables del inicio y la evolución de una terraza en el talud superior.
7. Aunque la dinámica mareal sea el proceso con mayor peso en los movimientos de las masas de agua en el talud continental en la zona oriental del golfo de Cádiz, el forzamiento atmosférico también influye en la columna de agua. De hecho, se demuestra como los cambios atmosféricos tiene una mayor relación con las masas de agua profunda que con las superficiales.
8. Momentos de levante fuerte en el estrecho de Gibraltar provocan un efecto en el Estrecho de bloqueo de entrada de agua Atlántica en el Mediterráneo que a su vez genera una acumulación de esta agua Atlántica en la plataforma oriental del golfo de Cádiz, provocando a su vez que otras aguas que hay en la parte inferior de esta agua (Mediterránea) deba de desplazarse a profundidades mayores al aumentar la presencia de agua Atlántica.
9. Las variaciones de presión atmosférica en regiones alejadas como el mar de Liguria, generan ondas barotrópicas que una vez llegan al SoG contribuyen, junto con los levantes, a esta variabilidad de la presencia de esta masas de agua sobre el talud.

Capítulo 7

LÍNEAS DE INVESTIGACIÓN FUTURAS

Los resultados obtenidos a lo largo de la presente Tesis invitan al planteamiento de prometedoras líneas futuras de investigación, algunas de ellas ya en fases iniciales de estudio; a continuación, se enumeran las principales propuestas:

1. Profundizar en el análisis de la interacción entre el Agua Antártica Intermedia (AAIW), y el agua Mediterránea (MOW) en la zona de máxima velocidad del agua Mediterránea.
2. Analizar la influencia mareal en zonas profundas para conocer cuál es la relevancia de esta variabilidad en la morfología del fondo.
3. Identificar las posibles zonas de generación de ondas internas en el Golfo de Cádiz, con el fin de poder conocer las interacciones de estos procesos con la morfología del fondo.
4. Ampliar los estudios en distintas zonas de la plataforma del Golfo de Cádiz donde se observan ciertas morfologías de fondo, cuyo origen es debido a las corrientes y generación de ondas internas cerca de estas morfologías.
5. Realizar un estudio en distintos lugares del planeta con similares características del Golfo de Cádiz para conocer si los procesos físicos que han sido estudiados pueden observarse en otros lugares.
6. Estudiar los procesos a escalas de tiempo menores en la zona de la plataforma que generan procesos energéticos y que afectan al fondo.

Capítulo 8

BIBLIOGRAFÍA

Álvarez, O, Izquierdo, A., Tejedor, B., Man, R.,1999. The Influence of Sediment Load on Tidal Dynamics, a Case Study Cádiz Bay. Estuarine, coastal and Shelf Science (48) 439–50. https://doi.org/10.1006/ecss.1998.0432

Álvarez, M., Pérez, F.F., Bryden H., Ríos, A.F.: Physical and Biogeochemical Transports Structure in the North Atlantic Subpolar Gyre. Journal of Geophysical Research: Oceans 109(C3), https://doi.org/10.1029/2003JC002015, 2004.

Álvarez Fanjul, E., Pérez Gómez, B. and Rodríguez Sánchez Arévalo, I. (2001). Nivmar: a storm surge forecasting system for Spanish waters. Scientia Marina. 65, S1 (Jul. 2001), 145–154. https://doi.org/10.3989/scimar.2001.65s1145.

Ambar, I., Howe, M.: Observations of the Mediterranean Outflow- I. Mixing in the Mediterranean outflow. Deep-Sea Research, Vol 26A, pp 535 to 554, https://doi.org/10.1016/0198-0149(79)90095-5, 1979.

Ambar, I., Howe, M.: Observations of the Mediterranean Outflow- I. The deep circulation in the vicinity of the Gulf of Cadiz. Deep-Sea Research, Vol 26A, pp 555 to 568, https://doi.org/ 10.1016/0198-0149(79)90096-7, 1979.

Ambar, I., Serra, N., Brogueira, M. J., Cabeçadas, G., Abrantes, F., Freitas, P., Gonçalves, C., Gonzalez, N. 2002. Physical, Chemical and Sedimentological Aspects of the Mediterranean Outflow off Iberia. Deep-Sea Research Part II: Topical Studies in Oceanography 49 (19): 4163–77. https://doi.org/10.1016/S0967-0645(02)00148-0

Baringer, M.O., Price, J.F.: Momentum and energy balance of the Mediterranean outflow. Journal of Physical Oceanography 27 (8), 1678–1692, https://doi.org/10.1175/1520-0485(1997)027<1678: MAEBOT>2.0.CO;2, 1997.

Baringer, M.O., Price, J.F.: A review of the physical oceanography of the Mediterranean outflow. Marine Geology 155, 63–82, https://doi.org/10.1016/S0025-3227(98)00141-8, 1999.

Barrier, N., Cassou, C., Deshayes, J., Treguier, A.M.: Response of North Atlantic Ocean Circulation to Atmospheric Weather Regimes. Journal of Physical Oceanography 44(1):179–201, https://doi.org/10.1175/JPO-D-12-0217.1,2014.

Bellanco, M.J., Sánchez-Leal, R.F.: Spatial Distribution and Intra-Annual Variability of Water Masses on the Eastern Gulf of Cadiz Seabed. Continental Shelf Research 128(October):26–35, https://doi.org/10.1016/j.csr.2016.09.001, 2016.

Bolado-Penagos, M., González, C.J., Chioua, J., Sala, I., Gomiz-Pascual J.J., Vázquez A., Bruno M. (2020). Submesoescale processes in the coastal margins of the Strait of Gibraltar. The Trafalgar-Alboran coonection. Progress in Oceanography, Volume 181, 102219. https://doi.org/10.1016/j.pocean.2019.102219.

Bolado-Penagos, M., Sala, I., Gomiz-Pascual, J. J., Romero-Cózar, J., González-Fernández, D., Reyes-Pérez, J.,Vázquez, A., Bruno, M.. (2021). Revising the effects of local and remote atmospheric forcing on the Atlantic Jet and Western Alboran Gyre dynamics. Journal of Geophysical Research: Oceans, 126, e2020JC016173. https://doi.org/10.1029/2020JC016173

Borenäs, K.M., Wahlin, A.K., Ambar, I., Serra, N.: The Mediterranean outflow splitting-a comparison between theoretical models and CANIGO data. Deep-Sea Research II 49, 4195–4205, https://doi.org/10.1016/S0967-0645(02)00150-9, 2002.

Bostock, H., Sutton, P., Williams, M.J.M., Opdyke, B.: Reviewing the circulation and mixing of Antarctic Intermediate Water in the South Pacific using evidence from geochemical tracers and Argo float trajectories, Deep-Sea Res. I, 73, 84-98, https://doi.org/10.1016/j.dsr.2012.11.007, 2013.

Bozzano, G., Violante, R.A., Cerredo, M.E.: Middle slope contourite deposits and associated sedimentary facies off NE Argentina. Geo-Marine Letters, 31, 495-507, https://doi.org/10.1007/s00367-011-0239-x, 2011.

Brogueira, M. J., Cabeçadas, G., Gonçalves, C.: Chemical Resolution of a Meddy Emerging of Southern Portugal. Continental Shelf Research 24(15):1651–57, https://doi.org/10.1016/j.csr.2004.05.012, 2004.

Brackenridge, R.E., Stow, D.A.V., Hernández-Molina, F.J., Jones, C., Mena, A., Alejo, I., Ducassou, E., Llave, E., Ercilla, G., Nombela, M.A., Pérez-Arlucea, M., Frances, G., 2018. Textural characteristics and facies of sand-rich contourite depositional systems. Sedimentology,65 (7), 2223–2252.

Brandt, P., Alpers, W., Backhaus, J. O., 1996. Study of the generation and propagation of internal waves in the Strait of Gibraltar using a numerical model and synthetic aperture radar images of the European ERS 1 satellite, J. Geophys. Res. C Ocean., 101(C6), 14237–14252, doi:10.1029/96JC00540

Bruno, M., Juan Alonso, J., Cózar, A., Vidal, J., Ruiz-Cañavate, A., Echevarría, F., Ruiz, J., 2002. The boiling-water phenomena at Camarinal Sill, the strait of Gibraltar, Deep. Res. Part II Top. Stud. Oceanogr., 49(19), 4097–4113, doi:10.1016/S0967-0645(02)00144-3

Bruno, M., Mañanes, R., Jose Juan, A., Izquierdo, A., Tejedor, L., Kagan, B., 2000. Vertical Structure of Tidal Currents over the Camarinal Sill at the Strait of Gibraltar. Journal of Geophysical Research: Oceans 105 (C8): 19709–28. https://doi.org/10.1029/2000jc900066

Bruno, M., Vázquez, A., Gómez-Enri, J., Vargas, J.M., García Lafuente, J., Ruiz-Cañavate, A., Mariscal, L., Vidal, L., 2006. Observations of Internal Waves and Associated Mixing Phenomena in the Portimao Canyon Area. Deep-Sea Research Part II: Topical Studies in Oceanography 53 (11–13): 1219–40. https://doi.org/10.1016/j.dsr2.2006.04.015

Bruno, M., Chioua, J., Romero, J., Vázquez, A., Macías D., Dastis C., Ramírez-Romero, E., Echevarria F., J. Reyes J., García, C.M. The importance of sub-mesoscale processes for the exchange of properties through the Strait of Gibraltar, Progress in Oceanography, Volume 116, 2013, Pages 66-79, ISSN 0079-6611, https://doi.org/10.1016/j.pocean.2013.06.006.

Cabeçadas, G., Brogueira, M.J., Gonçalves, C.: The Chemistry of Mediterranean Outflow and Its Interactions with Surrounding Waters. Deep-Sea Research Part II: Topical Studies in Oceanography 49(19):4263–70, https://doi.org/10.1016/S0967-0645(02)00154-6, 2002.

Camassa, R., & Tiron, R. (2011). Optimal two-layer approximation for continuous density stratification. Journal of Fluid Mechanics, 669, 32-54.

Candela, J, Winant, C., Ruiz, A., 1990. "Tides in the Strait of Gibraltar." Journal of Geophysical Research 95 (C5): 7313–35. https://doi.org/10.1029/JC095iC05p07313

Carracedo, L. I., M. Gilcoto, H. Mercier, F. F. Pérez.: Seasonal Dynamics in the Azores-Gibraltar Strait Region: A Climatologically-Based Study. Progress in Oceanography 122:116–30, https://doi.org/10.1016/j.pocean.2013.12.005, 2014.

Carrère, L., and Lyard, F. (2003), Modeling the barotropic response of the global ocean to atmospheric wind and pressure forcing - comparisons with observations, Geophys. Res. Lett., 30, 1275, doi:10.1029/2002GL016473, 6.

Cattaneo, A., Miramontes, E., Samalens, K., Garreau, P., Caillaud, M., Marsett, B., Corradi, N., Migeon, S. Contourite identification along Italian margins: The case of the Portofino drift (Ligurian Sea), Marine and Petroleum Geology, Volume 87, 2017, Pages 137-147, ISSN 0264-8172, https://doi.org/10.1016/j.marpetgeo.2017.03.026.

Cats, G. and Wolters, L., (1996) "The Hirlam project [meteorology]," in IEEE Computational Science and Engineering, vol. 3, no. 4, pp. 4-7, doi: 10.1109/99.556505.

Cheng H., Sinha A., Wang X., Cruz F. W., Edwards R. L.: The Global Paleomonsoon as seen through speleothem records from Asia and the Americas. Climate Dynamics 39: 1045–1062, https://doi.org/10.1007/s00382-012-1363-7, 2012.

Chérubin, L. M., Serra, N., and Ambar, I. (2003), Low-frequency variability of the Mediterranean undercurrent downstream of Portimão Canyon, J. Geophys. Res., 108, 3058, doi:10.1029/2001JC001229, C3.

Chioua, J., Dastis, C., González, C. J., Reyes, E., Mañanes, R., Ruiz, M. I., et al. (2017). Water exchange between Algeciras Bay and the Strait of Gibraltar: A study based on HF coastal radar. Estuarine, Coastal and Shelf Science, 196, 109–122. https://doi.org/10.1016/j.ecss.2017.06.030

Coulbourne, B., Foote, K.D.: Variability of Stratification and Circulation on the Flemish Cap during the Decades of 1950s-1990s. J. Nortw. Atla. Fish. Sci. 26, 103-122, 2000.

Criado-Aldeanueva, F., García-Lafuente, J., Vargas, J.M., Del Río, J., Vázquez, A., Reul, A., Sánchez, A., 2006. Distribution and Circulation of Water Masses in the Gulf of Cadiz from in Situ Observations. Deep-Sea Research Part II: Topical Studies in Oceanography 53 (11–13): 1144–60. https://doi.org/10.1016/j.dsr2.2006.04.012

Curry, W. B., Oppo, D. W.: Glacial Water Mass Geometry and the Distribution of δ 13C of ΣCO2 in the Western Atlantic Ocean. Paleoceanography 20(1):1–12, https://doi.org/10.1029/2004PA001021, 2005.

Dastis, C., Bruno, M., Izquierdo, A., & Reyes, E. (2018). Influence of the atmospheric pressure fluctuations over the Mediterranean Sea on the mesoscale water dynamics of the Strait of Gibraltar and the Alboran Sea. Fundamentalnaya i Prikladnaya Gidrofizika, 11(1), 28–39. https://doi.org/10.7868/S2073667318010033

Dauxois T., Didier A., Falcon E. (2004). Observation of near-critical reflection of internal waves in a stably stratified fluid", Physics of Fluids 16, 1936-1941.

de Castro, S., Hernández-Molina, F. J., de Weger, W., Jiménez-Espejo, F.J., Rodriguez-Tovar, F. J., Mena, A., Llave, E., Sierro, F.J., 2020b. Contourite characterisation and its discrimination from other deep-water deposits in the Gulf of Cadiz contourite depositional system. Sedimentology. doi.org/10.1111/sed.12813

Dee, D. P., Uppala, S. M., Simmons, A. J., Berrisford, P., Poli, P., Kobayashi, S., Andrae, U., Balmaseda, M. A., B alsamo, G., Bauer, P., Bechtold, P., Beljaars, A. C. M., van de Berg, L., Bidlot, J., Bormann, N., Delsol, C. , Dragani, R., Fuentes, M., Geer, A. J., Haimberger, L., Healy, S. B., Hersbach, H., Hólm, E. V., Isaksen, L., Kållberg, P., Köhler, M., Matricardi, M., McNally, A. P., Monge-Sanz, B. M., Morcrette, J.-J., Park, B.-K., Peubey, C., de Rosnay, P., Tavolato, C., Thépaut, J.-N., Vitart, F.: The ERA-Interim Reanalysis: Configuration and Performance of the Data Assimilation System. Quarterly Journal of the Royal Meteorological Society 137(656):553–97, https://doi.org/10.1002/qj.828, 2011.

De Oliveira Júnior, L., E. Garel, Relvas, P., The structure of incipient coastal counter currents in South Portugal as indicator of their forcing agents, Journal of Marine Systems, Volume 214, 2021, 103486, ISSN 0924-7963, https://doi.org/10.1016/j.jmarsys.2020.103486.

Downes, S. M., Bindoff, N. L., Rintoul, S.R.: Changes in the subduction of Southern Ocean water masses at the end of the twenty-first century in eight IPCC models. J. Climate, 23, 6526–6541, https://doi.org/10.1175/2010JCLI3620.1, 2010.

Echevarría, F., García Lafuente, J., Bruno, M., Gorsky, G., Goutx, M., González, N., García, C.M., Gómez, F., Vargas, J.M., Picheral, M., Striby, L., Varela, M., Alonso, J.J., Reul, A., Cózar, A., Prieto, L., Sarhan, T., Plaza, F., FJiménez-Gómez, F., 2002. Physical-Biological Coupling in the Strait of Gibraltar. Deep-Sea Research Part II: Topical Studies in Oceanography 49 (19): 4115–30. https://doi.org/10.1016/S0967-0645(02)00145-5

Expedition 339 Scientists.: Mediterranean outflow: environmental significance of the Mediterranean outflow water and its global implications. IODP Preliminary Report, p. 339 http://dx.doi.org/10.2204/iodp.pr.339.2012, 2012.

Farmer, D. M., Armi, L., 1985. The internal hydraulics of the Strait of Gibraltar and associated sills and narrows, Oceanol. acta, 8(1), 37–46. https://archimer.ifremer.fr/doc/00112/22325/

Farmer, D. M., Armi, L., Armi, L., Farmer, D. M., 1988. The flow of Atlantic water through the Strait of Gibraltar, Prog. Oceanogr., 21(1), 1, doi:10.1016/0079-6611(88)90055-9

Faugères, J.C., Mézerais M.L., Stow D.: Contourite drift types and their distribution in the North and South Atlantic Ocean basins. Sed. Geol. 82, 189–203, https://doi.org/10.1016/0037-0738(93)90121-K, 1993.

Fiuza A.F. de G., Macedo M.E., Guerreiro M.R., (1982). Climatological space and time variation of the Portuguese coastal upwelling. Oceanologica Acta Vol 5 nº1,31-40.

Fratantoni, D.M.: North Atlantic surface circulation during the 1990s observed with satellite-tracked drifters. J. Geophys. Res.106, 22067–22093, https://doi.org/10.1029/2000JC000730, 2001.

García M., Hernández-Molina F.J., Llave E., Stow D., León R., Fernández-Puga M.C., Díaz del Río V., Somoza L.: Contourite erosive features caused by the Mediterranean Outflow Water in the Gulf of Cadiz: quaternary tectonic and oceanographic implications. Mar Geol 257:24–40, https://doi.org/10.1016/j.margeo.2008.10.009, 2009.

García, M., Llave, E., Hernández-Molina, F. J., Lobo, F. J., Ercilla, G., Alonso, B., Casas, D., Mena, A., Fernández-Salas, L. M., 2020. The role of late Quaternary tectonic activity and sea-level changes on sedimentary processes interaction in the Gulf of Cadiz upper and middle continental slope (SW Iberia). Mar. Petrol. Geol., 121, 104595.

García-Lafuente, J., Delgado, J., & Criado, F. (2002). Inflow interruption by meteorological forcing in the Strait of Gibraltar. Geophysical Research Letters, 29(19), 1914. https://doi.org/10.1029/2002GL015446

García-Lafuente, J., Delgado, J., Criado-Aldeanueva, F., Bruno, M., del Río, J., Vargas, J.M. 2006. Water Mass Circulation on the Continental Shelf of the Gulf of Cádiz. Deep-Sea Research Part II: Topical Studies in Oceanography 53 (11–13): 1182–97. https://doi.org/10.1016/j.dsr2.2006.04.011

Garel, E., Laiz, I., Drago, T., Relvas, P., Characterisation of coastal counter-currents on the inner shelf of the Gulf of Cadiz, Journal of Marine Systems, Volume 155, 2016, Pages 19-34, ISSN 0924-7963, https://doi.org/10.1016/j.jmarsys.2015.11.001.

Gasser M., Pelegrí, J.L., Emelianov M., Bruno M., Gràcia E., Pastor M., Peters H., Rodríguez-Santana A., Salvardor J., Sánchez-Leal R.F., (2017). Tracking the Mediterranean outflow in the Gulf of Cadiz. Progress in

Oceanography, Volume 157, pages 47-71, ISSN 0079-6611. https://doi.org/10.1016/j.pocean.2017.05.015.

Gil, J., Sánchez, R., Cerviño, S., Garabana, D.: Geostrophic Circulation and Heat Flux across the Flemish Cap, 1988-2000. J. Northw. Atla. Fish. Sci. 34, 61-81, http://dx.doi.org/10.2960/J.v34.m510, 2008.

Gomiz, J.J., 2017. Conexión de Procesos Hidrológicos e Hidrodinámicos Entre El Golfo de Cádiz y El Mar de Alborán. Doctoral Thesis, Cadiz University, Spain. http://hdl.handle.net/10498/22798

Gomiz-Pascual, J.J., Bolado-Penagos, M., Gonzalez, C.J., Vazquez, A., Buonocore, C., Romero-Cozar, J., Perez-Cayeiro, M.L., Izquierdo, I., Alvarez, O., Mañanes, R., Bruno, M. The fate of Guadalquivir River discharges in the coastal strip of the Gulf of Cádiz. A study based on the linking of watershed catchment and hydrodynamic models, Science of The Total Environment, Volume 795, 2021, 148740, ISSN 0048-9697, https://doi.org/10.1016/j.scitotenv.2021.148740.

Gonzalez, C.J., Mañanes, R., Izquierdo, A., Bruno, M., Gomiz, J.J., Chioua, J., Lopez, L., 2013. "Baroclinic M 2 Tidal Circulation in Algeciras Bay and Its Implications for the Water Exchange with the Strait of Gibraltar: Observational and 3-D Model Results" 118: 5398–5411. https://doi.org/10.1002/jgrc.20404.

Grell, G. A., J. Dudhia, and D. R. Stauffer, (1994). A description of the fifth-generation Penn State/NCAR Mesoscale Model (MM5). NCAR Tech. Note NCAR/TN-398+STR, 122 pp.

Gründlingh. M.L. 1981. On the observation of a solitary event in the Mediterranean outflow west of Gibraltar. 'Meteor' Forsch-Ergebn., ser A, 23 (1981), pp. 15-46.

Hall, R. A., Huthnance, J. M., & Williams, R. G. (2013). Internal Wave Reflection on Shelf Slopes with Depth-Varying Stratification, Journal of Physical Oceanography, 43(2), 248-258.

Hernández-Molina, F.J., Stow, D.A.V., Alvarez-Zarikian, C.A., Acton, G., Bahr, A., Balestra, B.,Ducassou, E., Flood, R., Flores, J.A., Furota, S., Grunert, P., Hodell, D., Jimenez-Espejo, F., Kim, J.K., Krissek, L., Kuroda, J., Li, B., Llave, E., Lofi, J., Lourens, L.,Miller,M., Nanayama, F., Nishida, N., Richter, C., Roque, C., Pereira, H., Sanchez Goñi, M.F., Sierro, F.J., Singh, A.D., Sloss, C., Takashimizu, Y., Tzanova, A., Voelker, A., Williams, T., Xuan, C., 2014b. Onset of Mediterranean outflow into the north Atlantic. Science 344, 1244–1250.Izquierdo, A., Tejedor, L., Sein, D. V., Backhaus, J. O., Brandt, P., Rubino, A. and Kagan, B. A.: Control variability and internal bore evolution in the Strait of Gibraltar: A 2-D two-layer model study, Estuar. Coast. Shelf Sci., 53(5), 637–651, doi:10.1006/ecss.2000.0706, 2001

Hernández-Molina, F.J., Llave, E., Somoza, L., Fernández-Puga, M.C., Maestro, A., León, R., Medialdea, T., Barnolas, A., García, M., Díaz del Río, V., Fernández-Salas, L.M., Vázquez, J.T., Lobo, F., Alveirinho Dias, J.M., Rodero, J., Gardner, J. Looking for clues to paleoceanographic imprints: A diagnosis of the Gulf of Cadiz contournite depositional systems. Geology (2003) 31 (1).19:22. https://doi.org/10.1130/0091-7613(2003)031<0019:LFCTPI>2.0.CO;2.

Hernández-Molina, F.J., Serra N., Stow D.A.V., Llave E., Ercilla G., van Rooij D. Along-slope oceanographic processes and sedimentary products around the Iberian margin. Geo-Marine Letters (2011) 31:315. https://doi.org/10.1007/s00367-011-0242-2.

Hernández-Molina, F.J., Stow, D.A.V., Alvarez-Zarikian, C.: Expedition IODP 339 Scientists: IODP expedition 339 in the gulf of Cadiz and off west Iberia: decoding the environmental significance of the Mediterranean outflow water and its global influence. Sci. Drill. 16, 1–11, https://doi.org/10.5194/sd-16-1-2013, 2013.

Hernández-Molina, F. J., LLave, E., Preu, B., Ercilla, G., Fontan, A., Bruno, M., Serra, N., Gomiz, J.J., Brackenridge, R.E., Sierro, F.J., Stow, D.A.V., García, M., Juan, C., Sandoval, N., Arnaiz, A.: Contourite Processes Associated with the Mediterranean Outflow Water after Its Exit from the Strait of Gibraltar: Global and Conceptual Implications. Geology 42(3):227–30, http://dx.doi.org/10.1130/G35083.1, 2014.

Hernández-Molina, F. J., Sierro F. J., Llave E., Roque C., Stow D.A.V., Williams T., Lofi J., Van der Schee M., Arnáiz A., Ledesma S., Rosales C., Rodríguez-Tovar F.J., Pardo-Igúzquiza E., Brackenridge R. E. Marine Geology 377:7-39. https://doi.org/10.1016/j.margeo.2015.09.013

Iorga, M., Lozier, M.S.: Signatures of the Mediterranean outflow from a North Atlantic climatology 1. Salinity and density fields. J. Geophys. Res. 104, 25985–26009, https://doi.org/10.1029/1999JC900115, 1999.

Izquierdo A., Tejedor L., Sein D.V., Backhaus J.O., Brandt P., Rubino A., Kagan B. A., 2001; Control Variability and Internal Bore Evolution in the Strait of Gibraltar: A 2-D Two-Layer Model Study. Estuarine, Coastal and Shelf Science (2001) 53, 637–651. https://doi:10.1006/ecss.2000.0706

Izquierdo A., Tejedor L., Sein D.V., Backhaus J.O., Brandt P., Rubino A., Kagan B. A., 2001; Control Variability and Internal Bore Evolution in the Strait of Gibraltar: A 2-D Two-Layer Model Study. Estuarine, Coastal and Shelf Science (2001) 53, 637–651. https://doi:10.1006/ecss.2000.0706

Izquierdo, A., Mikolajewicz, U.2010. Impact of Tidally-Induced Local-Scale Processes on the Spreading of the Mediterranean Outflow Water. EGU General Assembly 2010, held 2-7 May, 2010 in Vienna, Austria, p.5122

Izquierdo, Alfredo, and Uwe Mikolajewicz, 2019. “The Role of Tides in the Spreading of Mediterranean Outflow Waters along the Southwestern Iberian Margin.” Ocean Modelling 133 (September 2018): 27–43. https://doi.org/10.1016/j.ocemod.2018.08.003.

Johnson, G. C.: Quantifying Antarctic Bottom Water and North Atlantic Deep Water Volumes. Journal of Geophysical Research: Oceans 113(5):1–13, https://doi.org/10.1029/2007JC004477, 2008.

Jung, S. J. A., Kroon, D., Ganssen, G., Peeters, F., Ganeshram. R.: Southern Hemisphere Intermediate Water Formation and the Bi-Polar Seesaw. PAGES News 18(1):36–39, 2010.

Kanzow, T., Cunningham, S.A., Johns, W.E., Hirschi, J. J-M., Marotzke, J., Baringer, M.O., Meinen, C.S., Chidichimo, M.P., Atkinson, C., Beal, L.M., Bryden, H.L., Collins, J.: Seasonal Variability of the Atlantic Meridional Overturning Circulation at 26.5°N. Journal of Climate 23(21):5678–98, https://doi.org/10.1175/2010JCLI3389.1, 2010.

Keulegan, G. H. 1953 Characteristics of internal solitary waves J. Res. Nat. Bureau of Standards 51, 133.

Khélifi, N., Sarnthein, M., Andersen, N., Blanz, T., Frank, M., Garbe-Schönberg, H., B.A., Stumf, R., Einelt, M., 2011. Amajor and long-term Pliocene intensification of theMediterranean outflow, 3–5–3.3 Ma ago. Geology 37, 811–814.

Khélifi, N., Sarnthein, M., Frank,M., Andersen, N., Garbe-Schönberg, D., 2014. Late Pliocene Variations of the Mediterranean Outflow. Mar. Geol. 357, 182–194.

Knoll, M., Hernández-Guerra, A., Lenz, B., López Laatzen, F., Machín, F., Müller, T.J., Siedler, G: The Eastern Boundary Current System between the Canary Islands and the African Coast. Deep-Sea Research Part II-Topical Studies In Oceanography 49(17):3427–40, https://doi.org/10.1016/S0967-0645(02)00105-4, 2002.

Krauss, W., Fahrbach, E., Aitsam, A., Elken, J., Koske, P.: The North Atlantic Current and its associated eddy field southeast of Flemish Cap. Deep Sea Res. 34, 1163-118, https://doi.org/10.1016/0198-0149(87)90070-7, 1987.

Kundu, P.K., Allen, J.S. Smith R.L., 1975. Modal descomposition of the velocity field near the Oregon coast, Journal of Physical Oceanography,5(4) 638-704. https://doi.org/10.1175/1520-0485(1975)005<0683:MDOTVF>2.0.CO;2

Lauton G., Pattiaratchi C. B., Lentini C. A. D. (2021). Observations of Breaking Internal Tides on the Australian North West Shelf Edge, Frontiers in Marine Science 8, 629372.

Lavander, K. L., Davis, R. E., Owens, W.B.: Mid-depth recirculation observed in the Labrador and Irminger seas by direct velovity measurements. Nature, 407, 66-68, https://doi.org/10.1038/35024048, 2000.

Lebreiro S.M., Antón L., Reguera M.I., Marzocchi A., Paleoceanographic and climatic implications of a new Mediterranean Outflow branch in the southern Gulf of Cadiz. Quaternary Science Reviews. Vol 197:92-111, https://doi.org/10.1016/j.quascirev.2018.07.036.

Llave E., Hernández-Molina F.J., Somoza L., Stow D.A.V., Díaz del Río V.: Quaternary evolution of the contourite depositional system in the Gulf of Cadiz. Economic and paleoceanographic importance of contourites. Geol Soc Lond Spec Publ 276:49–79, https://doi.org/10.1144/GSL.SP.2007.276.01.03, 2007.

Llave E., Schönfeld J., Hernández-Molina F.J., Mulder T., Somoza L., Díaz del Río V., Sánchez-Almazo I.: High-resolution sta tigraphy of the Mediterranean outflow contourite system in the Gulf of Cadiz during the late Pleistocene: the impact of Heinrich events. Mar Geol 227:241–262, https://doi.org/10.1016/j.margeo.2005.11.015, 2006.

Lofi, J., Voelker, A. H. L., Ducassou, E., Hernández-Molina, F. J., Sierro, F. J., Bahr, A., Galvani, A., Lourens, L. J., Pardo-Igúzquiza, E., and Pezard, P.: Quaternary chronostratigraphic framework and sedimentary processes for the Gulf of Cadiz and Portuguese Contourite Depositional Systems derived from Natural Gamma Ray records: Marine Geology, v. 377, p. 40-57, https://doi.org/10.1016/j.margeo.2015.12.005, 2016.

Loget, N., Van Den Driessche. J., 2006. On the Origin of the Strait of Gibraltar. Sedimentary Geology 188–189: 341–56. https://doi.org/10.1016/j.sedgeo.2006.03.012

Louarn, E. and Morin P.: Antarctic Intermediate Water Influence on Mediterranean Sea Water Outflow. Deep-Sea Research Part I: Oceanographic Research Papers 58(9):932–42, https://doi.org/10.1016/j.dsr.2011.05.009, 2011.

Lynett Patrick and Liu Philip L.–F., 2004. A two-layer approach to wave modelling, Proc. R. Soc. Lond. A.4602637–2669.

Machín, F. and Pelegrí J. L.: Northward Penetration of Antarctic Intermediate Water off Northwest Africa. Journal of Physical Oceanography 39(3):512–35, https://doi.org/10.1175/2008JPO3825.1, 2009.

Machín, F. J. et al.: Seasonal Flow Reversals of Intermediate Waters in the Canary Current System East of the Canary Islands. Journal of Physical Oceanography 40(8):1902–9, https://doi.org/10.1175/2010JPO4320.1, 2010.

Machín, F. J. and Pelegrí J. L.: Interaction of Mediterranean Water Lenses with Antarctic Intermediate Water off Northwest Africa. Scientia Marina 80(S1):205–14, http://dx.doi.org/10.3989/scimar.04289.06A, 2016.

Macías, D., Bruno, M., Echevarría, F., Vázquez, Á., García, C.M., 2008a. Meteorologically-induced mesoscale variability of the North-Western Alboran Sea (southern Spain) and related biological patterns. Estuarine, Coastal and Shelf Science 78, 250–266. doi:10.1016/j.ecss.2007.12.008.

Macias, D., Garcia-Gorriz, E. & Stips, A. The seasonal cycle of the Atlantic Jet dynamics in the Alboran Sea: direct atmospheric forcing versus Mediterranean thermohaline circulation. Ocean Dynamics 66, 137–151 (2016). https://doi.org/10.1007/s10236-015-0914-y

Mackie, J.: Paleocurrent and paleoclimate reconstruction of the Western Boundary Undercurrent and Labrador Current on the Grand Banks of Newfoundland, thesis, Dalhousie University, 2005.

Madelain, F.: Influence de la topographie du fond sur l'ecoulement méditerrané en entre le Detroit de Gibraltar et le Cap Saint-Vincent. Cahiers Oceanographiques 22, 43–61, 1970.

Makou, M. C., Oppo, D.W., Curry, W.B.: South Atlantic Intermediate Water Mass Geometry for the Last Glacial Maximum from Foraminiferal Cd/Ca. Paleoceanography 25(4):1–7, https://doi.org/10.1029/2010PA001962, 2010.

Maldonado A., Nelson C.H, (1999). Interaction of tectonic and depositonal process that control the evolution of the Iberian Gulf of Cadiz margin. Marine Geology, Volume 155, Issues 1-2, pages 217-242, ISSN 025-3227, https://doi.org/10.1016/S0025-3227(98)00148-0

Marchuk, G.I., Kagan, B.A., 1970. Internal gravitational waves in a really stratified ocean. Izvestiya Akad Nauk SSSR. Atmospheric and Oceanic Physics 6, 412–422.

Marshall, J., Hill, C., Perelman, L., and Adcroft, A. (1997), Hydrostatic, quasi-hydrostatic, and nonhydrostatic ocean modeling, J. Geophys. Res., 102(C3), 5733– 5752, doi:10.1029/96JC02776.

Mauritzen, C, Morel, Y., Paillet, J., 2001. On the influence of Mediterranean Water on the Central Waters of the North Atlantic Ocean. Deep-Sea Research I 48 (2001) 347-381. https://doi.org/10.1016/S0967-0637(00)00043-1

Melières, F.: Recherches sur la dynamique sédimentaire du Golfe de Cádiz (Espagne). These de Doctoral, University of Paris A, 235pp, 1974.

Millot C., Candela J., Fuda J.L, Tber Y., Large warming and salinification of the Mediterranean outflow due to changes in its composition, Deep Sea Research Part I: Oceanographic Research Papers, 53 (4), 656-666, 2006.

Miramontes, E., Penven, P., Fierens, R., Droz, L., Toucanne, S., Jorry, S.J., Jouet, G., Pastor, L., Silva Jacinto, R., Gaillot, A., Giraudeau, J., Raisson, F. The influence of bottom currents on the Zambezi Valley morphology (Mozambique Channel, SW Indian Ocean): In situ current observations and hydrodynamic modelling, Marine Geology, Volume 410, 2019, Pages 42-55, ISSN 0025-3227, https://doi.org/10.1016/j.margeo.2019.01.002.

Miramontes, E., Jouet, G., Thereau, E., Bruno, M., Penven, P., Guerin, C., Le Roy, P., Droz, L., Jorry, S.J., Hernandez-Molina, F.J., Thi´eblemont, A., Silva Jacinto, R., Cattaneo, A., 2020. The impact of internal waves on upper continental slopes: insights from the Mozambican margin (southwest Indian Ocean). Earth Surf. Process. Landforms 45, 1469–1482. https://doi.org/10.1002/esp.4818.

Muratli, J., Chase, Z., Mix A. C., McManus, J.: Increased Glacial-Age Ventilation of the Chilean Margin by Antarctic Intermediate Water. Nature Geoscience 3(1):23–26, https://doi.org/10.1038/ngeo715, 2010.

Nash, J. D., Hartmut, P., Kelly, S.M., Pelegrí, J.L., Emelianov, M., Gasser, M., 2012. Turbulence and High-Frequency Variability in a Deep Gravity Current Outflow. Geophysical Research Letters 39 (17): 1–6. https://doi.org/10.1029/2012GL052899

Navarro G., Ruiz J., (2006). Spatial and temporal variability of phytoplankton in the Gulf of Cadiz trough remote sensing images. Deep Sea Research Part II: Topical Studies in Oceanography. Volume 53, Issues 11-13, 1241-1260. ISSN 0967-0645. https://doi.org/10.1016/j.dsr2.2006.04.014.

Nelson, C. H., Baraza, J., Maldonado, A.: Mediterranean undercurrent sandy contourites, Gulf of Cadiz, Spain. Sed Geol 82:103–131, https://doi.org/10.1016/0037-0738(93)90116-M, 1993.

Nelson, C.H., Baraza, J., Maldonado, A., Rodero, J., Escutia, C., Barber, J.H. Jr.: Influence of the Atlantic inflow and Mediterranean outflow currents on Late Quaternary sedimentary facies of the Gulf of Cadiz continental margin. Mar Geol 155:99–129, https://doi.org/10.1016/S0025-3227(98)00143-1, 1999.

Lorente, P., Soto-Navarro, J., Alvarez Fanjul, E., & Piedracoba, S. (2014). Accuracy assessment of high frequency radar current measurements in the Strait of Gibraltar. Journal of Operational Oceanography, 7(2), 59–73. https://doi.org/10.1080/1755876X.2014.11020300

Lorente, P.; Piedracoba, S.; Sotillo, M. G.; Álvarez-Fanjul, E. (2019). "Long-Term Monitoring of the Atlantic Jet through the Strait of Gibraltar with HF Radar Observations" J. Mar. Sci. Eng. 7, no. 1: 3. https://doi.org/10.3390/jmse7010003

Oppo, D. W, Horowitz, M.: Glacial Deep Water Geometry: South Atlantic Benthic Foraminiferal Cd / Ca and / 53C Evidence. 15(2):147–60, https://doi.org/10.1029/1999PA000436, 2000.

Pahnke, K., Goldstein S. L., Hemming S. R.: Abrupt Changes in Antarctic Intermediate Water Circulation over the Past 25,000 Years. Nature Geoscience 1(12):870–74, DOI: 10.1038/ngeo360, 2008.

Pardo, P. C., Pérez F.F, Velo A., Gilcoto M.: Water Masses Distribution in the Southern Ocean: Improvement of an Extended OMP (EOMP) Analysis. Progress in Oceanography 103:92–105, https://doi.org/10.1016/j.pocean.2012.06.002, 2012.

Pearson, K.: On Lines and Planes of Closest Fit to Systems of Points in Space. Philosophical Magazine 2(11):559–72., 1901.

Peliz, A., Dubert, J., Santos, A.M.P., Oliveira, P.B., LeCann, B.: Winter upper ocean circulation in the Western Iberian Basin—fronts, eddies and poleward flows:an overview. Deep Sea Res. PartI: Oceanogr. Res.Pap. 52(4), 621–646, https://doi.org/10.1016/j.dsr.2004.11.005, 2005.

Peliz, A., Marchesiello, P., Santos, A.M.P., Dubert, J., Teles-Machado, A., Marta-Almeida, M., LeCann,B.: Surface circulation in the Gulf of Cadiz: 2. Inflow–outflow coupling and the Gulf of Cadiz slope current.J.Geophys.Res. 114,C03011. http://dx.doi.org/10.1029/2008jc004771, 2009.

Pérez, F.F., Mercier, H., Vázquez-Rodríguez, M., Lherminier, P., Velo, A., Pardo, P.C., Rosón, G., Ríos, A. F.: Atlantic Ocean CO2 uptake reduced by weakening of the meridional overturning circulation. Nature Geosci. 6, 146–152, http://dx.doi.org/10.1038/ngeo1680, 2013.

Pérez-Hernández, M. D., Hernández Guerra, A., Fraile-Nuez, E., Comas-Rodríguez, I., Benítez-Barrios, V.M., Dominguez-Yanes, J.F., Vélez-Belchí, P., De Armas, D.: The Source of the Canary Current in Fall 2009. Journal of Geophysical Research: Oceans 118(6):2874–91, https://doi.org/10.1002/jgrc.20227, 2013.

Pickart, R.S., McKee, T.K., Torres, D.J., Harrington, S.A.: Mean Structure and Interannual Variabillity of the Slopewater System South of Newfoundland. J. Phys. Oceanog. 29, 2541-2558, https://doi.org/10.1175/1520-0485(1999)029<2541:MSAIVO>2.0.CO;2, 1999.

Pollard, R. T., Pu. S.: Structure and Circulation of the Upper Atlantic Ocean Northeast of the Azores. Progress in Oceanography 14(C):443–62, https://doi.org/10.1016/0079-6611(85)90022-9, 1985.

Poole, R., Tomczak, M.: Optimum Multiparameter Analysis of the Water Mass Structure in the Atlantic Ocean Thermocline. Deep-Sea Research I 46(2):1895–1921, https://doi.org/10.1016/S0967-0637(99)00025-4, 1999.

Potter, R. a. 2004. On the Warming and Salinification of the Mediterranean Outflow Waters in the North Atlantic. Geophysical Research Letters 31 (1): 1–4. https://doi.org/10.1029/2003GL018161

Preu, B., Hernández-Molina, F.J., Violante, R., Piola, A.R., Paterline, C.M., Schwenk, T., Voigt, I., Krastel, S., Spiess, V.: Morphosedimentary and Hydrographic Features of the Northern Argentine Margin: The Interplay between Erosive, Depositional and Gravitational Processes and Its Conceptual Implications. Deep-Sea Research Part I: Oceanographic Research Papers 75:157–74, https://doi.org/10.1016/j.dsr.2012.12.013, 2013.

Preu, B., Schwenk, T., Hernández-Molina, F.J., Violante, R., Paterlini, M., Krastel, S., Tomasini, J., Spieß, V.: Sedimentary growth pattern on the northern Argentine slope: The impact of North Atlantic Deep Water on southern hemisphere slope architecture. Marine Geology 329–331, 113-125, https://doi.org/10.1016/j.margeo.2012.09.009, 2012.

Price, J.F., Baringer, M.O., Lueck, R, G., Johnson, G.C., Ambar, I., Parrilla, G., Cantos, A., Kennelly, M.A., Sanford, T.B., 1993. Mediterranean Outflow Mixing and Dynamics. Science 259 (5099): 1277–82. https://doi.org/10.1126/science.259.5099.1277.

Quaresma, L.S., Pichon, A., 2013. Modelling the Barotropic Tide along the West-Iberian Margin. Journal of Marine Systems 109–110 (SUPPL.): S3–25. https://doi.org/10.1016/j.jmarsys.2011.09.016

Rahmstorf, S., 2006. Thermohaline Ocean Circulation. Encyclopedia of Quaternary Sciences, 1–10. https://doi.org/10.1016/B0-44-452747-8/00014-4

Raymo, M.E., Oppo, D.W., Flower, B.P., Hodell, D.A., McManus, J.F., Venz, K.A., Kleiven, K.F., McIntyre, K.: Stability of North Atlantic Water masses in face of pronounced natural climate variability, Paleoceanography, 19, PA2008, doi:10.1029/2003PA000921, 2004.

Rebesco, M., Hernández-Molina, F.J., Van Rooij, D., Wåhlin, A.: Contourites and associated sediments controlled by deep-water circulation processes: state of the art and future considerations. Mar. Geol. 352, 111–154, https://doi.org/10.1016/j.margeo.2014.03.011, 2014.

Relvas, P., Barton, E.D. 2002. Mesoscale Patterns in the Cape São Vicente (Iberian Peninsula) Upwelling Region. Journal of Geophysical Research C: Oceans 107 (10): 28–1. https://doi.org/10.1029/2000jc000456

Reyes, María Manuela. (2015). “Modelado de Alta Resolucion Para El Estudio de La Respuesta Oceanica Al Forzamiento Del Viento En El Estrecho de Gibraltar (Unpublished Doctoral Dissertation).”: 230. http://hdl.handle.net/10498/17501

Rhein, M.: Oceanography: Drifters reveal deep circulation. Nature 407, 30-31, https://doi.org/10.1038/35024186, 2000.

Rios, A.F. Perez,F.F., Fraga,F., Water masses in the upper and middle North- Atlantic Ocean East of the Azores. Deep Sea Research. Part A Oceanogr. Res.Pap.39 (3-4A), 645–658, 1992.

Rogerson, M., Rohling, E.J., Bigg, G.R., Ramirez, J.: Paleoceanography of the Atlantic-Mediterranean exchange: Overviewand first quantitative assessment of climatic forcing:Rev. Geophys., v. 50, RG2003, doi:http://dx.doi.org/10.1029/2011RG000376, 2012.

Roque, D., Parras-Berrocal, I., Bruno, M., Sanchez-Leal, R., Hernandez-Molina, F.J., 2019. Seasonal variability of intermediate water masses in the Gulf of Cadiz: Implications of the Antarctic and subarctic seesaw. Ocean Science, 15(5), 1381–1397. https://doi.org/10.5194/os-15-1381-2019.

Roque, C., Duarte, H., Terrinha, P., Valadares, V., Noiva, J., Cachão, M., Ferreira, J., Legoinha, P., Zitellini, N.: Pliocene and Quaternary depositional model of the Algarve margin contourite drifts (gulf of Cadiz, SW Iberia): seismic architecture, tectoni control and paleoceanographic insights. Mar. Geol. 303–306, 42–62, https://doi.org/10.1016/j.margeo.2011.11.001, 2012.

Sabine, C. L., Feely, R.A., Gruber, N., Key, R.M., Lee, K., Bullister, J.L., Wanninkhof, R., Wong, C.S., Wallace, D.W.R., Tilbrook, B., Millero, F. J., Peng T.H., Kozyr, A. Ono, T., Ríos, A.F.: The Oceanic Sink for Anthropogenic CO2. Science 305(5682):367–71, DOI: 10.1126/science.1097403, 2004.

Sala I, Navarro G, Bolado-Penagos M, Echevarría F, García CM. (2018) High-Chlorophyll-Area Assessment Based on Remote Sensing Observations: The Case Study of Cape Trafalgar. Remote Sensing; 10(2):165. https://doi.org/10.3390/rs10020165

Sammartino, S., García Lafuente, J., Naranjo, C., Sánchez Garrido, J. C., Sánchez Leal, R., and Sánchez Román, A. (2015), Ten years of marine current measurements in Espartel Sill, Strait of Gibraltar, J. Geophys. Res. Oceans, 120, 6309– 6328, doi:10.1002/2014JC010674.

Sánchez Garrido, J. C., García Lafuente, J., Criado Aldeanueva, F., Baquerizo, A., Sannino, G., 2008. Time-spatial variability observed in velocity of propagation of the internal bore in the Strait of Gibraltar, J. Geophys. Res. Ocean., 113(7), 1–6, doi:10.1029/2007JC004624

Sánchez-Garrido, J. C., Sannino, G., Liberti, L., García Lafuente, J., Pratt, L., 2011: Numerical modeling of three-dimensional stratified tidal flow over Camarinal Sill, Strait of Gibraltar, J. Geophys. Res. Ocean., 116(12), 1–17, doi:10.1029/2011JC007093

Sánchez-Leal, R.F., Bellanco, M.J., Fernández-Salas, L.M., García-Lafuente, J., Gasser-Rubinat, M., González-Pola, C., Hernández-Molina, F.J., Pelegrí, J.L., Peliz, A., Relvas, P., Roque, D., Ruiz-Villarreal, M., Sammartino, S., Sánchez-Garrido, J.C.: The Mediterranean Overflow in the Gulf of Cadiz: A rugged journey. Scientific Reports3(11), DOI:10.1126/sciadv.aao0609, 2017.

Sánchez-Leal, R., Bellanco, M.J., Naranjo, C., García-lafuente, J., Gonz, C., 2020. On the Seasonality of Waters below the Seasonal Thermocline in the Gulf of Cadiz. Continental Shelf Research, 204 https://doi.org/10.1016/j.csr.2020.104190

Schlitzer, R., Ocean Data View, https://odv.awi.de, 2018

Schönfeld, J., Zahn, R.: Late glacial to Holocene history of the Mediterranean Outflow. Evidence from benthic foraminiferal assemblages and stable isotopes at the Portuguese margin. Palaeogeogr. Palaeoclimatol. Palaeoecol. 159 (1–2), 85–111, https://doi.org/10.1016/S0031-0182(00)00035-3, 2000.

Schönfeld, J., Zahn, R., Abreu, L.: Surface and deep water response to rapid climate changes at the Western Iberian Margin. Glob. Planet. Chang. 36, 237–264, https://doi.org/10.1016/S0921-8181(02)00197-2, 2003.

Shanmugam, G., 2006. Deep-Water Processes and Facies Models: Implications for Sandstone Petroleum Reservoirs, Vol. 5 Amsterdam, the Netherlands: Elsevier Science.

Shanmugam, G., 2012. New perspectives on deep-water sandstones: origin, recognition, initiation, and reservoir quality. Handbook of Petroleum Exploration and Production, 9. Elsevier, Amsterdam, 524 pp. Available at: https://www.elsevier.com/books/new-perspectives-on-deepwater-sandstones/shanmugam/978-0-444-56335-4.

Shanmugam, G., 2020. Mass transport, gravity flows, and bottom currents: Downslope and alongslope processes and deposits. Elsevier. 608.Spakman, W., Chertova, M. V., van den Berg, A., and van Hinsbergen, D. J. (2018) Puzzling features of western Mediterranean tectonics explained by slab dragging. Nature Geoscience, 11, 211-216.

Shmidtko, S., Johnson, G.C.: Multidecadal Warming and Shoaling of Antarctic Intermediate Water, J. Climate, 25, 207-221, https://doi.org/10.1175/JCLI-D-11-00021.1, 2012.

Siedler, G., and Paul, U. (1991), Barotropic and baroclinic tidal currents in the eastern basins of the North Atlantic, J. Geophys. Res., 96(C12), 22259– 22271, doi:10.1029/91JC02319.

Sierro, F.J., Hodell, D.A., Andersen, N., Azibeiro, L.A., Jimenez-Espejo, F.J., Bahr, A., Flores, J.A., Ausin, B., Rogerson, M., Lozano-Luz, R., Lebreiro, S., Hernandez-Molina, F.J., 2020. Mediterranean Overflow over the last 250 ky. Freshwater forcing from the tropics to the ice sheets. Paleoceanogr. Paleoclimatol., 35, e2020PA003931.

Soto-Navarro, J., Lorente, P., Álvarez-Fanjul, E., Sánchez-Garrido, J. C., & García-Lafuente, J. (2016). Surface circulation at the Strait of Gibraltar: A combined HF radar and high resolution model study. J. Geophys. Res. Oceans, 121, 2016–2034. https://doi.org/10.1002/2016JC012335

Stein, M.: Oceanography of the Flemish Cap and Adjacent Waters. J. Northw. Atla. Fish. Sci. 37, 135-146, doi:10.2960/J. v37.m652, 2007.

Stow, D.A.V., Hernández-Molina, F.J., Alvarez Zarikian, C.A., the Expedition 339 Scientists, 2013b. Proceedings IODP, 339. Integrated Ocean Drilling Program Management International, Tokyo http://dx.doi.org/10.2204/iodp.proc.339, 2013.

Stramma, L., Siedler, G.: Seasonal changes in the North Atlantic subtropical gyre, J. Geophys. Res., 93(C7), 8111–8118, doi:10.1029/JC093iC07p08111, 1988.

Stramma, L., England, M.: On the Water Masses and Mean Circulation of the South Atlantic Ocean. Journal of Geophysical Research 104:20863–83, https://doi.org/10.1029/1999JC900139, 1999.

Talley, L. D.: Shallow, Intermediate, and Deep Overturning Components of the Global Heat Budget. Journal of Physical Oceanography 33(3):530–60, https://doi.org/10.1175/1520-0485(2003)033<0530:SIADOC>2.0.CO;2, 2003.

Talley, L. D.: Some aspects of ocean heat transport by the shallow, intermediate and deep overturning circulations. In Mechanisms of Global Climate Change at Millennial Time Scales, Geophys. Mono. Ser., 112, American Geophysical Union, ed. Clark, Webb and Keigwin, 1-22, https://doi.org/10.1029/GM112p0001, 1999.

Teles-Machado, A., Peliz, A., Dubert, J., Sánchez, R.F., 2007. On the Onset of the Gulf of Cadiz Coastal Countercurrent. Geophysical Research Letters 34 (12): 1–5. https://doi.org/10.1029/2007GL030091

Thiéblemont, A., Hernández-Molina, F.J., Miramontes, E., Taisson, F., Penven, P. Contourite depositional systems along the Mozambique channel: The interplay between bottom currents and sedimentary processes, Deep

Sea Research Part I: Oceanographic Research Papers,Volume 147, 2019, Pages 79-99, ISSN 0967-0637, https://doi.org/10.1016/j.dsr.2019.03.012.

Thran, A.C., Dutkiewicz, A., Spence, P., Müller, R.D., 2018. Controls on the global distribution of contourite drifts: Insights from an eddy-resolving ocean model. Earth Planet. Sci. Lett. 489, 228–240

Tomczak, M., Large, D.: Optimum Multiparameter Analysis of Mixing in the Thermocline of the Eastern Indian Ocean. Journal of Geophysical Research 94(Cll):16141–49, https://doi.org/10.1029/JC094iC11p16141, 1989.

Tomczak, M., Godfrey, J S.: Regional Oceanography: An Introduction 2nd edn. pp.63-82, 2003.

Tsimplis, M. N., 2000. Vertical structure of tidel currents over the Camarinal Sill at the Strait of Gbraltar, J. Geophys. Res., 105, 19709–19728.

Tsuchiya, M., Talley L.D., Michael S., McCartney, M.S.: An Eastern Atlantic Section from Iceland Southward across the Equator. Deep Sea Research Part A. Oceanographic Research Papers 39(11–12):1885–1917, https://doi.org/10.1016/0198-0149(92)90004-D, 1992.

Van Aken, H. M.: The Hydrography of the Mid-Latitude Northeast Atlantic Ocean I. The Deep Water Masses, https://doi.org/10.1016/S0967-0637(99)00092-8, 2000.

Van Aken, Hendrik M.: The Hydrography of the Mid-Latitude Northeast Atlantic Ocean, DOI: 10.1016/S0967-0637(99)00092-8, 2000.

Van Aken, Hendrik M.: The Hydrography of the Mid-Latitude Northeast Atlantic Ocean - Part III: The Subducted Thermocline Water Mass. Deep-Sea Research Part I: Oceanographic Research Papers 48(1):237–67, https://doi.org/10.1016/S0967-0637(00)00059-5, 2001.

Vandorpe T., Van Rooij D., de Haas H. Statigraphy and paleoceanography of a topography-controlled contourite drift in the Pen Duick area, southern Gulf of Cádiz. Marine Geology Vol 349: 136-151. https://doi.org/10.1016/j.margeo.2014.01.007.

Vandorpe T., Martins I., Vitorino J., Hebbeln D., García M., Van Rooij D.: Bottom currents and their influence on the sedimentation pattern in the El Arraiche mud volcano province, southern Gulf of Cadiz. Marine Geology Vol 378:114-126. https://doi.org/10.1016/j.margeo.2015.11.012.

Vargas, M., Sarhan, T., García-Lafuente, J., Cano, N.,1999. An Advection-Diffusion Model to Explain Thermal Surface Anomalies off Cape Trafalgar. Boletin - Instituto Espanol de Oceanografia 15 (1–4): 91–99.

Vargas-Yáñez, M., Plaza, F., García-Lafuente, J., Sarhan, T., Vargas, J. M., & Vélez-Belchi, P. (2002). About the seasonal variability of the Alboran Sea circulation. Journal of Marine Systems, 35, 229–248. https://doi.org/10.1016/S0924-7963(02)00128-8

Vazquez, A, Stashchuk, N., Vlasenko, V., Bruno, M., Izquierdo, A., Gallacher, P.C., Violette, L., 2006. Evidence of Multimodal Structure of the Baroclinic Tide in the Strait of Gibraltar. 33: 2–7. https://doi.org/10.1029/2006GL026806

Vázquez, A., Bruno, M., Izquierdo, A., Macías, D., Ruiz-Cañavate, A. 2008. Meteorologically forced subinertial flows and internal wave generation at the main sill of the Strait of Gibraltar, Deep. Res. Part I Oceanogr. Res. Pap., 55(10), 1277–1283, doi: 10.1016/j.dsr.2008.05.008.

Vázquez, A., Bruno, M., Izquierdo, A., Macías, D., Ruiz-Cañavate, A., 2008. Meteorologically Forced Subinertial Flows and Internal Wave Generation at the Main Sill of the Strait of Gibraltar. Deep-Sea Research Part I: Oceanographic Research Papers 55 (10): 1277–83. https://doi.org/10.1016/j.dsr.2008.05.008

Velez-Belchi, P., Perez-Hernandez, M. D., Casanova-Masjoan, M, Cana, L., Hernandez-Guerra, A.: On the Seasonal Variability of the Canary Current and the Atlantic Meridional Overturning Circulation. 122:4518–38, https://doi.org/10.1002/2017JC012774, 2017.

Viana, A.R., Hercos, C.M., Almeida Jr., W., Magalhães, J.L.C., Andrade, S.B.: Evidence of bottom current Influence on the Neogene to Quaternary sedimentation along the Northern Campos Slope, SW Atlantic Margin, Deep-Water Contourite Systems: Modern Drifts and Ancient Series, Seismic and Sedimentary Characteristics. Geological Society, London, Memoirs 22, pp. 249-259, https://doi.org/10.1144/GSL.MEM.2002.022.01.18, 2002.

Visbeck, M., 2002. "Deep Velocity Profiling Using Lowered Acoustic Doppler Current Profilers: Bottom Track and Inverse Solutions." Journal of Atmospheric and Oceanic Technology 19 (5): 794–807. https://doi.org/10.1175/1520-0426(2002)019<0794:DVPULA>2.0.CO;2

Vlasenko, V., Sanchez Garrido, J.S., Stashchuk, N., Garcia Lafuente, J., Losada, M., 2009. Three-Dimensional Evolution of Large-Amplitude Internal Waves in the Strait of Gibraltar. Journal of Physical Oceanography 39 (9): 2230–46. https://doi.org/10.1175/2009JPO4007.1

Voelker, A.H.L., Lebreiro, S.M., Schönfeld, J., Cacho, I., Erlenkeuser, H., Abrantes, F.: Mediterranean outflow strengthening during northern hemisphere coolings: a salt source for the glacial Atlantic? Earth Planet Sci. Lett. 245, 39e55. https://doi.org/10.1016/j.epsl.2006.03.014, 2006.

Voelker A.H.L., Colman A., Olack G., Waniek J. J., Hodell D., Oxygen and hydrogen isotope signatures of Northeast Atlantic water masses, Deep Sea Research Part II: Topical Studies in Oceanography, 116: 89-106, 2015.

Voigt, I., Henrich, R., Preu, B.M., Piola, A.R., Hanebuth, T.J.J. Schwenk, T., Chiessi, M.: A submarine canyon as a climate archive – Interaction of the Antarctic Intermediate Water with the Mar de Plata Canyon (Southwest Atlantic). Marine Geology, 341: 46-57, https://doi.org/10.1016/j.margeo.2013.05.002, 2013.

Wainer, I., Goes M., Murphy L. N., Brady E.: Changes in the Intermediate Water Mass Formation Rates in the Global Ocean for the Last Glacial Maximum, Mid-Holocene and Pre-Industrial Climates. Paleoceanography 27(3):1–11, https://doi.org/10.1029/2012PA002290, 2012.

Wallace J.M. and Dickinson R.E., 1972. Empirical orthogonal representation of time series in the frequency domain. Part I: Theorical considerations. Journal of Applied Meteorology, 11(6), pp 887-892. https://doi.org/10.1175/1520-0450(1972)011<0887: EOROTS>2.0.CO;2

Wesson, J.C., Gregg, M.C., 1994. Mixing at Camarinal Sill in the Strait of Gibraltar. Journal of Geophysical Research 99 (C5), 9847–9878.

Yashayaev, I, Clarke, A.: Evolution of North Atlantic water masses inferred from Labrador Sea salinity series. Oceanography 21, 30-45, https://doi.org/10.5670/oceanog.2008.65, 2008.

Yin, S., Hernández-Molina, F.J., Zhang, W., Li, J., Wang, L., Ding, W., Ding, W., 2019. The influence of oceanographic processes on contourite features: a multidisciplinary study of the northern South China Sea. Mar. Geol. 415, 105967.